Quantitative electron probe microanalysis of light elements using energy dispersive x-ray spectrometry.

Bloomfield, D. J.

Award date:
1983

Awarding institution:
University of Bath

QUANTITATIVE ELECTRON PROBE MICROANALYSIS OF LIGHT ELEMENTS USING ENERGY DISPERSIVE X-RAY SPECTROMETRY

submitted by

D. J. BLOOMFIELD B.Sc.

for the degree of Ph.D.

of the University of Bath.

1983

DJ Bloomfield

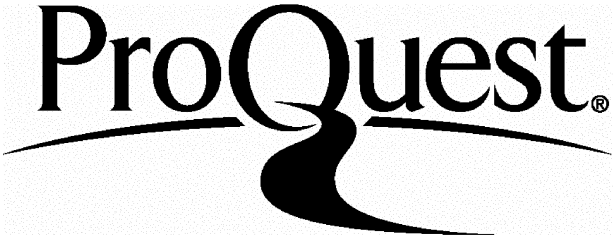

SUMMARY

Prospects for energy dispersive (ED) analysis of light elements in the electron probe are assessed, with particular concern for the accuracy which can be achieved in quantitative analysis. A comprehensive study of the ED system and the low energy spectrum it produces has revealed several problems. These have been thoroughly investigated and techniques developed to overcome them.

Reasons for the failure of a commonly used dead time correction system are discussed and the magnitude of errors in quantitative work are determined. An alternative correction method is developed and its accuracy confirmed. It is also shown that differences in methods used for signal discrimination in ED systems lead to different presentations of the low energy spectrum. These effects must be clearly understood before measurements of soft x-ray peak intensities are attempted. The problem of electronic noise counts which appear at low energy is discussed and a way of removing them from spectra is demonstrated. A new component of the spectrum background below 500 eV is identified and characterised, to provide a means of accounting for it in recorded spectra.

Two remaining problems, although common to conventional ED analysis, are more difficult to solve in the soft

x-ray region. The first concerns prediction of x-ray continuum, and here a promising technique based on the use of a reference standard is developed, extending it's range down to 0.1 keV. The second problem is deconvolution of overlapping peaks and a least squares fitting procedure is adopted for this work.

The accuracy of ED analysis incorporating these techniques is demonstrated by comparison with wavelength dispersive analysis of selected specimens. Finally realistic sensitivity levels are measured for light elements at a range of probe voltages.

ACKNOWLEDGEMENTS

I am very grateful for the help and guidance I have received from my supervisors Dr. V.D. Scott and Dr. G. Love, and I would like to thank them for giving me the opportunity to carry out this work.

The Science and Engineering Research Council provided the funds for my studentship and the equipment used in the work, and I appreciate the additional support of the 'Procurement Executive, M.O.D.'

I am also indebted to the School of Materials Science at Bath University for the various facilities made available to me during the work.

Finally I must thank my family for tolerating my 'devotion' to the project and my wife Jean, for her excellent typing.

CONTENTS

1. ELECTRON PROBE MICROANALYSIS

Electron probe microanalysis (EPMA) is based on the use of a finely focused electron beam to induce x-ray emission from a small volume, typically 1 μm^3, in a specimen. These x-rays are then analysed with a spectrometer to yield information about the elements within that region of the specimen. Furthermore, comparison of x-ray line intensities from specimens of unknown composition with those from standards allows quantitative measurement of elemental weight concentrations.

Section 1, will describe the physical principles of x-ray emission, development of the electron probe microanalyser and the theory of quantitative analysis. A detailed introduction to energy dispersive spectrometry and a discussion of light element analysis, which form the subject of this thesis will follow in section 2.

1.1 X-ray Emission in EPMA

When an incident electron enters the specimen it undergoes multiple scattering until it loses most of it's kinetic energy or escapes from the specimen surface. The electron can lose energy in two types of inelastic collision giving rise to 'characteristic' and 'continuum' x-ray emissions.

1.1.1 Characteristic X-ray Emission.

Electrons or x-rays with sufficient energy are able to cause inner shell ionisation of atoms within the specimen. It is the relaxation of these 'excited' atoms which gives rise to the characteristic x-ray emission.

Figure 1.1 shows the electron energy levels for zinc, and illustrates the excitation of electrons from the K, L and M shells to the valence band. An incident electron or x-ray is able to cause such ionisation only if it's energy is greater than the 'binding energy' of the orbital concerned. This is therefore termed the 'critical excitation energy' and it's dependence upon atomic number is shown in figure 1.2 for K, L and M shells. At least one shell in any element can be ionised by electrons or x-rays with energy 5 keV or more.

The ionised atom is in an 'excited' state and subsequently relaxes by the transition of an electron from a higher level into the vacancy. The energy released is equal to the difference between the orbital energies involved and since this is specific to the atom concerned it can be used to identify elements in the specimen. With elements of atomic number greater than 3 the photons produced are x-rays having energies greater than 0.1 keV (wavelengths less than 120 nm).

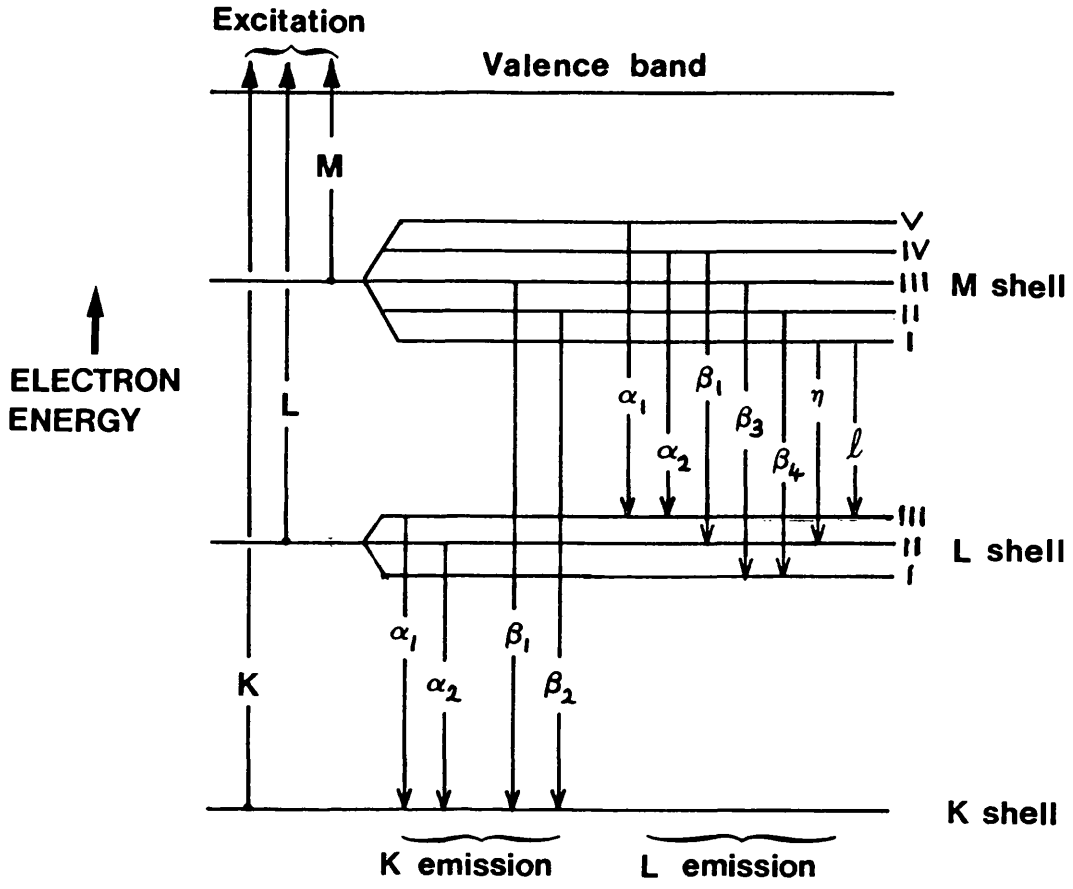

Fig. 1.1 Schematic diagram of electron energy levels in zinc, showing excitation transitions, and allowed relaxation transitions with designation of x-ray emissions.

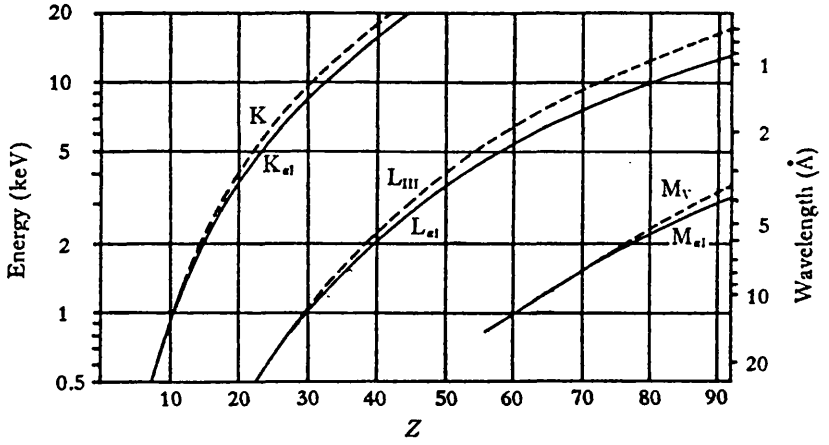

Fig. 1.2 Energy and wavelength of the most important X-ray lines, and their critical excitation energies, as a function of atomic number (Z). (Dashed lines indicate critical excitation energy E_c.)

(From Reed 1975a)

Quantum theory only permits certain electron transitions between energy levels. Those allowed between K, L and M shells in zinc are shown in fig. 1.1 with the corresponding line designations. X-rays are known primarily by the letter of the original ionised shell with a subscript denoting the source of the electron which fills the vacancy. For example x-rays produced by electron transitions from the M.IV to the L.II sub orbital are called L.β1 emissions. Figure 1.2 also shows the energies and wavelengths of the most important K, L and M characteristic x-rays from elements with atomic number between 6 and 92. Although each line energy is unique some are closely spaced such as the molybdenum Lα and the sulphur Kα at 2.293 and 2.307 keV (5.407 and 5.372 nm) respectively. The ability to separate adjacent lines depends upon the resolving power of the x-ray spectrometer.

As mentioned previously both electrons and x-rays are able to produce inner shell ionisation and hence give rise to characteristic x-ray emission. The term used when x-rays themselves cause such emission is 'fluorescence'. In the electron probe ionisation is caused primarily by the incident electron beam, but characteristic and continuum x-rays generated within the specimen can themselves produce secondary characteristic emission by fluorescence. The effect occurs most strongly when the x-ray energy is just above the critical excitation energy of an electron shell; this is the case

when a K photon from one element encounters an atom 1 or 2 lower in atomic number.

The relaxation of an ionised atom does not always give rise to photon emission. An alternative, 'radiationless' process termed Auger emission is possible in which the energy is released by ejection of another electron. The probability of an x-ray being emitted rather than an Auger electron is called the fluorescent yield.

1.1.2 X-ray Continuum

Continuum or bremsstrahlung radiation consists of the photons produced directly by the 'slowing down' of incident electrons within the specimen. These photons can have a wide range of energies between zero and the full energy of the incident electron (E_o), this maximum energy is known as the Duane-Hunt limit. In EPMA the incident electron energy is generally between 5 and 50 keV and the photons emitted in the slowing down process are therefore predominantly x-rays. Kramers (1923) used the Thomson-Whiddington law (Whiddington 1912) for electron energy loss and a classical approach to the scattering cross section to determine the intensity of continuum x-rays generated in a solid target. His result may be expressed as;

$$N(E)dE = \frac{b.Z(E_o-E)\ dE}{E}$$

where $N(E)dE$ is the number of photons generated per

second with energy in the range dE at E; Z is the atomic number of the specimen; and b is a constant $\sim 2\times10^{-9}$, s^{-1} eV^{-1} $electron^{-1}$. This distribution is illustrated by the dotted line in figure 1.3.

Some of the generated continuum x-rays will be re-absorbed in the specimen, particularly the 'less penetrating' soft x-rays, so the actual emission from the specimen is similar in shape to the solid line in fig.1.3.

The continuum gives no easily accessible information about the composition of the specimen and can sometimes cause problems in EPMA by masking characteristic lines.

1.2 Instrumental Development

1.2.1 The Electron Probe Microanalyser

Characteristic x-rays were discovered in 1909 by Barkla and Sadler; and it was soon after this, in 1912, that von Laue conceived the principle of x-ray spectrometry in which x-rays are separated in terms of wavelength by a diffracting crystal. Wavelengths could be selected in turn by altering the angle of diffraction and the x-rays were detected by an ionisation chamber or photographic plate. Moseley (1913,1914) first demonstrated the use of this technique for spectrographic chemical analysis, by recording and identifying

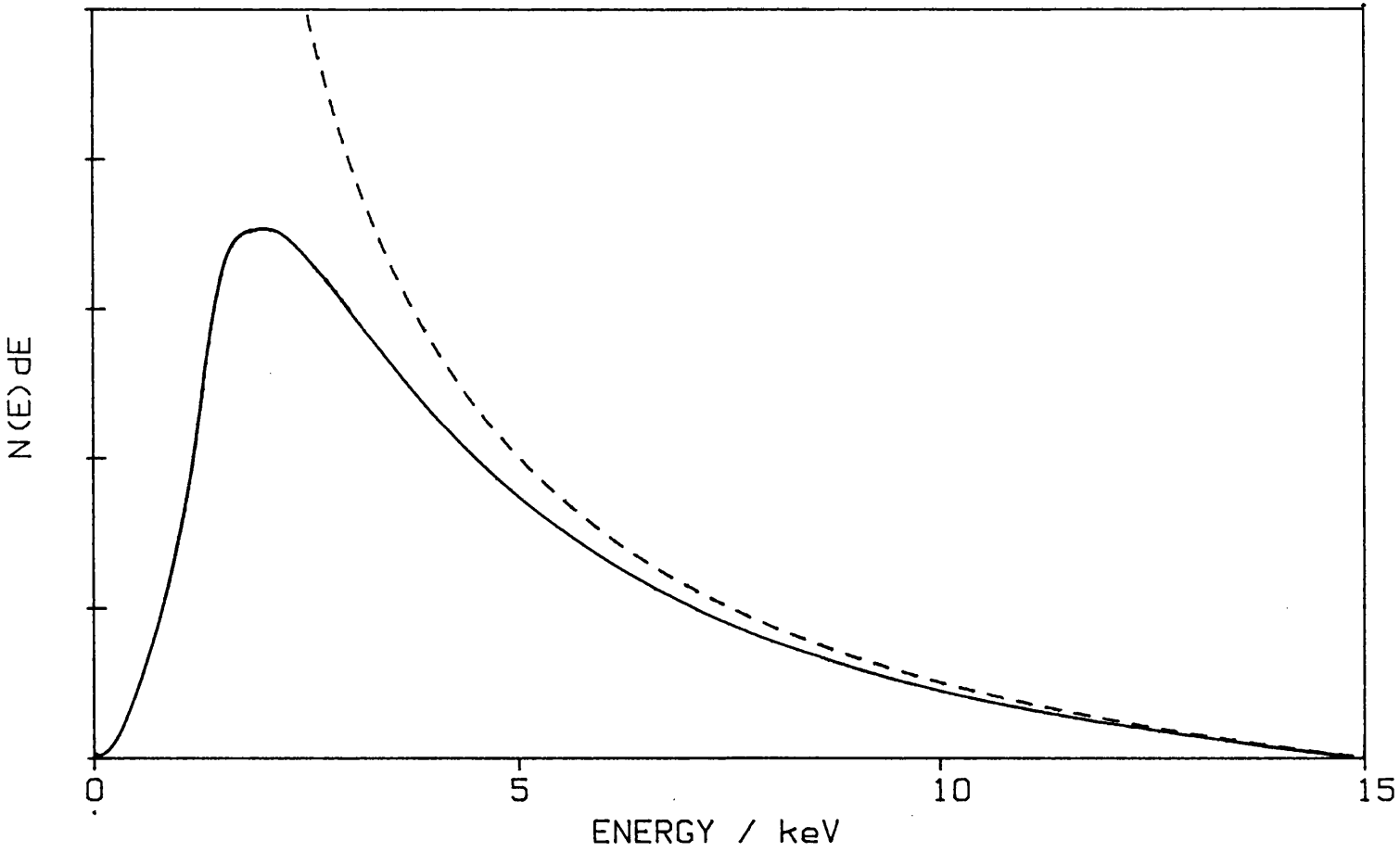

Fig. 1.3 Dotted line shows the intensity distribution (photons s^{-1} eV^{-1} $electron^{-1}$) of continuum x-rays generated in a solid target, as given by Kramers (1923). Solid curve shows the actual emitted intensity which is lower due to self absorption.

characteristic emission lines from targets in an x-ray tube.

In subsequent years spectrometers were developed, mainly for x-ray fluorescence analysis, whilst electron beam techniques were delayed by the limited capability of electron focusing systems. In the 1930's spectrometer design was improved by the use of curved crystals and focusing geometry, (Johann 1931, Johansson 1932). The greater efficiency of this type of spectrometer enabled useful analysis to be carried out with much lower electron beam currents (<100 nm) than was previously possible and so aided the development of EPMA.

It was in 1951 that Castaing reported the successful combination of a transmission electron microscope and x-ray spectrometer as a prototype electron probe microanalyser; in which a 1 um diameter beam could be used for practical x-ray analysis of specimens. In his thesis Castaing presented the principles of the technique and the foundations for correction procedures needed in quantitative analysis.

The general layout of an electron probe microanalyser is illustrated in figure 1.4. Electrons are generated by a heated tungsten filament and accelerated down the evacuated column by means of a potential (typically 5 to 30 kV) applied between the filament and an anular anode. The beam is focused by electromagnetic lenses producing

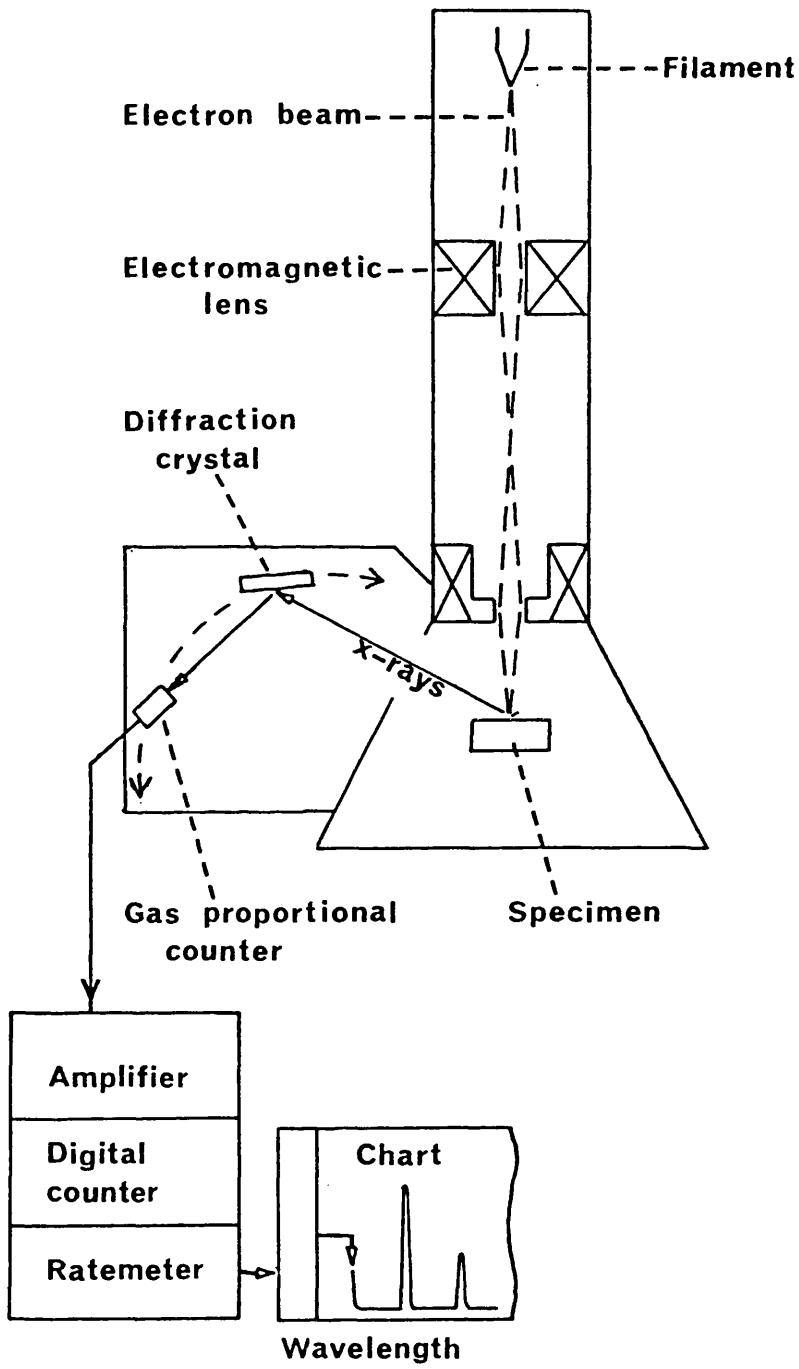

Fig.1.4 Electron probe microanalyser

a probe perhaps 0.1 to 1.0 μm in diamter with currents of 1 to 100 nA.

Most early instruments operated with a static electron beam, but in 1956 Cosslett and Duncumb developed a scanning system in which the beam traced a raster on the specimen surface. Signals from the surface, such as x-rays, secondary or backscattered electrons, could be used to modulate the brightness of a cathode ray tube (CRT) scanned in synchronism with the electron beam; producing a highly magnified image or map of the specimen on the CRT. This type of imaging system proved very useful in allowing accurate positioning of the probe for analysis of selected features.

The basic layout of the crystal, or wavelength dispersive (WD) spectrometer (shown in figure 1.4) has changed very little from the 1930's. X-rays from the specimen pass through an aperture to an externally mounted chamber containing the analysing crystal and x-ray detector. The detector most commonly used today is the gas flow proportional counter, the output of which is amplified and fed either to a rate meter and chart recorder or to a scaler for numerical readings.

The condition for diffraction at the crystal is given by the Bragg law,

$$n\lambda = 2d \sin\theta$$

where λ is the x-ray wavelength; d is the crystal lattice

spacing; θ is the angle of incidence; and n is an integer, the 'order'of the diffraction.

Generally the first order diffraction, where n=1, is the most intense and is used for practical analysis. Diffractions of higher order (n>1) are however common and appear at progressively higher angles θ where they may interfere with the first order lines of longer wavelength x-rays. Since the interfering line is of higher energy than the line of interest it can usually be removed by pulse height discrimination, and the necessary electronics is included in most modern systems.

The characteristic x-ray lines appear as peaks superimposed on a continuum background and the resolution of the spectrometer is often defined in terms of the full width of the peak at half it's height above background (FWHM). This is typically 0.1 Å (0.01 keV) for a 10 Å (1 keV) line and allows easy separation of major elemental lines. Another benefit is that background counts are relatively low giving peak to background ratios (P/B) of up to 1000 for pure elements. The sensitivity for low concentrations is generally limited by the accuracy with which the background level can be determined. For example with a 1% error in background measurement and a P/B ratio of 1000 the ultimate limit of detection is 0.001% or 10ppm although 100ppm is a more realistic level in practice.

Due to physical restrictions each diffracting crystal can

be used only for wavelengths from about 0.4d to 1.7d so crystals with different 'd' spacings are interchanged within the spectrometer to cover a wider wavelength range. Furthermore it can be seen from figure 1.2 that elements below 12 in atomic number produce K lines of wavelength 12 Å or more. In the 1950's and early 1960's there were no crystals available with 'd' spacings large enough to deal with these wavelengths so analysis of light elements was not feasible.

The range of elements with atomic number less than 12 includes carbon, nitrogen and oxygen, important elements not only in minerological and biological materials but also common constituents of inclusions in metals. Consequently there has been much interest in the development of EPMA to include light element analysis.

1.2.2 Early Developments in Light Element Analysis

Pulse height analysis

One solution to the problem of light element analysis was that developed by Dolby (1959,1963) based on pulse height analysis with a gas proportional counter. In this type of detector one ionisation can be produced for every 25 to 30 eV of incident electron energy. Furthermore, although x-rays in the range 1 to 10 keV produce only 40 to 400 ionisations each, acceleration of ions in the electric field causes an avalanche effect, termed

'internal amplification'. This greatly improves the signal to noise ratio of the output, which remains proportional, in amplitude, to the x-ray energy. Pulse height analysis can therefore be used to sort the x-ray photons according to energy and hence produce an energy dispersive spectrum. Unfortunately the statistics associated with the ionisation process lead to large variations in output signal for a particular x-ray energy. So the ability to separate neighbouring characteristic lines was very poor and special deconvolution techniques using electronic networks had to be developed. With this type of system Ranzetta and Scott (1964) were able to produce x-ray maps of 'light' elements in metal matrices; but the system was not easy to use on a routine basis.

Diffraction gratings

Another approach to analysis of long wavelength x-rays was the use of diffraction gratings. Line spacings were generally rather broad for x-ray work but the gratings could be used at low angles of incidence and had good reflection efficiency. Various types such as 'phase' and 'blaze' gratings were developed (e.g. Sayce and Franks 1964) for improved efficiency in soft x-ray analysis. The wavelength resolution was generally better than with crystal spectrometers; so gratings proved useful for studies of light element peak shapes (Holliday 1966). Gratings, however, required more stringent positional accuracy than crystals and could not

be fitted to conventional spectrometers.

WD analysis of soft x-rays

Diffraction gratings and energy dispersive systems with gas counters were generally superseded when crystals with large 'd' spacings became available for use in WD spectrometers. Natural crystals such as rubidium acid phthalate (RAP), could deal with K x-rays from elements with atomic number greater than 8; and synthetic stearate (STE) crystals with 'd' spacings up to 50 Å covered a range including the nitrogen K line at 31.6 Å and boron K at 67.6 Å. These crystals could be fitted to standard WD spectrometers and so extended the range of WDS to include the light elements.

1.2.3 Energy Dispersive Analysis with Solid-State Detectors

Interest in the energy dispersive technique was re-awakened in 1966 by improvements in solid-state detectors which, had previously been used mainly in high energy physics.

The early ED systems (Bowman et al 1966) offered an energy resolution of about 0.6 keV FWHM at 10keV compared with about 1.5 keV for systems using the gas proportional counter. A particular advantage of the ED approach was that the detector could be placed much

closer to the specimen than in WDS, thus improving x-ray detection efficiency. In x-ray fluorescence (XRF) work this meant that x-ray tubes used for excitation could be replaced by radio-active sources. So early ED systems were incorporated in compact XRF analysis packages, (Barclay, Jones and Carpenter 1968; Langheinrich and Forster 1968).

The use of ED systems was soon considered more seriously in EPMA, (Fitzgerald, Keil and Heinrich 1968). The energy resolution with these systems was such that adjacent K lines could only be separated for elements above 20 in atomic number. Nevertheless the high x-ray collection efficiency enabled analysis with lower beam currents than in WDS, which was useful when examining 'beam sensitive materials'. Also the ability to analyse a wide range of energies simultaneously was convenient for quick assessment of specimens of unknown composition.

The poor energy resolution in these early systems was due to noise levels in the detector and amplifiers. Fortunately rapid advances were made in amplifier design and in the early 1970's the resolution was improved to about 160 eV FWHM at 6 keV. This enabled separation of all characteristic K lines down to atomic number 11 and was little short of the resolution attainable today. Recently, with growing interest in ED analysis of soft x-rays, which could benefit from improved resolution, attention

has returned to the problems of noise levels in ED systems (Statham 1983).

1.3 Quantitative Analysis

An important aspect of EPMA is the ability to obtain quantitative information about specimen composition. The principle, first developed by Castaing (1951), is that the measured intensity (I_A) of characteristic x-ray emission from a particular element (A) within a specimen is approximately proportional to it's weight concentration (C_A) in that specimen.

Thus $C_A = b.I_A$ where 'b' is a constant

For a pure standard

$$C_A^S = b.I_A^S \quad \text{and} \quad C_A^S = 1$$

hence $$C_A = I_A/I_A^S \qquad (1.1)$$

The value of 'b' depends upon factors such as beam current, analysis time, and detector efficiency so the values I_A and I_A^S must be obtained under identical conditions.

1.3.1 ZAF Corrections

Although equation 1.1 gave reasonable results under certain conditions it soon became apparent that other factors need to be taken into account. Various approaches

have been proposed but the procedure adopted by Castaing is still widely used. He showed that the relevant factors could be considered as independent effects termed atomic number (Z), absorption (A) and fluorescence (F) such that

$$I_A/I_A^S = C_A ZAF \qquad (1.2)$$

The nature of these effects can be understood by considering the depth distribution of x-rays generated within a specimen, traditionally represented by a $\phi(\rho z)$ curve.

Depth distribution of generated x-rays

A typical x-ray distribution curve is shown in figure 1.5 where the horizontal axes represents the mass depth within the specimen. The vertical scale, $\phi(\rho z)$, gives the generated x-ray line intensity from an incremental thickness $\Delta\rho z$ at depth ρz, and is normalised with respect to the intensity $\phi(\Delta\rho z)$ given by an isolated thin film of thickness $\Delta\rho z$. Thus the total number of x-rays generated within the specimen, I_{gA} is given by integration,

$$I_{gA} = \phi(\Delta\rho z) \int_0^\infty \phi(\rho z)\ \delta\rho z$$

X-rays leaving the specimen are subject to absorption and the intensity I_e escaping through a mass distance ρs is given by Beer's law;

$$I_e = I_g \exp(-\tfrac{\mu}{\rho} .\rho s)$$

where μ/ρ is the mass absorption coefficient for the x-rays in the material concerned.

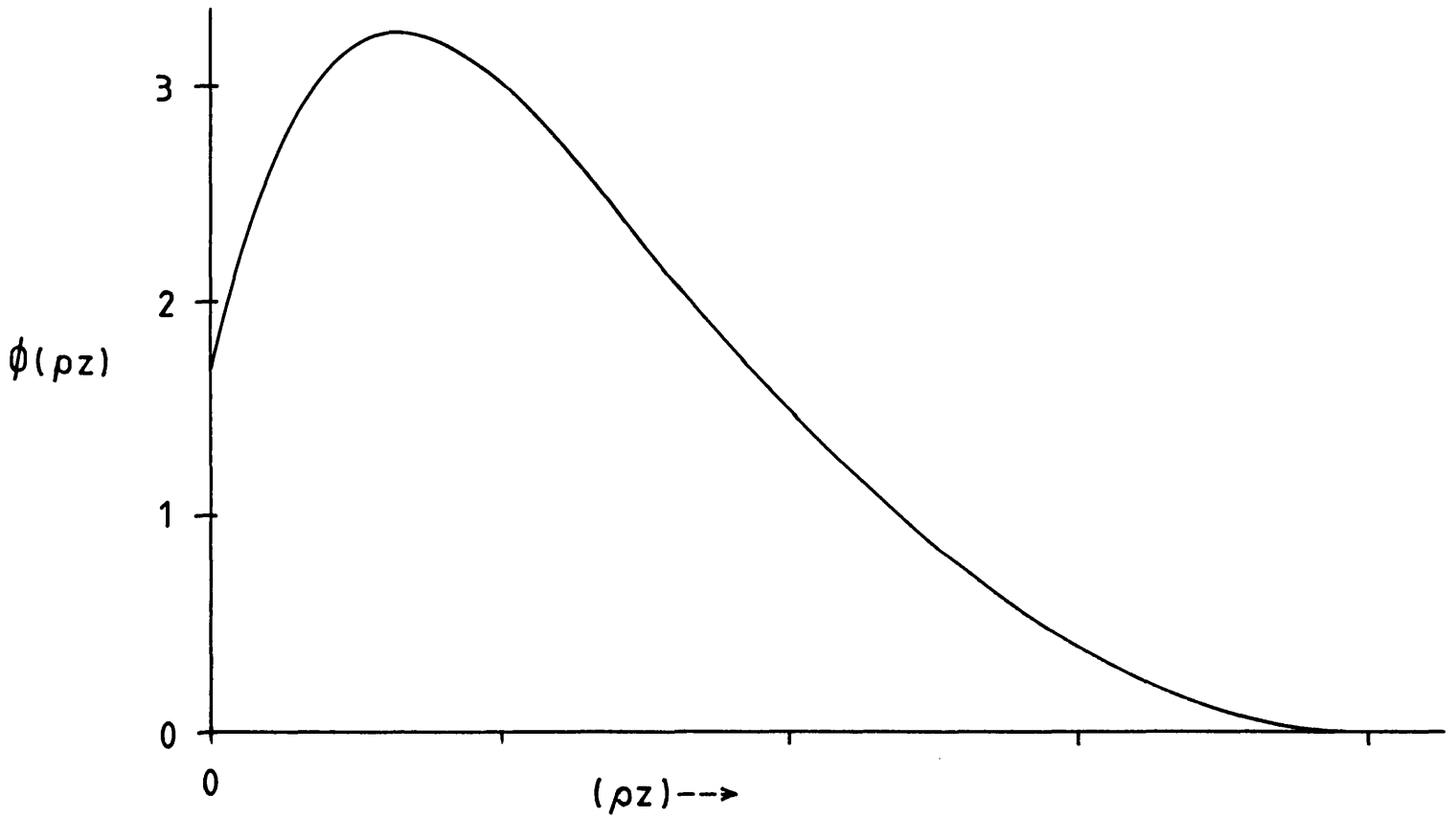

Fig. 1.5 Typical distribution of x-ray generation with mass depth.

With an x-ray take off angle of θ the path length in the specimen for x-rays generated at depth ρz is $\rho z.\text{cosec}\ \theta$. Thus the emitted intensity I_{eA} is given by

$$I_{eA} = \phi(\Delta\rho z) \int_0^\infty \phi(\rho z).\exp(-\chi\rho z)\ \delta\rho z$$

where $\chi = \frac{\mu}{\rho}.\text{cosec}\ \theta.$

If a term describing the effect of absorption, $f(\chi)$, is defined as I_{eA}/I_{gA} then,

$$I_{eA} = I_{gA}.f(\chi)$$

Within the specimen, photons of higher energy may cause generation of additional characteristic x-rays by fluorescence. If the fractional contributions to the line of interest, from fluorescence by continuum and characteristic x-rays are represented by γ and ε then the emitted intensity becomes,

$$I_{eA} = I_{gA}.f(\chi).(1+\gamma+\varepsilon)$$

Finally, taking the ratio of intensities from specimen and pure standard and inserting I_{gA} in full we obtain,

$$\frac{I_{eA}}{I_{eA}^S} = \frac{\phi(\Delta\rho z) \int_0^\infty \phi(\rho z).\delta\rho z\ f(\chi)\ (1+\gamma+\varepsilon)}{\phi(\Delta\rho z)^S \left(\int_0^\infty \phi(\rho z).\delta\rho z\right)^S f(\chi)^S(1+\gamma+\varepsilon)^S} \qquad (1.3)$$

The ratio of intensities from isolated thin films is in fact equal to the concentration C_A, of 'A' in the specimen, so equation 1.3 can be re-written in the form of equation 1.2,

$$I_{eA}/I^{S}_{eA} = C_A.Z.A.F$$

where $C_A = \dfrac{\phi(\Delta\rho z)}{\phi(\Delta\rho z)^S}$ $\qquad$ $Z = \dfrac{\int_0^\infty \phi(\rho z)\delta\rho z}{\left(\int_0^\infty \phi(\rho z)\delta\rho z\right)^S}$

$$A = \frac{f(\chi)}{f(\chi)^S} \qquad \text{and} \qquad F = \frac{(1+\gamma+\varepsilon)}{(1+\gamma+\varepsilon)^S}$$

The factor Z is termed the atomic number correction and accounts for differences in the integrated size of the $\phi(\rho z)$ curves for specimen and standard. The differences arise for the following reasons. The probability of an incident electron causing ionisation of a specimen atom is given by the atom's 'cross section' for ionisation which depends upon the energy of the electron. So the change in the electron's energy along it's path is fundamental in determining the $\phi(\rho z)$ curve. The electron energy loss, or 'retardation' is a function of the mean atomic number of the specimen, and it's effect on x-ray generation is known as the 'stopping power' factor, (S).

A further change in the $\phi(\rho z)$ curve is attributed to loss of incident electrons due to backscattering. This

again depends upon atomic number, and a corresponding correction factor (R) is required, so the overall atomic number correction is given by

$$Z = R/S$$

The factor A is termed the absorption correction and accounts for the differing effects of x-ray absorption in specimen and standard. It is necessary because the absorption coefficient for the characteristic line will not generally be the same in specimen and standard; and also, because there will be differences in the distribution of path lengths for emerging x-rays, which depend upon the $\phi(\rho z)$ depth distributions.

The factor F accounts for differing effects of fluorescence in specimen and standard. As described in section 1.2 x-rays generated by the electron beam can themselves generate characteristic lines and so enhance the emitted intensity. The F factor reflects the efficiency with which the line of interest can be fluoresced, by continuum and other x-ray lines, and the number of such x-rays present in the specimen.

Calculation and application of ZAF corrections

The importance of correction factors in quantitative EPMA has led to much work being carried out to determine the best ways of calculating them. Many of the proposed methods, and their ranges of application have been

comprehensively reviewed, for example by Beaman and Isasi (1970) and more recently by Love and Scott (1981).

The magnitude of the correction factors is generally between 0.8 and 1.0 for most common EPMA specimens, and a relative accuracy of 1 or 2% can be expected in the calculated weight concentrations. When one or more of the corrections becomes large, for example when analysing a light element in a heavy matrix with large absorption effects, the results become more susceptible to errors and typical accuracies are 5 to 10%.

The value of each correction factor depends, naturally, upon the composition of the specimen concerned. So corrections have to be calculated from an estimated composition and used to provide an improved estimate from the x-ray intensity measurements. This is repeated interatively until a near constant result is obtained and accepted as the best estimate of composition.

Corrections for light element analysis

The widely adopted ZAF correction methods were developed mainly for analysis of elements with atomic number above ~13 and are not well suited for use with light elements. The absorption correction for example becomes much larger for soft x-rays and consequently, errors in it's calculation have a more pronounced effect on the accuracy of the result. The problems are compounded by lack of experimental data involving soft

x-rays, such as absorption coefficients at low energies. Special attention has been given to this subject (Scott 1974, Love 1975) to obtain more appropriate experimental data and develop alternative models. The work has led to improved accuracy in ZAF correction, and procedures which are more suitable for use with soft x-rays, (Love and Scott 1978).

1.3.2 X-Ray Line Intensity Measurements

The basis of all quantitative work is measurement of the ratio of characteristic x-ray intensities from the specimen concerned and a standard of known composition. When making this measurement two important experimental considerations are preparation of specimens and stability of the instrumentation. Firstly, the emitted intensities can vary significantly on specimens with irregular surfaces so mounting and polishing must be carried out with care, (see for example Reed 1975a : 175). A conductive coating is often required to prevent specimen charging and various elements such as gold, carbon, aluminium and copper can be evaporated or sputtered onto the specimen. The coating should ideally be applied to both specimen and standard at the same time, to produce equal thickness and minimise any effect on intensity ratios. Secondly the intensity measurements on specimen and standard must be carried out under, as near as possible, identical conditions. It is therefore important that the electron beam current does

not alter significantly during the analysis and that the beam does not drift across the specimen surface.

The intensity measurements are made by accumulating counts for a measured analysis time, and the statistical confidence in the result is governed by the number of counts acquired. This is because the x-ray intensity varies with a Poisson distribution about it's mean value and the standard deviation in I counts is approximately $\sqrt{I}$. It is general practice to collect more than 10,000 counts for a particular line so the standard deviation is less than 1%.

Peak measurements in WDS

The WDS system detects one particular wavelength interval at a time, so for maximum counting efficiency the spectrometer is set at the centre of the peak; position P in figure 1.6. Background, due to x-ray continuum or stray x-rays reaching the detector, is always present but is generally low compared with characteristic peaks. So the background level beneath the peak can be estimated by taking the mean of intensities either side, at points B1 and B2 in figure 1.6.

The presence of high order diffractions in WD spectra was discussed in section 1.2.1. If these peaks lie close to the line of interest they can hinder measurement of background levels beside a peak, or in the worst case

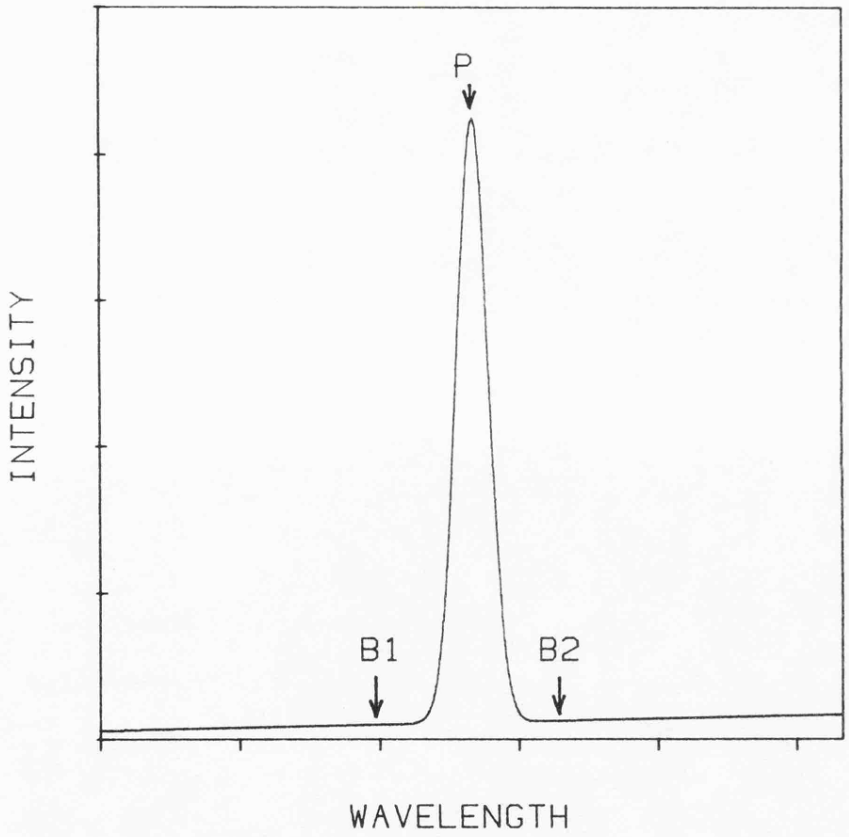

Fig. 1.6 Measurement of WD peak intensity at P; estimating background level as the average of intensities at B1 and B2.

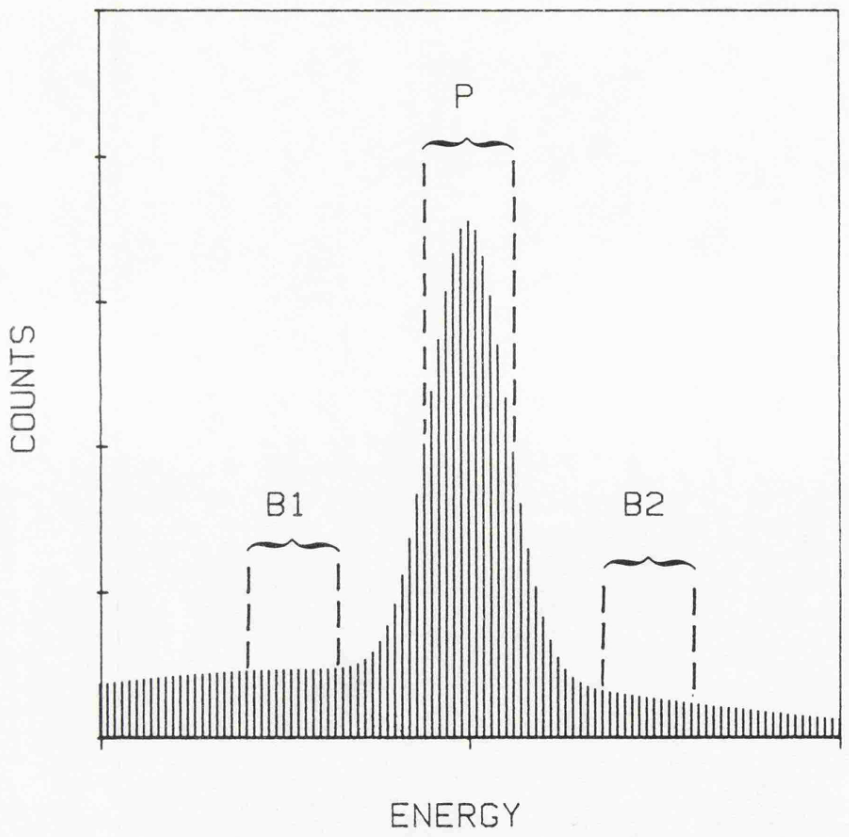

Fig. 1.7 Measurement of ED peak intensity by integration at P; estimating background level as the average of integrated counts at B1 and B2.

interfere with the peak itself. Pulse height analysis can generally be used to discriminate against these higher energy x-rays; although some loss of intensity in the measured line may have to be tolerated due to the limited energy resolution of the gas proportional counter.

Peak measurements in EDS

The energy dispersive system accumulates x-rays simultaneously, sorts them according to energy and presents the spectrum as a histogram of counts per energy interval, or 'channel', versus energy. Furthermore, characteristic peaks are spread over several energy channels, and maximum counting efficiency is achieved by integrating a number of channels near the centre of the peak, as indicated in figure 1.7. The optimum integration width is close to the FWHM of the peak (Reed 1975a:304), since a broader range will include excessive contributions from background. Allowance for the background can be made by integrating equal sized regions either side of the peak and taking the mean. This technique, known as linear interpolation, is generally adequate for single isolated peaks but is unsuitable when the background is markedly curved or when adjacent peaks conceal the level beside a peak of intest.

The broad peaks and low peak-to-background ratios in ED

spectra mean that difficulty in estimating background levels and measuring peak intensities is a general feature of ED spectra. More advanced methods for measuring peak intensities will be discussed in section 2, where the operation of ED systems and spectrum processing techniques are described in detail.

2. ENERGY DISPERSIVE X-RAY ANALYSIS

2.1 Principles of Energy Dispersive Systems

2.1.1 The Solid-State Detector

The operation of a solid-state detector is analogous to that of a gas counter, both having a high resistivity medium across which a large electric field is applied. An incident x-ray is absorbed by the photoelectric effect producing one or more high energy electrons which dissipate their energy by further ionisation of the detector medium. The charged products of ionisation are accelerated rapidly by the field and produce a pulsed charge output at the electrodes.

Ionisation in the solid-state detector corresponds to excitation of electrons across the energy gap, 1.1 eV for silicon and 0.8 eV for germanium. Allowing for other energy loss processes the average energies required per ionisation are about 3.6 eV (silicon) and 2.9 eV (germanium), both low compared with the equivalent value (25 to 30 eV) for gas counters. The number of ionisation produced by a given x-ray are therefore much higher in solid-state detectors, the effects of ionisation statistics are reduced and the theoretical energy resolution is correspondingly improved.

The use of solid-state detectors however, presents

several practical problems. The semiconductor material must have high resistivity so that leakage currents, and hence noise, are minimised. Also the concentration of trapping or recombination centres must be low to ensure that free charges survive long enough to reach the electrodes. These requirements have limited detector material to silicon and germanium which is produced in high purity for the electronics industry. Even these contain residual impurities, such as boron in silicon, and an important step in the development of solid-state detectors was the technique demonstrated by Pell, (1960). He showed that lithium ions could be diffused into a semiconductor and 'drifted' in an electric field to provide a distribution which exactly compensated for impurities. This has since been adopted as a standard technique in the manufacture of solid-state x-ray detectors.

Another problem is related to the detector output signal. In a gas counter a 10 keV x-ray will produce in the region of 400 ion pairs; but as these are accelerated towards the electrodes, collisions with other atoms cause an avalanche effect. This provides enormous amplification (about 10,000 times) and gives a high signal-to-noise ratio in the output. In the solid-state detector on the other hand, there is no avalanche effect and although a 10 keV x-ray produces about 3000 electron-hole pairs this corresponds to an output signal of only about 5×10^{-16} coulombs. Amplifier systems with extremely

high gain and low noise are needed to deal with such small signals and these were developed in the late 1960's and early 1970's, (Elad 1971). This led to improvements in the resolution of ED systems from about 600 eV to the value of 160 eV FWHM at 6keV more typical of modern systems.

2.1.2 The Lithium Drifted Silicon Detector

The use of both silicon and germanium as detector materials has been thoroughly investigated (Aitken and Woo 1971, Barbi and Lister 1981). The fact that a given x-ray would produce more ionisations in germanium than in silicon means that better energy resolution would be expected with germanium detectors. This advantage however, is often countered by other material characteristics. In particular peaks in the region of 3 keV appear with significant low energy tails due to incomplete charge collection when x-rays are absorbed close to the germanium surface. This effect also occurs with silicon detectors (see section on peak shape) but to a much lesser extent. The expected benefits of germanium detectors are not obtained until x-rays of energy greater than 30 keV are analysed. Thus silicon has become the most commonly used detector material in ED systems today.

Figure 2.1 illustrates a typical lithium drifted silicon, or Si(Li), x-ray detector. The silicon crystal is

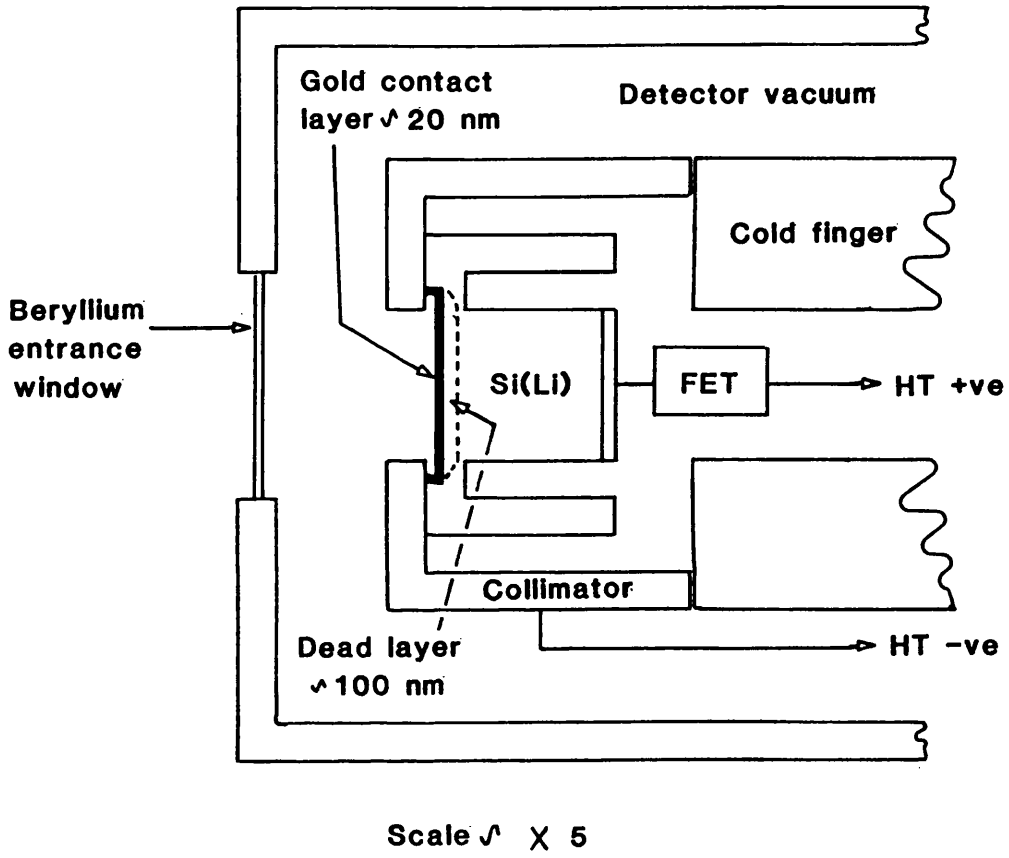

Fig.2.1 Cross section of typical Si(Li) x-ray detector.

approximately 8 mm in diameter and 5 mm thick. The front surface is coated with about 20 nm of gold so that a high electric field can be applied along it's axis, and an aperture limits the sensitive area to 10 mm^2. A field effect transitor, (FET), connected to the rear of the crystal provides the first stage amplification of output signals with minimum interference from noise. The crystal is surrounded by a vacuum enclosure to isolate it from contamination and the detector assembly is mounted on the end of a cold finger so that it can be cooled to the temperature of liquid nitrogen. Operation at cryogenic temperature serves several functions; the FET gives much better signal-to-noise ratio and in the crystal itself migration of the lithium ions and thermal excitation of carriers are minimised.

Beneath the gold contact layer is a region of silicon typically 100 nm thick in which collection of free charges is less efficient than in the bulk material. This region is known as the silicon dead layer (Statham 1981a) and it is likely that trapping or recombination of charge carriers occurs here due to the presence of defects, impurities or surface states. The effect of this layer on ED spectra will be discussed in the section dealing with spectrum characteristics.

X-rays are admitted to the detector by a thin window of typically 8 μm thick beryllium. The transmission characteristics of such a window are shown, for low

energy x-rays in figure 2.2; also indicated are the energies of K emission lines from light elements. It is apparent that soft x-rays from elements with atomic number less than 11 are severely attenuated by the window thus ruling out analysis of the light elements with this type of ED system.

The configuration of an ED system, attached to a microprobe is illustrated in figure 2.3. The largest component of the ED detector is the liquid nitrogen container and the main amplifier is also mounted on the detector unit to minimise interference from noise. The figure shows how the Si(Li) crystal can be positioned close to the specimen giving greater x-ray collection efficiency than with WDS.

2.1.3 Electronic Pulse Processing

Electronic processing of signals from the Si(Li) detector is carried out by a multichannel pulse height analyser, the details of which have been described many times in the literature, (see for example Williams 1971 and Reed 1975a). Most commercial systems use essentially the same techniques although Statham (1981b) describes a pulse processor developed originally by Kandiah which is based on a somewhat different approach.

The operation of conventional systems will be described briefly here. The signal produced when an x-ray is

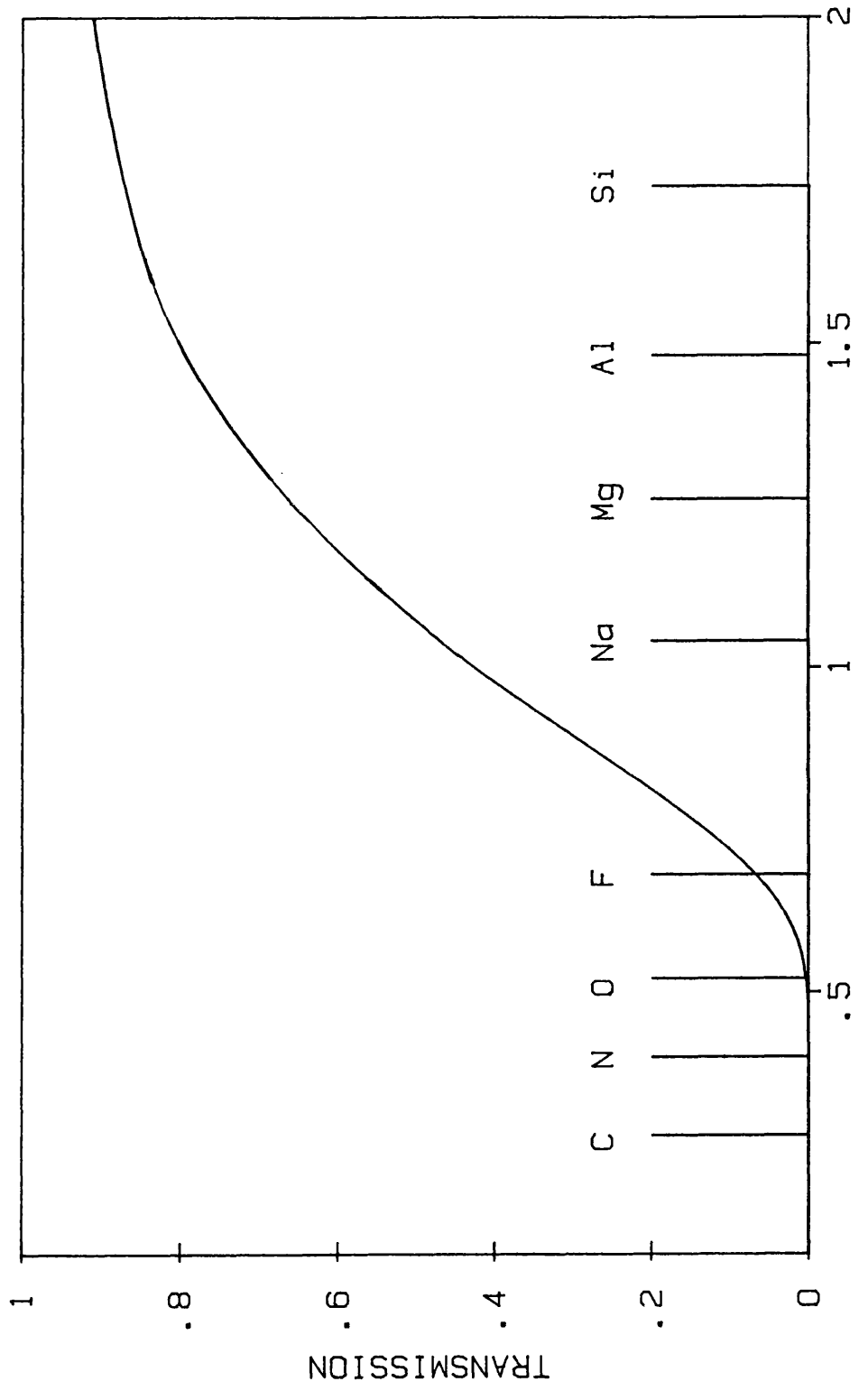

Fig. 2.2 Transmission characteristics of 8 μm beryllium window as a function of incident photon energy: and the K emission lines of light elements.

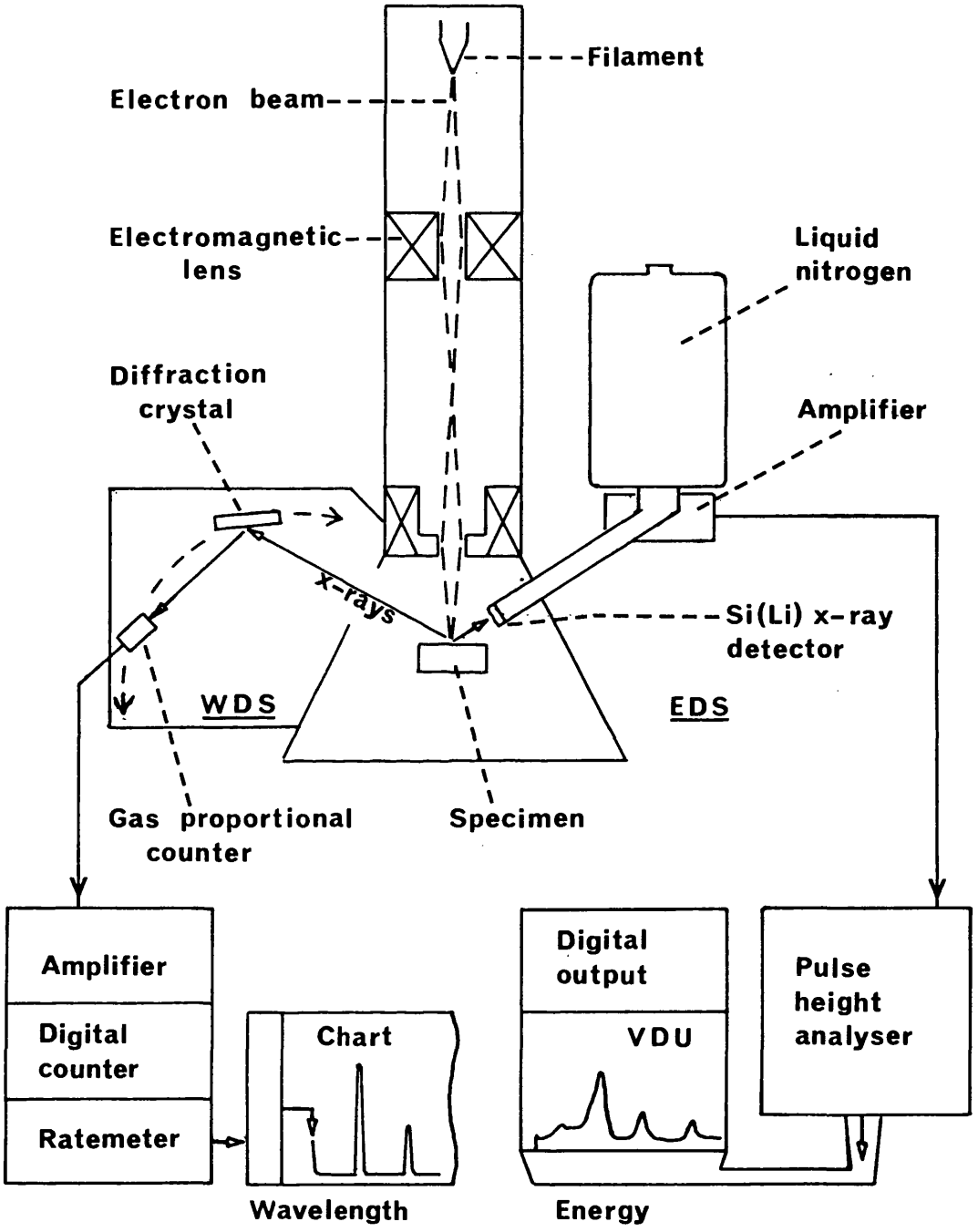

Fig.2.3 Electron probe microanalyser, with wavelength dispersive and energy dispersive x-ray spectrometers.(WDS and EDS)

absorbed in the silicon crystal is amplified in several stages, firstly by the cryogenic FET and subsequently by pre-amplifier and main amplifier. In this process it is shaped into a pulse extending over about 100 μs in duration to minimise the effect of random noise fluctuations. The height of this pulse is then measured by an analogue-to-digital converter. Here a common approach is to charge a capacitor to the peak voltage of the pulse and then discharge it at a constant current. The discharge time, which is measured digitally, is proportional to the pulse height and hence to the original x-ray energy; it therefore identifies the appropriate energy channel for that count. The number of counts recorded in that channel is simply incremented by one to add the new count to the spectrum.

The energy dispersive spectrum thus produced is in the form of a histogram, showing the number of x-rays detected in narrow energy bands, or channels, usually 10 or 20 eV wide. The characteristic lines appear as peaks spread over several channels and superimposed on a background of x-ray continuum. A typical ED spectrum from copper, obtained with a 15 kV probe, is shown in figure 2.4. The copper Kα emission line appears at 8.04 keV, the Kβ at 8.8 keV and the Lα line is at 0.93 keV.

2.2. Characteristics of Energy Dispersive Spectra

2.2.1 Energy Resolution

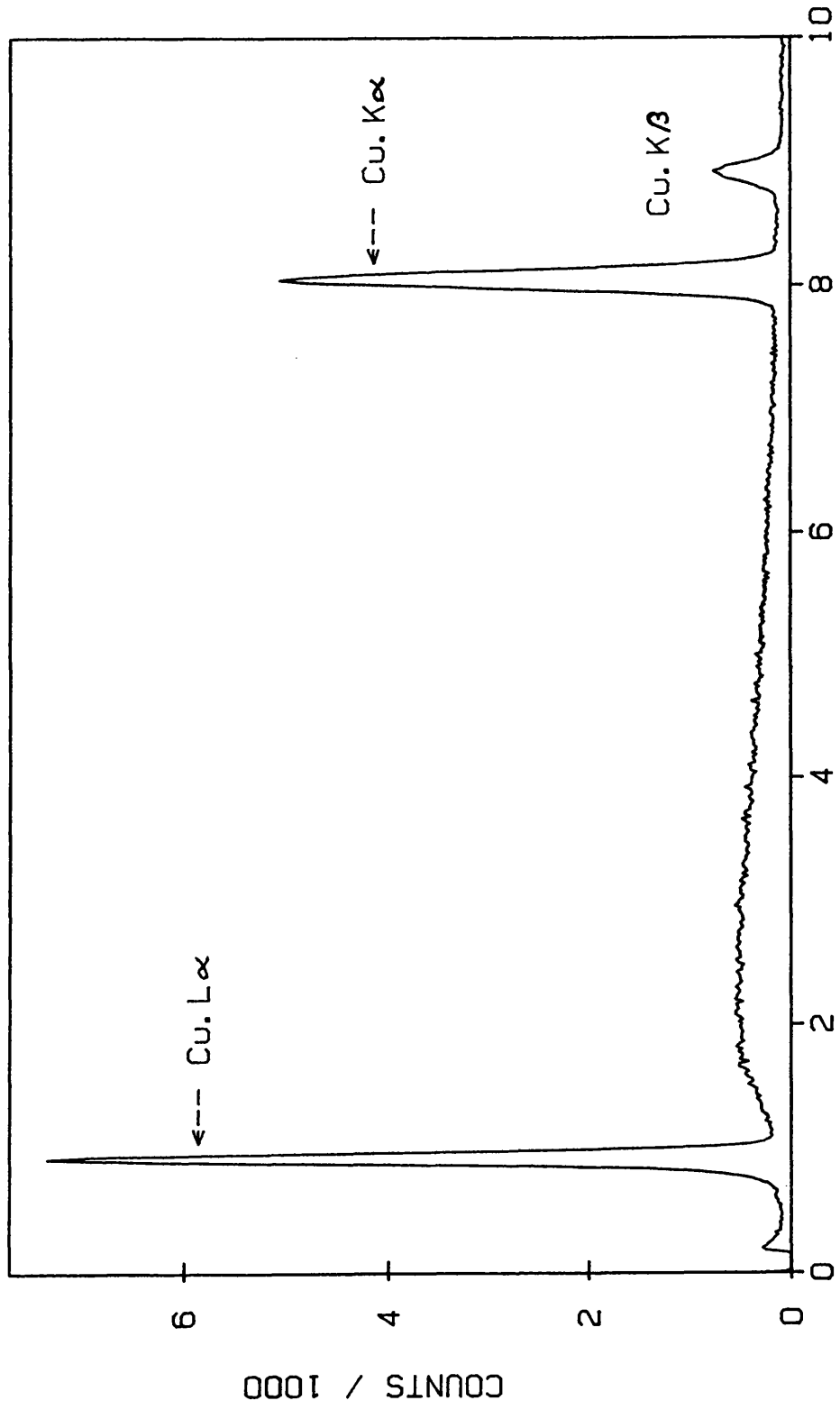

Fig.2.4 Energy dispersive spectrum obtained from pure copper with 15 kV probe.

The width of characteristic x-ray peaks, measured as the full width at half maximum height (FWHM), determines the ability of the spectrometer to resolve neighbouring lines. In EDS the resolution is given as the FWHM of the manganese Kα line at 5.89 keV (conveniently produced by iron-55 radioactive sources) and is typically in the region of 150 eV in modern systems. Two factors which determine this resolution will now be considered.. Firstly the number of ionisations produced in the detector medium by an incident x-ray of energy E has a statistical distribution with standard deviation σ given by

$$\sigma = \sqrt{FE/e}$$

where e is the average energy required per ionisation, and F is a constant called the Fano factor (Fano 1947). This produces a corresponding distribution in the size if the detector output signal. The energy measurement therefore has a standard deviation due to ionisation statistics (σ_S) given by,

$$\sigma_S = \sigma.e = \sqrt{eFE}$$

In the case of silicon e is 3.8 eV per ionisation and the Fano factor F is found to be about 0.12,

$$\text{thus} \qquad \sigma_S = 0.675\sqrt{E} \qquad (2.1)$$

Secondly, the signals from the detector pass through

several amplification stages and are inevitably affected by random fluctuations due to electronic noise. This leads to further statistical variations in measured x-ray energy, and the standard deviation is denoted by σ_N.

The actual standard deviation in measured x-ray energy, (σ), is obtained by adding the effects of ionisation statistics and noise in quadrature, giving

$$\sigma^2 = \sigma_N^2 + \sigma_S^2 \qquad (2.2)$$

The result is that a characteristic x-ray line appears in the ED spectrum as a 'normal' or Gaussian distribution centred on the true energy. The FWHM of this distribution ΔE is equal to 2.355 σ, so from equation 2.2,

$$\Delta E^2 = (2.355\ \sigma_N)^2 + (2.355\ \sigma_S)^2$$

Representing the noise term by ΔE_N and inserting σ_S from equation 2.1 we have,

$$\Delta E^2 = \Delta E_N^2 + 2.53\ E$$

For a typical ED system $\Delta E_N \simeq 100$ eV, so $\Delta E \simeq 160$ eV when E=6keV

2.2.2 Peak Shape

Although characteristic peaks conform well with the expected Gaussian distribution of counts, slight asymmetry

can be produced by an effect in the Si(Li) detector. A proportion of x-rays incident upon the detector are absorbed in the silicon dead layer (discussed earlier in this section) where charge collection efficiency is lower than in the rest of the detector. These x-rays appear in the spectrum at energies below their true value so forming a tail on the low energy side of a peak as illustrated in figure 2.5.

The tailing effect is more pronounced with x-rays having a high absorption coefficient in silicon since a greater proportion of these are likely to be absorbed in the dead layer. This is the case for characteristic x-rays from elements such as phosphorus, sulphur and chlorine which have energies just above the silicon absorption edge at 1.84 keV.

2.2.3 Escape Peak

The presence of a small peak, at an energy 1.74 keV below that of a major peak in the ED spectrum, is another effect attributable to the Si(Li) detector. It arises because a silicon x-ray can be produced, within the detector, by fluorescence following the absorption of an incident x-ray. If this silicon x-ray escapes from the detector it takes with it an energy of 1.74 keV. The measured energy of the incident x-ray is therefore 1.74 keV less than the true value and contributes to the artificial peak described above.

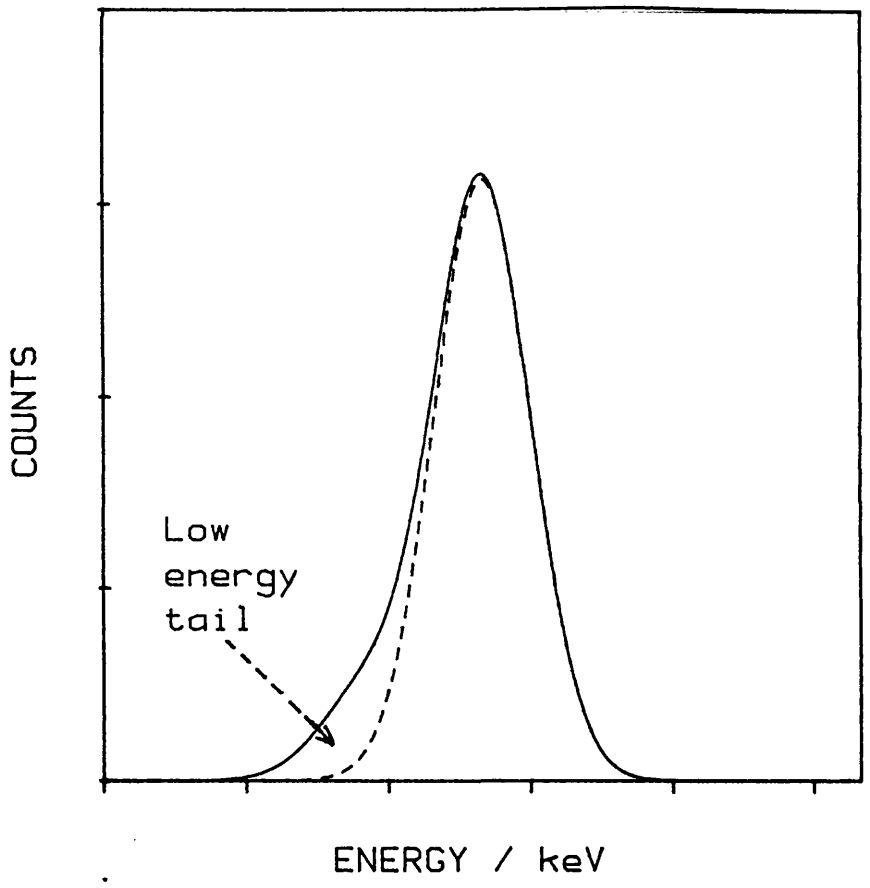

Fig. 2.5 Low energy tail on ED peak resulting from x-rays absorbed in the silicon dead layer: dotted line shows ideal Gaussian peak shape.

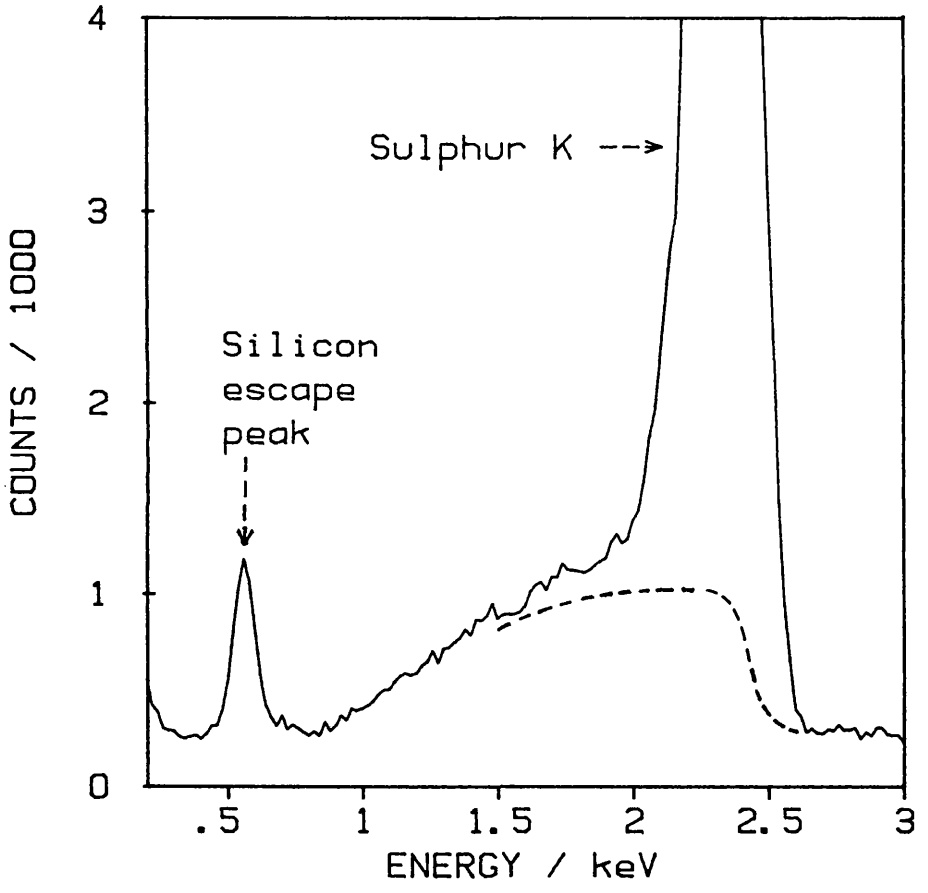

Fig. 2.6 Silicon escape peak in spectrum from pure sulphur; and step in continuum level (dotted line) caused by the sulphur K absorption edge. 15 kV probe.

The escape effect occurs most strongly when the incident x-ray has an energy just above the silicon absorption edge at 1.84 keV and the probability of causing K shell ionisation is greatest. Then, the escape peak is about 2% of the size of the main peak, this value falling to 0.1% for incident x-rays of 10 keV. The escape peak for the sulphur K line is shown in figure 2.6.

If the escape peak caused by one characteristic x-ray line lies close to another line of interest it can cause problems both for peak identification and measurement. Fortunately methods for removing escape peaks from spectra have been developed (Reed and Ware 1972, 1973). An expression is given which allows the fraction of counts suffering the escape effect to be calculated for any energy. Correction is applied to each channel in turn, recovering the appropriate number from the channel 1.74 eV lower in energy. It is necessary to work from high to low energy to ensure that the number of counts in a given channel is free of escape counts from higher energy before its own losses are calculated. This has proved a useful technique and is often included as an optional processing routine in modern ED systems.

2.2.4 Pulse Pile-up

Pulse pile-up can occur if an x-ray arrives at the detector less than about 20 μs after the preceding one

(Reed 1972a). The second signal from the detector is accepted by the main amplifier as part of the first, to produce one pulse of larger amplitude. A single count is then added to the spectrum at an erroneously high energy.

These pile-up counts are eliminated in modern ED systems by the use of an auxilliary 'fast' amplifier which processes signals in parallel with the main amplifier (Williams 1968). The 'fast' amplifier produces pulses of only 1 μs duration, compared with 100 μs for the main amplifier. These 1 μs pulses are monitored by a pile-up detector and if it 'sees' two pulses with less than 20 μs between them it instructs the main amplifier to reject the inevitable pile-up pulse. In this way most of the problems of pile-up are eliminated and erroneous counts do not appear in the spectrum. Only the relatively rare pile-up of pulses with less than 1 μs between them cannot be detected, even by the fast amplifier.

2.2.5 Dead Time

The dead time of a counting system (discussed in detail by Beaman, Isasi, Birnbaum and Lewis 1972, and Reed 1972b) may be defined as the interval following the arrival of a pulse during which the system does not register further pulses. This interval consists of essentially two parts, the first being associated with pulse acceptance or rise

time and the second with system recovery or pulse decay time.

Dead time can be of two types; if the arrival of a second pulse within a dead time interval actually increases the dead time it is called 'extendable'; if the interval is of fixed length the dead time is termed 'non extendable'. In ED systems, dead time is usually 'extendable' and is equal to about 100 μs per pulse, this being the duration of pulses in the main amplifier (discussed in section 2.1.3).

Figure 2.7 shows the effect this has on the rate of accumulation of counts. The horizontal axis represents the x-ray intensity incident upon the detector and is called the 'input' count rate; the vertical axis gives the actual rate at which counts are added to the spectrum, called the 'recording' rate. The dotted line shows ideal behaviour but, in practice, dead time causes a reduction in the recording rate and the system response falls below this line. The effect of extendable dead time in an ED system is illustrated by the solid curve which indicates that at a certain input rate (about 10,000 s^{-1} in this case) the system begins to saturate and to reach it's maximum recording rate. Higher input rates simply increase the overall dead time and actually reduce the recording rate.

Most ED systems compensate for dead time by incorporating

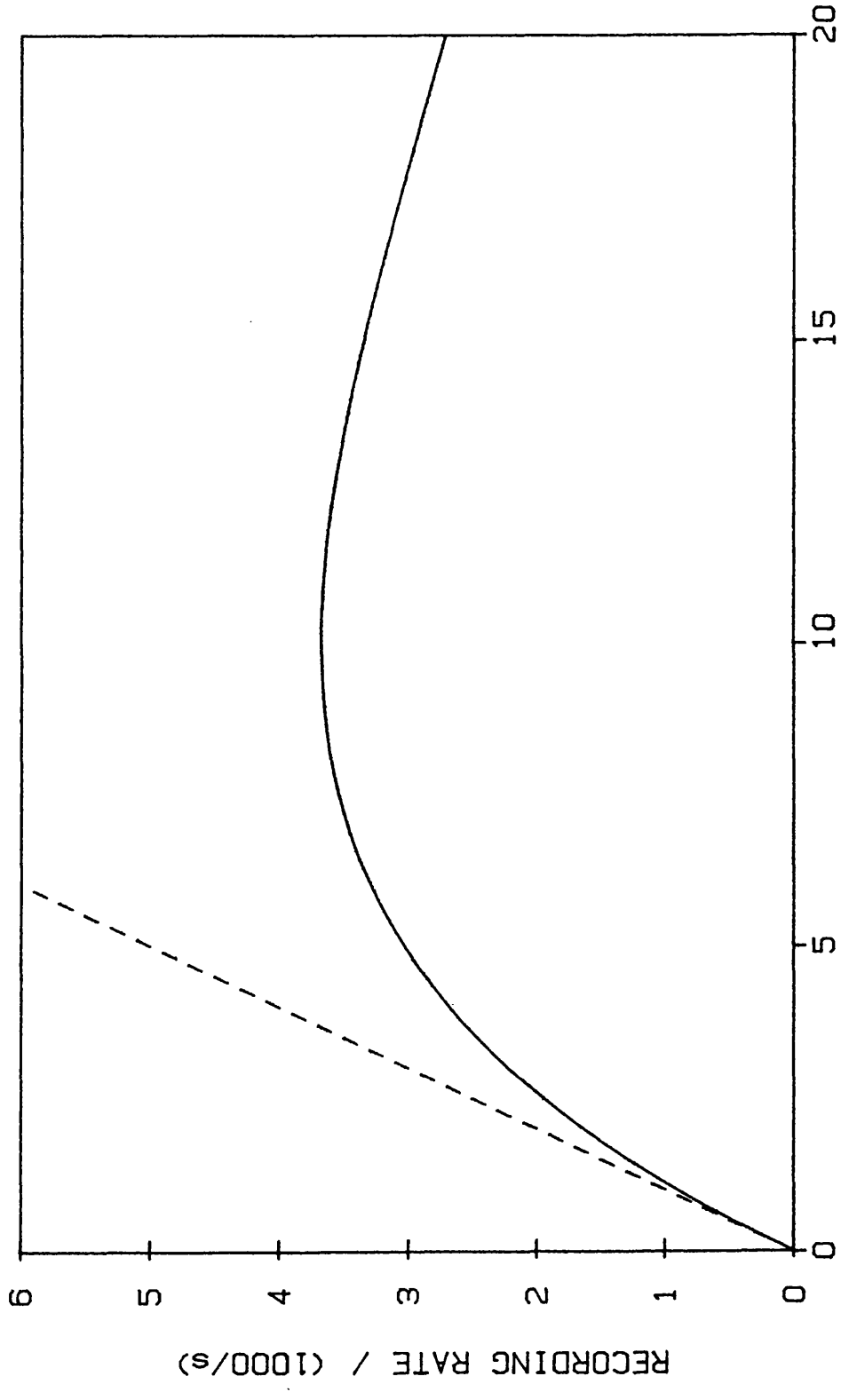

Fig. 2.7 Effect of extendable dead time of 100 us per pulse on recording rate.

a 'live time' clock which is controlled automatically by the electronics. The clock records actual analysis time exclusive of dead time and so appears to run slowly compared with real time.

2.3. Spectrum Processing

Quantitative electron probe microanalysis is based essentially upon comparing intensities of characteristic x-ray emission from specimen and standard under identical beam conditions. Intensity measurements are somewhat difficult to make on ED spectra because the relatively poor energy resolution of the technique broadens the x-ray peaks and leads to fairly low peak-to-background ratios. Hence the x-ray peaks often require deconvoluting one from another and accurate background prediction is essential.

2.3.1 Linear Interpolation of Background

In section 1.3.2 a simple approach was described for obtaining characteristic x-ray line intensities from energy dispersive spectra. The technique was basically an adaptation of the method used in WDS. One measurement is made on the peak, and the background intensity is estimated by linear interpolation of the levels either side of the peak.

Unfortunately in EDS peaks are much wider (about 160 eV

FWHM at 6 keV compared with 15 eV in WDS), and the interpolation must be made over a broad energy range of about 500 eV. Furthermore, the background in this region is not generally linear but contains an 'absorption step' as illustrated in figure 2.6 where the dotted line shows the probable level of continuum beneath the sulphur K peak. The step is due to a change in absorption coefficient for x-rays within the specimen and occurs at the critical excitation energy of the sulphur K shell. It can be seen that a linear interpolation is unlikely to give the correct background level.

A low energy tail is present on some peaks, due to incomplete charge collection in the detector (section 2.2.2), and can make measurement of the background beside the peak difficult. In some cases the background is obscured by a neighbouring peak as illustrated in figure 2.8. This is a relatively simple example in which the titanium Kβ peak reduces the accuracy in estimation of the background level on the high energy side of the Kα peak. When additional elements are present the problem can be much worse.

Because of the reasons given above, linear interpolation is generally limited to cases where characteristic peaks are situated well clear of any neighbours, and where the peak-to-background ratio is high. Then errors in the estimated background level are minimised and are small compared with the size of the peak.

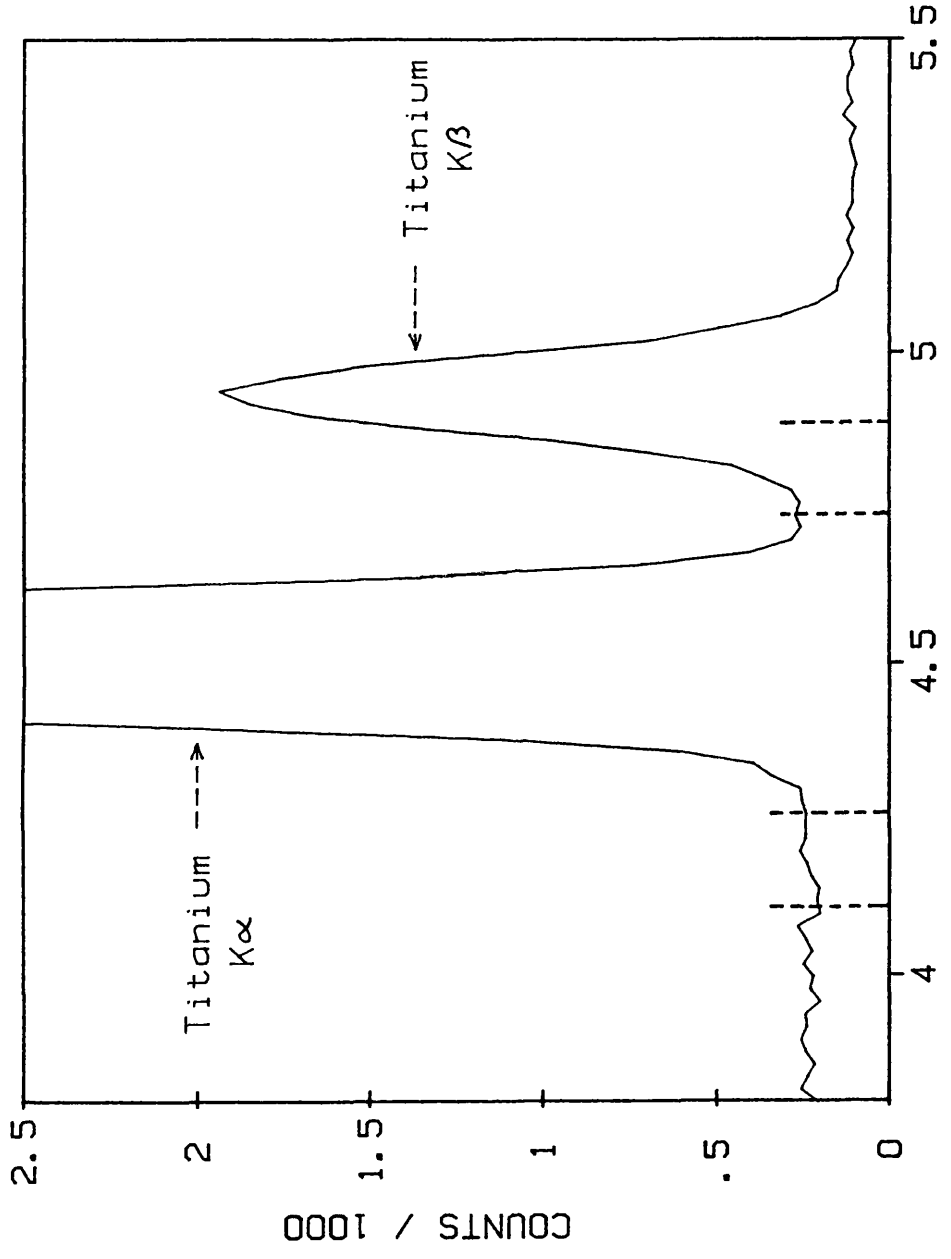

Fig.2.8 ED spectrum from pure titanium; the Kβ peak obscures one background integration region for the Kα peak. 15 kV probe.

The adoption of more advanced techniques for peak measurement in EDS depends very much on the availability of computers to carry out mathematical operations on the recorded spectra. However, with the development of compact, powerful computers it has become standard practice to incorporate a dedicated 'mini' or 'micro' computer in ED systems. These can be used with software supplied by the manufacturer and often may be programmed in high level language by the analyst.

2.3.2 Mathematical Techniques

The energy dispersive x-ray spectrum is stored in the multichannel analyser or computer as a series of integers representing the counts recorded in each energy channel. The techniques referred to here as 'mathematical', are those which treat this spectrum simply as a series of numbers and process or analyse it according to mathematical rules or procedures. Certain assumptions are made about the 'shape' or other properties of the spectrum but no physical theories relating to x-ray intensities or detector performance are incorporated. Such methods are very flexible and are capable of processing most types of spectra. Consequently some of the earliest work carried out on ED spectra was performed using mathematical routines developed originally for related techniques such as gamma-ray spectrography. This included for example, computer algorithms to locate peaks (Mariscotti 1967, Connelly and Black 1970), and in some cases could deal

with overlap, (Brouwer and Jansen 1973).

Filtering

A variety of techniques have been developed under the general name of 'filtering'. The principle on which they are based can be understood most easily by referring to filtering carried out using the fourier transform (Cochran et al 1967). In this instance, the energy axis of a spectrum is treated as a time scale so that the spectrum itself appears to be a 'waveform'. The fourier transform is then applied to calculate the 'frequency' components of this waveform. The resulting frequency spectrum can be modified in different ways, to amplify or attenuate certain frequencies for example, and this is described as 'frequency filtering' or simply 'filtering'. By applying the reverse fourier transform, the filtered data can be restored to its original form, ie. with a 'time' (or in our case 'energy') axis.

However, the results obtained by 'fourier filtering' can also be achieved in another way. When this alternative procedure, known as 'convolution', is applied to a spectrum the value in each energy channel is replaced by a weighted sum of neighbouring channels. The actual 'weighting' values used represent the 'convolution function'.

In general the two technques described above are

equivalent and produce the same result when the 'convolution function' is equal to the fourier transform of the 'frequency filter'. For this reason some methods of spectrum processing which are actually carried out by convolution are often termed 'filtering' techniques, although the effective filter function is not explicitly identified.

Resolution enhancement

In principle, filtering or convolution with the appropriate function could be used to reverse the statistical spreading of peaks in a recorded ED spectrum. This would enhance the energy resolution, improve peak-to-background ratios and separate overlapping peaks.

The above technique was attempted (Inouye, Harper and Rasmussen 1969, Colby 1972) using a fourier filter, and improvements in resolution were claimed. It appears however that the use of this type of 'filter' leads to distortion of the spectrum, producing small spurious peaks beside the major peaks. This is obviously undesirable because it could cause errors in identification or measurement of peaks. Ryder (1981) has discussed this approach and identifies the random variations due to counting statistics as the factor which limits the use of filters for resolution enhancement.

Top hat filters

Another type of filtering which has been commonly used is termed 'top hat' filtering (Statham 1977, McCarthy and Schamber 1981). It provides an approximate separation of the 'highly curved' peaks from the relatively flat background. In this process the ED spectrum is greatly distorted but by applying the same filter to spectra from standards reliable specimen-to-standard peak intensity ratios can still be obtained.

The filtering is carried out by use of convolution rather than fourier transformation and it is the convolution function which has the characteristic 'top hat' shape giving the technique its name. The actual 'filter' which is being invoked by this convolution is not generally considered and factors such as the 'width' of the top hat have been developed empirically. Robertson et al (1972) however, discussed the filtering effect in more detail to deduce the optimum form of the convolution function.

2.3.3 Continuum Prediction

As an alternative to mathematical filtering of ED spectra the background may be removed by predicting it's shape. This can be achieved by use of the physical principles of x-ray emission and experimental data from actual spectra.

Explicit calculation

Ware and Reed (1973) have developed an expression which can be used to calculate the intensity of continuum radiation from any specimen. It is assumed that the intensity actually generated within the specimen is given by Kramers (1923) law (section 1.1.2) and is thus calculated for the energy of each channel in the spectrum. The generated intensity must then be modified to allow for absorption of continuum by the specimen itself. For this purpose Ware and Reed chose the Philibert (1963) absorption correction method. Further attenuation occurs when the x-rays pass through the ED detector window, gold contact and silicon dead layer, so another correction factor is required to predict the magnitude of this effect. Finally, because the agreement between predicted and experimental continuum shape was not adequate, Ware and Reed incorporated an empirical energy term which could be used to improve the agreement.

The continuum is calculated channel-by-channel over the required energy range, scaled to match the recorded spectrum and finally subtracted to leave the characteristic peaks.

Several modifications to this technique have been proposed, for example by Rao-Sahib and Wittry (1974), Fiori et al (1976) and Statham (1976). The main problems appear to be that Kramers' expression is not sufficiently

accurate and that the most readily available corrections for x-ray absorption and electron backscattering apply to characteristic rather than continuum x-rays. Even so, calculated continuum shapes have been shown to correspond well with the background in ED spectra, although agreement below 2 or 3 keV is usually poor.

Prediction from reference standard

A novel approach to continuum prediction has been proposed by Smith, Gold and Tomlinson (1975). A continuum spectrum from a reference standard is first obtained and corrected channel by channel for all specimen dependent effects; this is analogous to the atomic number and absorption corrections used in the conventional ZAF approach for characteristic radiation. The resulting spectrum represents the continuum, from a hypothetical specimen of atomic number one producing no electron backscattering or x-ray absorption, as recorded by the ED detector (ie. the 'true' emitted distribution modified by the spectrometer efficiency). Smith termed this the 'normalised background'. The continuum intensity for the sample of interest is then determined by carrying out the same procedure in reverse; on this occasion modifying the normalised background by applying atomic number and absorption corrections relevant to the sample.

An advantage of the reference standard method over that of Ware and Reed is that the detector effiency need not

be known as it is constant for specimen and standard.

Both of the above techniques are superior to the filter approach in that they provide realistic absorption edges beneath characteristic peaks. A disadvantage however, is that prediction of background requires a knowledge of specimen composition. This must first be estimated, then refined using an iterative procedure.

2.3.4 Peak Overlap

One approach to the problem of overlapping peaks is to use overlap factors. These represent the fraction of integrated peak intensity from one element which appears in the region over which the neighbouring peak is integrated. For example in figure 2.9 the factor describing the overlap of peak A into the integration region of B (denoted ab) is given by Y/X. These factors can be obtained experimentally (Smith and Gold 1976), or theoretically using Gaussian models to represent the peaks, (Myklebust, Fiori and Heinrich 1981). The true peak intensities (A and B) can be found from the uncorrected measurements (S_1 and S_2) by an iterative procedure, or by solving simultaneous equations of the form,

$$A + B.ba = S_1$$
$$A.ab + B = S_2$$

A second approach is the least squares fitting technique,

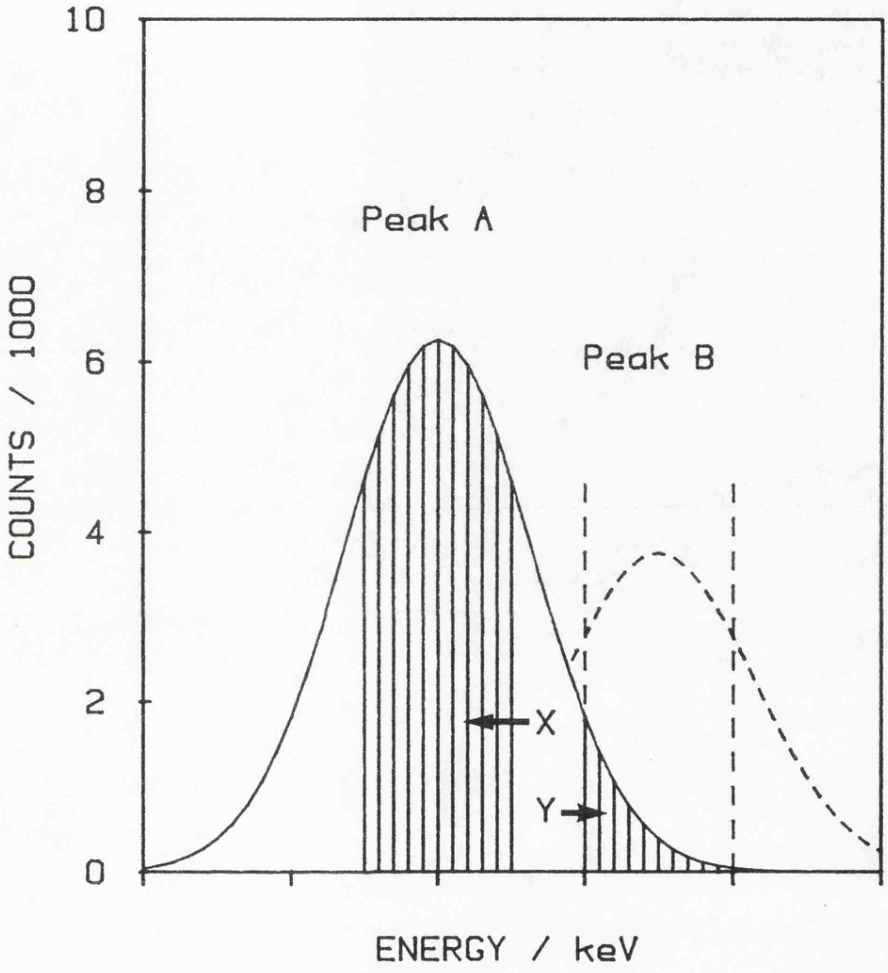

Fig.2.9 Schematic diagram showing the integration region (X) of peak A and the overlap (Y) of A into the integration region of peak B.

in which mathematically generated Gaussian peaks or actual x-ray lines recorded from standards are used to represent the peaks in the overlap. These individual peaks can be added together in an attempt to duplicate the overlap, and when the relative sizes are correct the sum will match the recorded spectrum. The least squares technique allows the required size of each peak to be calculated directly to give an optimum fit to the overlap spectrum. The criterion for the best fit is based on minimisation of the sum of the squared deviations, (Schamber 1981).

When a filtering technique is used to supress background the spectrum can be greatly distorted. Nevertheless providing the same filter is applied to all peaks then the least squares approach can still be used to match filtered peaks to the filtered spectrum, (Statham 1977).

3. LIGHT ELEMENT ED ANALYSIS

3.1. Developments in Light Element ED Analysis

In the late 1960's energy dispersive spectrometry was developed using Si(Li) detector, but the analysis of soft x-rays was not possible owing to the need for an entrance window on the detector. This window served to protect the silicon crystal from contamination and to absorb stray electrons and light photons which would add unwanted counts to the spectrum. Since the crystal was mounted in a vacuum enclosure the window had to withstand atmospheric pressure when the detector was removed from the microscope chamber.

Beryllium was the most common choice of window material because it has low absorption coefficient and high strength, and does not produce any x-rays that would be seen in the ED spectrum. The window thickness was usually about 25 μm which was sufficient to attenuate completely all x-rays from elements below atomic number eleven, (c.f. figure 2.2).

Even if this window could have been eliminated, there were still difficulties which prevented soft x-ray analysis. ED systems are faced with the problem of measuring extremely small electrical signals from solid-state detectors. Consequently the effects of random fluctuations due to noise in the electronics placed severe limitations on the energy resolution which could be

achieved in early equipment. Typically, the noise levels were equivalent to several hundred eV. It was therefore difficult to resolve adjacent elements in the periodic table below atomic number 20, where the difference in K emission energy falls below about 400 eV, (Calcium Kα at 3.69 keV and potassium Kα at 3.31 keV). In addition the signals generated by x-rays with energy less than 1 keV would be swamped by the random noise fluctuations, so the low energy region of the spectrum could not be analysed.

3.1.1 Experimental Systems

When advances in electronics began to improve the energy resolution of ED systems, analysis of soft x-rays became feasible. Jaklevic and Goulding (1971) attached a modified Si(Li) detector to an x-ray tube in which the target could be irradiated by an electron gun. The detector was fitted with a conventional beryllium window to maintain it's internal vacuum when exposed to the atmosphere. However, whilst inside the x-ray tube the window could be interchanged with a thin aluminium foil which allowed soft x-rays to reach the Si(Li) crystal.

A further refinement allowed them to reduce the number of noise counts in the low energy region, which would otherwise swamp the soft x-ray peaks. They used a pulsing technique to switch the electron gun on and off

rapidly. The signals from the Si(Li) detector were only passed on to the multi-channel analyser when the electron beam was on. This meant that the ED system was actively recording counts only when the probability of an x-ray arriving was a maximum. At other times, when no x-rays were expected, the system was effectively inactive and did not accumulate noise counts.

Using the above technique they were able to record x-ray peaks from oxygen, nitrogen and carbon, demonstrating that ED analysis of light elements was practical.

3.1.2 Commercial Systems

The possibility of removing the beryllium window from a Si(Li) detector inside an electron microscope, to allow light element EPMA with an ED system, was discussed by Russ (1971). He concluded that a cold trap would be needed close to the crystal to minimise condensation of vapours on it's surface. Also a magnetic or electric field would be required to deflect approaching electrons which add unwanted counts to the spectrum if they reach the detector.

Aitken and Woo (1971) suggested that a thin plastic window such as mylar ($C_5H_5O_2$) or formvar ($C_5H_7O_2$) could be used in place of the beryllium window. An aluminium coating, some 10's of nm thick on the plastic would exclude light photons (which add noise to the spectrum)

from luminescent specimens and the window would reduce the circulation of contaminants between the specimen chamber and crystal.

The main practical problem appears to have been the development of a mechanical arrangement for changing the windows inside the electron microscope. In the first commercially available ED systems offering soft x-ray analysis (Barbi et al 1974) the operating mechanism was bulky and it was not possible to place the detector close to the specimen. However the design was later improved (Russ et al 1976) and the system became much easier to use on a routine basis in the electron probe microanalyser.

3.1.3 Processing Soft X-ray Spectra

Techniques for processing ED spectra have been reviewed, for example by Russ (1977a) and Statham (1981c), and were also discussed in section 2.3. Whilst these methods appear to work satisfactorily for ED spectra above 1 or 2 keV, it has been demonstrated (Russ 1977b) that they are not directly applicable to the low energy region. Although difficulties were expected due to the large number of potential overlaps at low energies the main problem was in removing the background beneath the low energy peaks.

Russ (1977b) found that the linear interpolation method

was unsuitable, because the continuum shape is highly curved, and absorption edges are large at low energies, producing a very non-linear background. Filtering techniques could not deal with the noise counts which appear as a Gaussian peak centered at zero energy. The noise peak should be treated as unwanted background but the filter method is unable to distinguish it from a characteristic peak. The direct calculation of background gave the wrong shape below about 2 keV because it could not predict with sufficient precision the effects of absorption which become large at low energies.

When discussing the problem of overlap, Russ suggested that conventional techniques may be adequate for soft x-ray work. Overlap factors could be determined experimentally for low energy peaks, or least squares fitting used with peaks recorded from standards. If mathematically generated peak shapes were to be used they would have to incorporate additional parameters to allow for the low energy tails which appear on soft x-ray peaks. Nevertheless, the accuracy of peak intensity measurement was expected to be poor in the low energy region, because overlap situations would be both common and severe.

In more recent work (Russ 1978, Sandborg and Merkle 1981, Russ and Sandborg 1981), the possibility of quantitative ED analysis of light elements has been considered. The general inadequacy of conventional spectrum processing

techniques has been recognised but little has been done to provide more suitable alternatives.

3.2. The Aims of This Work

The ability to carry out light element analysis with ED systems offers several benefits. One immediate application is in the case of scanning electron microscopes where the addition of an EDS facility is an economical alternative to the electron microprobe for analytical work. Also, in work with beam sensitive materials the high collection efficiency of ED detectors allows use of much lower electron beam intensities with corresponding reduction in specimen damage.

Another feature of ED systems is the ability to present an entire spectrum quickly. This is often useful even where WDS facilities are available, since it allows rapid assessment of specimens, which can then be examined by WDS with prior knowledge of the elements present.

Although quantitative ED measurements are not generally so accurate as in WDS, useful results can often be achieved. The possibility of extending quantitative ED analysis to include light elements has been considered, but a full assessment of the technique is still required. The aim of this work is therefore to establish sensitivity limits for light element ED analysis and to

determine the accuracy with which quantitative measurements can be carried out.

Quantitative work can be divided into two stages; measuring peak intensity ratios and applying ZAF correction factors to determine elemental weight concentrations. The latter stage is common to both WD and ED techniques and is already the subject of other work. Thus the objective here is to study the first stage, of measuring peak intensities, since this is more fundamental to the ED technique itself. Assessment of the accuracy of these measurements will be made by direct comparison with corresponding WDS intensity ratios, thus avoiding the problem of matrix corrections for soft x-rays.

The emphasis will be placed on studying the ED spectrum below 1 keV, to identify the problems experienced with conventional processing techniques. Where necessary existing methods will be adapted or new methods developed, to provide an accurate means of measuring soft x-ray peak intensities.

3.3 The Equipment Used

Most of the work has been carried out on an EDAX 711 analyser with an ECON x-ray detector. This detector has three interchangeable window positions; two of which allow use of a conventional 8 μm beryllium window and an open

aperture, whilst the third supports a window prepared by the analyst. In the soft x-ray studies carried out here an aluminised formvar window has been used for reasons discussed in section 3.1.2. The windows were prepared by first dipping glass slides in a solution of 2% formvar in 1.2 dichloro-ethane. The slides were then exposed to air, allowing the solvent to evaporate and leaving thin films of formvar on the glass surfaces. These films were 'floated' off in water and transferred to the ECON window holder. Window thickness was not measured, but owing to their fragility a compromise was necessary between minimum thickness to allow transmission of soft x-rays and adequate strength for a useful life (several months) before breakage. A double layer window, consisting of two films produced as described above was found suitable. The aluminium coating of about 15 nm was applied by standard vapour deposition.

The ECON detector was attached initially to a JEOL JXA50A electron probe microanalyser and later to a JEOL JSM35C scanning electron microscope. The x-ray take off angle was 35 degrees for both ED detector and WD spectrometers. Some additional experiments were undertaken on; an EDAX 9100 analyser, a LINK Systems 860 series 2 analyser with 'windowless' detector and a LINK Systems 2010/1057 with fixed beryllium window.

4. DEAD TIME CORRECTION

In quantitative analysis measurement of x-ray intensity is of primary importance, but pulse counting systems generally suffer from dead time effects which prevent them from measuring the true intensity. This is of particular significance in ED systems where loss of counts can be as high as 25% for intensities of 2000 s^{-1}. The cause of dead time was discussed in section 2.2.5 and electronic correction based on a live time clock was mentioned. The system's clock records live time exclusive of dead time so it appears to run slowly compared with real time. During investigation of the low energy spectrum however, the system clock was found to remain exactly in step with real time, even at high count rates, indicating that the system was failing to apply an adequate correction. It was necessary therefore, to study the different methods used to correct for dead time in ED systems and to identify the problems which can give rise to errors. The magnitude of errors was measured for a range of analysis conditions and the effect of these on quantitative work was considered. Finally alternative techniques were examined, whereby accurate calculation of live analysis time could be achieved.

4.1 Methods of Dead Time Correction

Compensation for dead time effects is carried out with electronic circuitry and different EDS systems dc this

in different ways.

Harms' (1967) method of dead time correction is to generate an extra count (a duplicate of a real one) whenever a pulse is missed during a 'dead' interval. Alternative methods make use of the principle of a 'live time' clock, the system clock being used to record the live analysis time as discussed on the previous page.

Two ways in which 'live time' is determined during analysis have been described. In the Covell procedure (Covell, Sandomire and Eichen 1960) the clock is stopped during each 'dead' interval while the main amplifier is busy processing a pulse. In the Barnhart method (Russ, Sandborg, Barnhart, Soderquist, Lichtinger and Walsh 1973) the number of counts missed during dead time is accumulated separately; the clock is then stopped periodically, allowing the system to process the exact number of extra counts needed to compensate for those missed.

The way in which these techniques are applied in practice can be understood by examining pulse processing in a typical modern ED system. Figure 4.1 shows the main processing route taken by signals from the x-ray detector, passing through amplification and measurement stages to the memory and display. The fast amplifier which was discussed in section 2.2.5 is also shown here and will be considered in more detail because it is utilised in one approach to dead time correction.

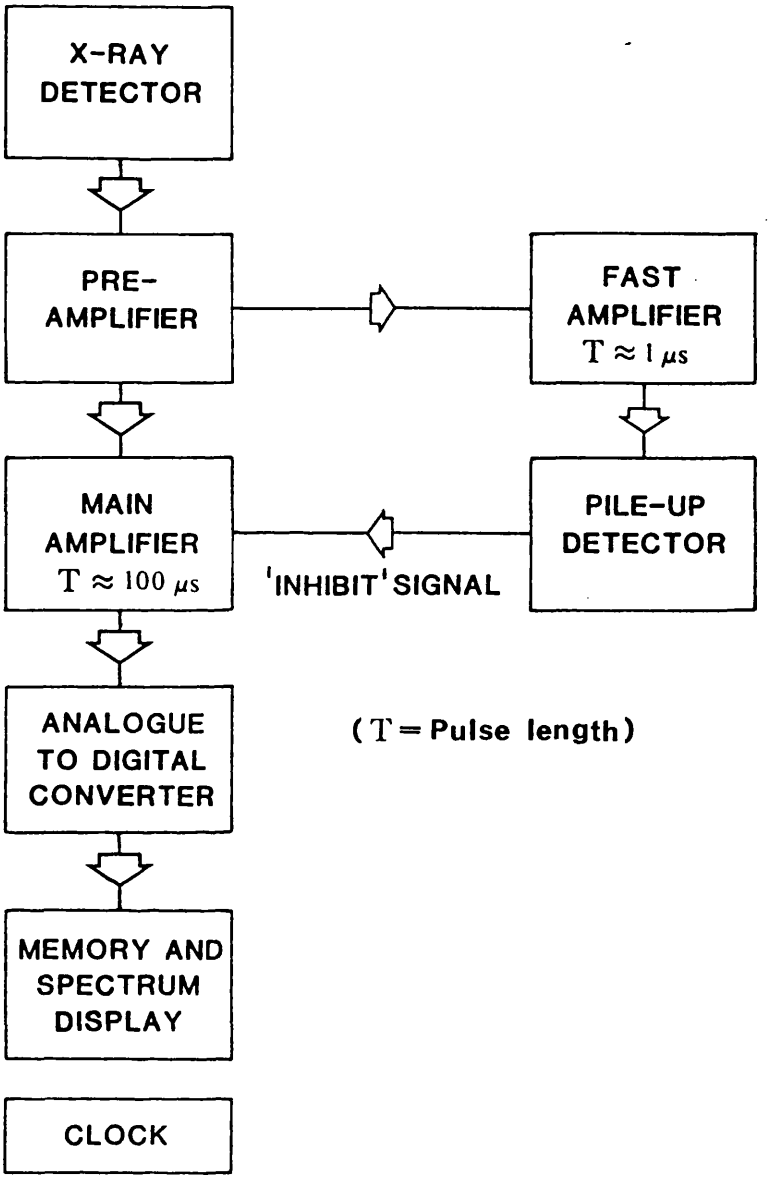

Fig.4.1 Signal processing in EDS systems

Main processing route

Pile-up rejection circuit (Williams 1968)

The fast amplifier is incorporated in the ED system essentially to eliminate pulse pile up (Williams 1968). It produces pulses of only 1 μs duration (compared with 100 μs in the main amplifer) so the pile-up detector is able to examine the intervals between pulses as long as they are more than ∿1 μs apart. If the pile-up detector 'sees' two pulses with less than ∿20 μs between them it rejects the inevitable pile-up pulse in the main amplifier by sending it an 'inhibit' signal. In this way most of the problems of pulse pile up are eliminated. Only the relatively rare pile up of pulses within ∿1 μs of each other cannot be detected.

4.1.1 Principles of the Covell Method

The principle of the correction for dead time as described by Covell et al (1960) is shown schematically in figure 4.2 as a 'dashed' line. When the main amplifier accepts a voltage pulse at its input it begins processing the pulse and sends out a 'busy' signal to stop the system clock. Only when the amplifier has finished processing and is ready to accept the next pulse, is the clock restarted. The clock is therefore stopped during dead time intervals and gives the effective live analysis time.

The method, however, does not allow for the loss of information due to pile-up. Ideally, each live time interval ends with the acquisition of an x-ray count

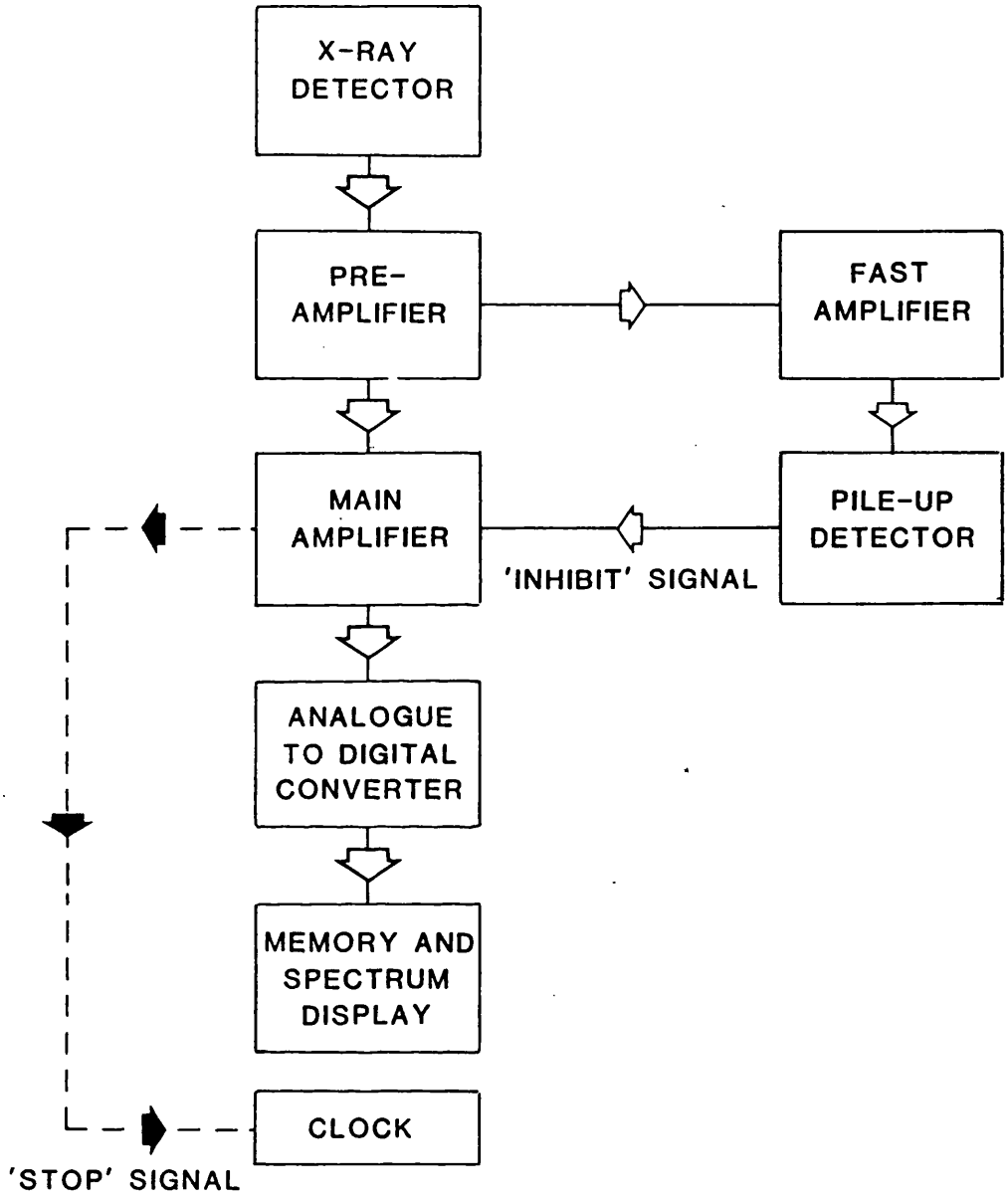

Fig.4.2 EDS signal processing with pile-up rejection and automatic correction for dead time.

Main processing route.

Pile-up rejection circuit.

Dead time correction system of Covell et al (1960)

but when a pile-up occurs the overlapping pulses are rejected. Thus the previous 'live' interval is effectively wasted and should not be included on the total live analysis time. An additional electronic correction is needed to compensate for this effect and Bartosek, Masek, Adams and Hoste (1972) describe a method which can be used in conjunction with the Covell dead time correction. Here, when a pile-up rejection is carried out, the clock is forced to remain off even after the amplifier recovers. Thus the clock is stopped for the next 'live' interval until a new pulse is recorded. Only after this compensating count has been acquired is the clock allowed to restart.

4.1.2 Principles of the Barnhart Method

Figure 4.3 shows schematically an EDS system with the addition of the dead time correction of Barnhart (Russ et al 1973). The method is based upon the assumption that although the main amplifier misses many counts because of dead time, the 'fast' amplifier is able to process almost all of them. The output of the 'fast' amplifier can therefore be taken as the best estimate of the true x-ray count rate. A digital counter records the difference between the number of pulses processed by the ADC and the number seen by the fast amplifier. This difference is equal to the number of pulses missed by the main amplifier during dead time. Periodically, when the digital counter reaches a set number, it stops

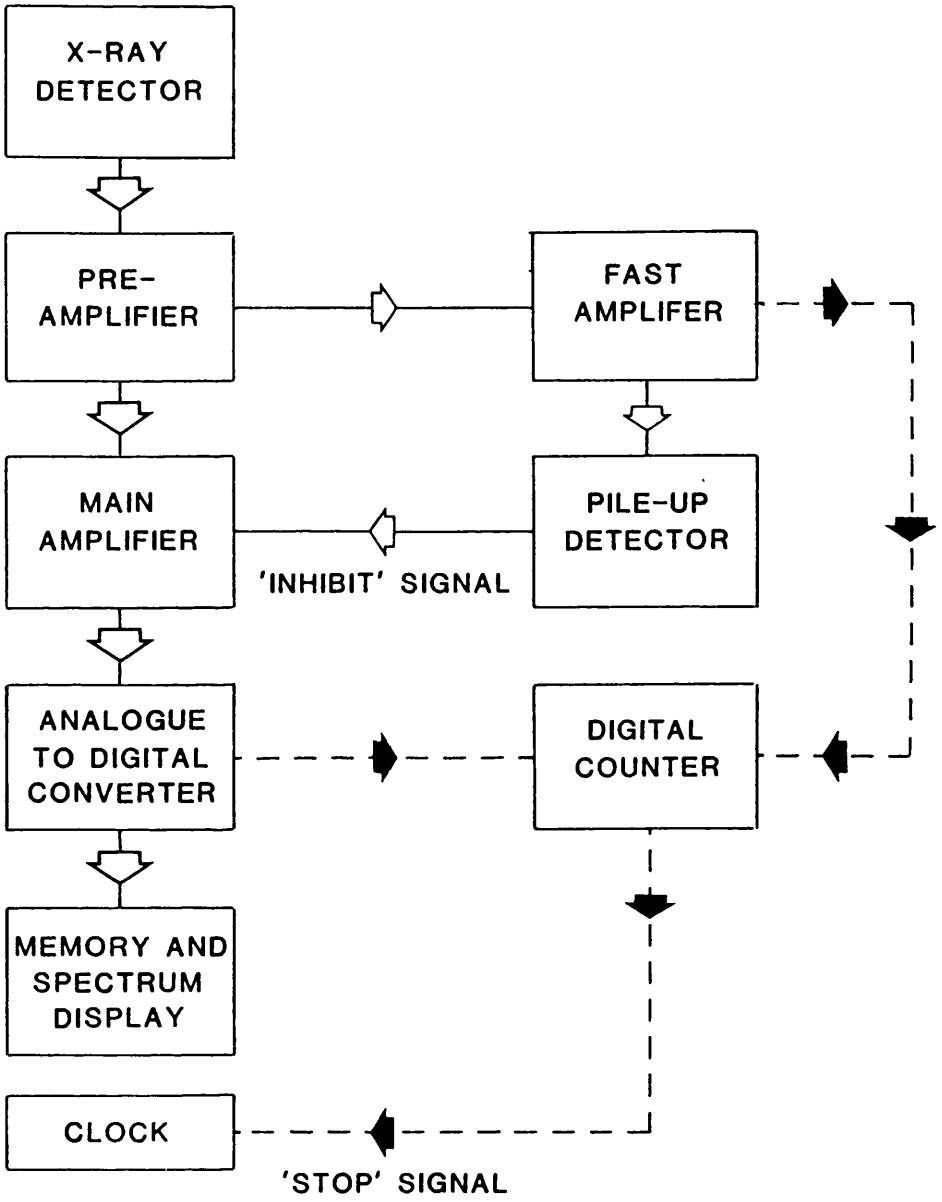

Fig.4.3 EDS signal processing with pile-up rejection and automatic dead time correction.

Main processing route.

Pile-up rejection circuit.

Barnhart dead time correction system (see Russ et al 1973)

the clock and allows the analyser to collect exactly that number of extra pulses. The analyser then has the correct number of counts for the live time period shown by the system clock. The effect is that the measured x-ray intensity is regularly adjusted to match that seen by the 'fast' amplifier. As well as correcting for dead time in the main amplifier, this method has the advantage of automatically correcting for the loss of counts caused by 'pile-up' rejection.

4.2 Assessment of Correction Methods

The amplifiers used in EDS systems require a minimum signal threshold setting in order to prevent noise entering the system. In the case of the main amplifier, with its slow processing time but relatively good energy resolution (full width half maximum for low energy photons ∿100 eV), the setting is ∿160 eV (figure 4.4a). On the other hand, the energy resolution of the fast amplifier (∿700 eV) has been sacrificed for speed and the threshold setting is much higher, ∿800 eV (figure 4.4b). Hence when processing x-ray energies which lie close to the threshold of the fast amplifier problems may be anticipated. Such effects would occur not only during analysis of the light elements (oxygen, carbon etc) but also when L or M radiations from heavier elements appear in this energy region.

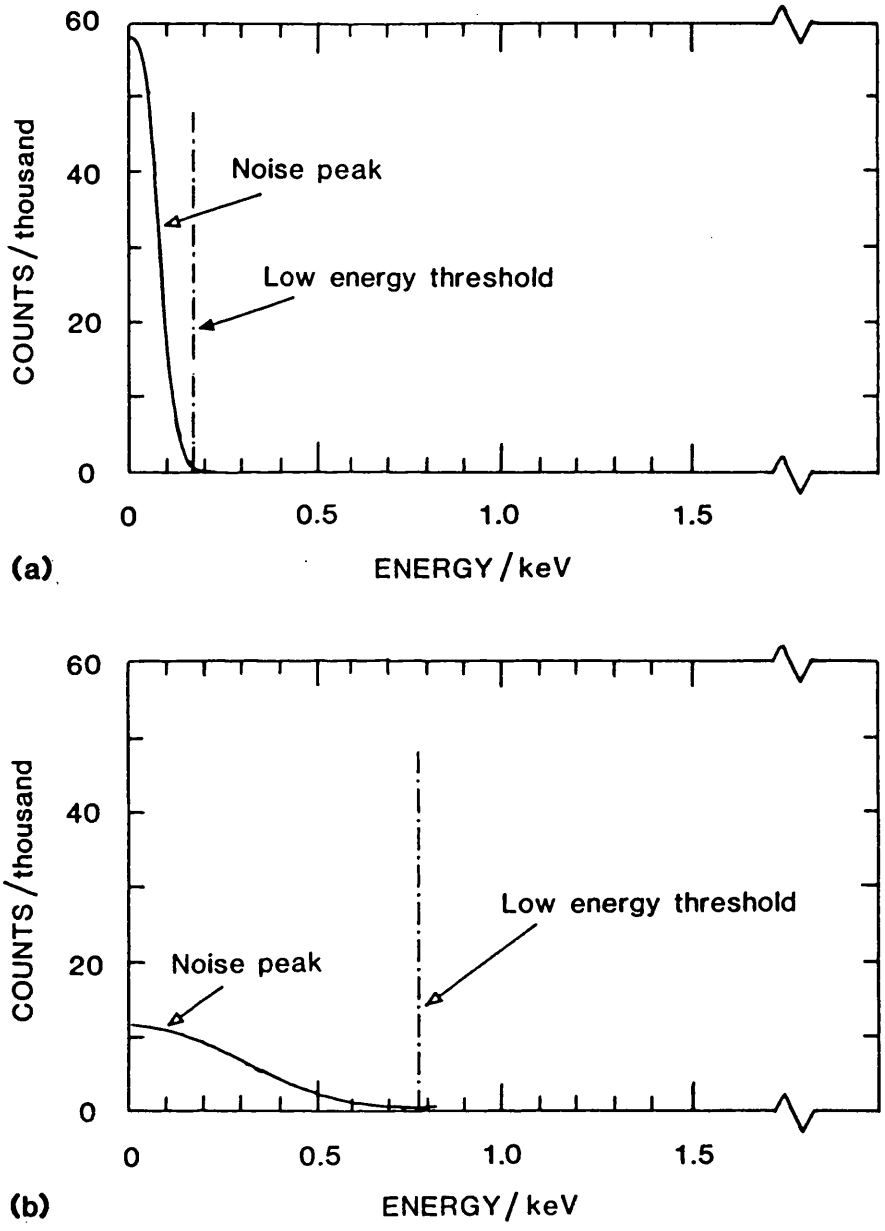

Fig. 4.4 Response to noise in the input signal for

(a) main amplifier and

(b) fast amplifier.

The Barnhart dead time correction method was evaluated using EDAX 711 and 9100 analysers and that of Covell using a LINK Systems 860 series 2 and a 2010/1057.

The first series of experiments involved measurements of pure specimens of silicon, chromium and zinc with the beryllium detector window in position. The elements silicon and chromium were selected because they produce no x-ray peaks in the energy region close to the threshold of the fast amplifier; (the chromium L radiation, $\sim$500 eV, is absorbed by the beryllium). Zinc was chosen because its L line has an energy of $\sim$1000 eV, just above the threshold energy of the fast amplifier. A more comprehensive range of specimens was included in the second series of experiments in order to investigate any dependence of the dead-time correction upon atomic number. In the case of the Barnhart system the latter measurements were repeated with a formvar window substituted for the beryllium; and with the Covell method a carbon window was used on the detector attached to the LINK 860 Series 2 system.

The following experimental measurements were made: (a) the total number of counts accumulated during an analysis (N), (b) the 'live' analysis time given by the system clock (t_ℓ), and (c) the 'real' analysis time measured with a stop watch (t_r). The term N/t_ℓ gives the incident x-ray count rate as determined by the EDS system incorporating its internal correction for dead time.

This will be referred to as the 'corrected' count rate.

The term N/t_r is the uncorrected count rate and gives the actual rate at which the analyser was capable of accumulating x-ray counts during the analysis.

4.2.1. The Barnhart Method

Figure 4.5 shows uncorrected count rate vs 'corrected' count rate for specimens of silicon and chromium at various probe voltages with the beryllium window in position. It may be seen that a smooth curve can be drawn through the points. Also included in figure 4.5 are results for the zinc specimen and these all lie above the curve; one point is shown (8 kV, $N/t_r = 1600s^{-1}$) where no dead-time correction at all has been applied by the system, as indicated by its position on the dotted line drawn at 45^{o}.

The position and shape of the zinc Lα peak together with the low energy threshold setting are shown for the main amplifier and fast amplifier in figures 4.6a and 4.6b, respectively. Note that with the fast amplifier the combination of poor energy resolution (∿700 eV) and high threshold (∿800 eV) results in a substantial proportion (shaded area) of the pulses associated with Zn Lα radiation being missed; it is apparent that any peak of energy up to ∿1500 eV would similarly suffer. Since the dead time correction

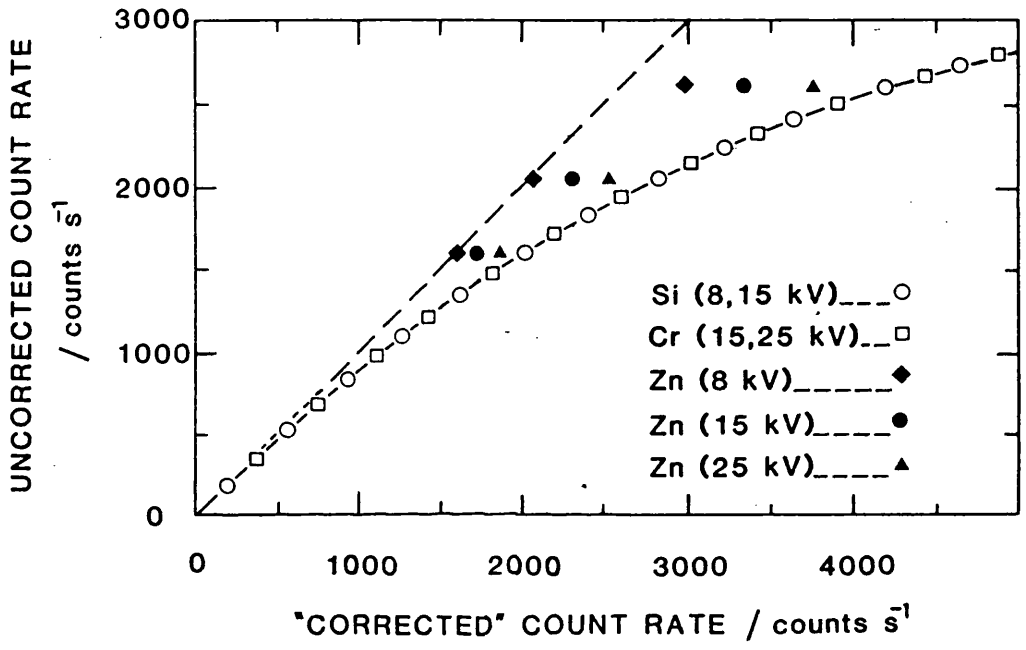

Fig. 4.5 Plot of uncorrected vs "corrected" count rate using Barnhart dead time correction system : beryllium window.

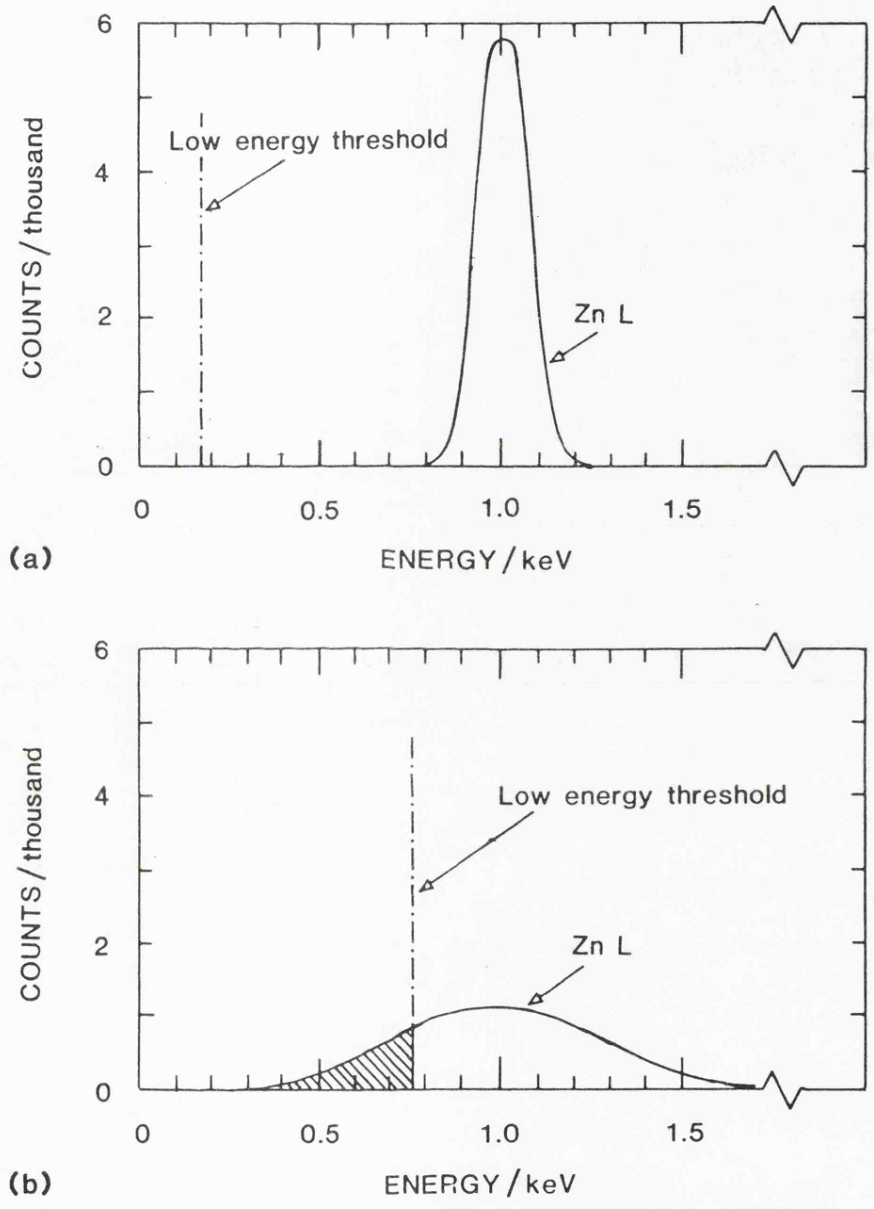

Fig.4.6 Response to signals generated by Zn L radiation for

(a) main amplifier and

(b) fast amplifier .

is carried out by matching the measured x-ray intensity with the count rate 'seen' by the fast amplifier, this means that appreciable underestimation of the true count rate occurs and insufficient dead-time correction is applied. The lower the probe accelerating voltage, the higher is the proportion of Zn Lα emission compared with the total spectrum and the greater is the under-correction, as evidenced in figure 4.5.

The magnitude of the undercorrection was calculated by taking the ratio of the number of counts 'missed' to the 'corrected' count rate read from the curve in figure 4.5, and expressing the value as a percentage. For example , with the zinc result at 8 kV, referred to above where no dead time correction was applied, the error would be given by $\left[(2000 - 1600)/2000\right]$ x 100%, i.e. 20%. The error in the dead-time correction is dependent upon the counting rate and with the higher 'uncorrected' count rate of $2060s^{-1}$ the zinc measurement at 8 kV gives a value of $\left[(2820 - 2060)/2820\right]$x 100% = 27%.

In order to compare data obtained from a range of specimens, all errors were estimated for uncorrected count rates of $2000s^{-1}$, this being a convenient figure to adopt when carrying out electron-probe microanalysis studies. The data are plotted against atomic number in figure 4.7a. At higher atomic numbers ($Z \geq 34$),

errors in the dead time correction are small owing to the fact that the energies of the L radiations from these elements all lie well above (they are greater than ∿1500 eV) the threshold setting of the fast amplifier. With decrease in atomic number from Z = 34 through to Z = 29, the energy of the L peak decreases from ∿1500 eV to ∿900 eV and the error gets progressively larger as more and more of the pulses fall below the threshold setting. However, as Z is further reduced the undercorrection then becomes less since the L peak is increasingly absorbed by the beryllium window and the counting system does not have to deal with them; in the case of chromium (Z = 24), few of the L x-rays reach the detector and the error is insignificant. Measurements on aluminium and magnesium show substantial errors since their K radiations produce pulses with energy close to the fast amplifier threshold. It should be noted that errors do not depend greatly upon accelerating voltage with these elements because the proportion of K radiations in the total spectrum is not appreciably changed with kV. It is interesting to note too that errors were recorded on a sulphur specimen owing to the escape peak appearing in the vicinity of the threshold.

Results obtained with the formvar detector window in position instead of beryllium are plotted as before against atomic number in figure 4.7b. The errors are increased generally, owing to the greater proportion

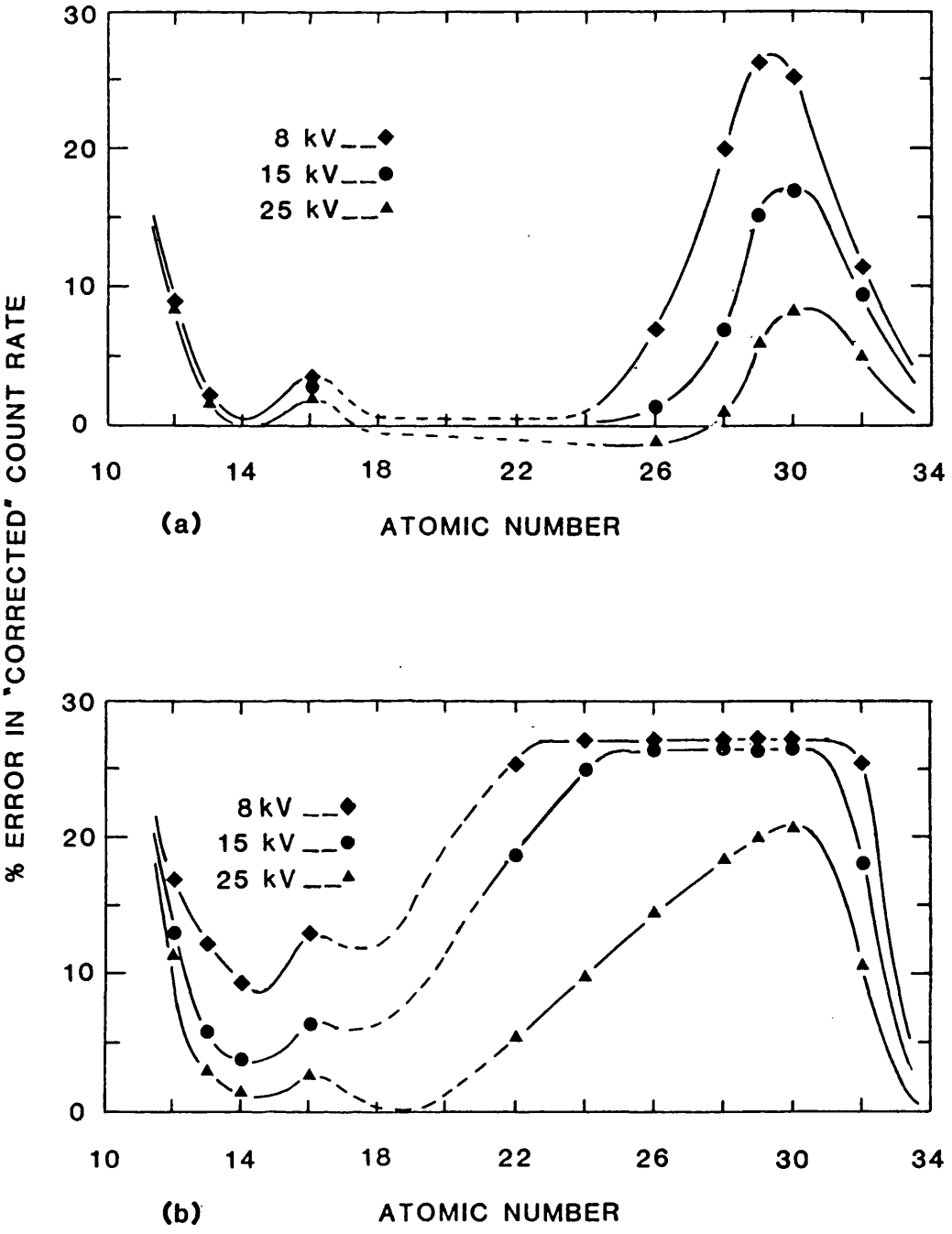

Fig.4.7 Plot of % error in "corrected" count rate vs specimen atomic number using Barnhart dead time correction system : uncorrected count rate 2000 s^{-1}.

(a) Beryllium window.

(b) Formvar window.

of low energy x-rays now admitted to the detector, although the form of the curves remains much the same as those obtained with the beryllium window in position (figure 4.7a). Errors are zero when $Z \geq 34$ and increase to a maximum for Z = 30. With an accelerating voltage of 25 kV, the errors progressively decrease with atomic numbers below Z = 30, but use of the formvar window now results in substantial errors from chromium and titanium since their L radiations are absorbed much less in this window material than in beryllium. As with the data plotted in figure 4.7a a marked dependence upon accelerating voltage is apparent and horizontal portions of the curves for 8kV and 15 kV show that little or no dead time correction is being applied in many instances. The errors which arise when silicon (Z = 14) is being analysed are associated with the portion of continuum radiation transmitted by the formvar containing energies below the threshold setting of the fast amplifier; this affects also the measurements on sulphur and other neighbouring elements.

The marked dependence of the magnitude of errors upon the detector window material manifested itself in other ways during this investigation. Earlier work (Love, Scott, Dennis and Laurenson 1981) had shown that the cooled window surface was a prime site for condensation of organic material, and that this caused substantial attenuation of the softer x-ray emissions. The dead time correction errors were then correspondingly less. With

a contaminated beryllium window (Bloomfield, Love and Scott 1981), the error was 17% when recording zinc radiation at 8 kV compared with 25% when using a recently cleaned window; a contaminated formvar window gave rise to similar effects.

In order to investigate the extent to which errors in the dead time correction might affect practical micro-analysis results, some measurements were made upon a specimen of $CuAl_2$ and reference standards of pure copper and pure aluminium. Data were obtained at 15 kV using the EDS system with the beryllium window in position. The probe current was adjusted so that $\sim$2000 counts s^{-1} were recorded in the total spectrum from pure copper. The copper Kα intensities were then measured on the standard and on the $CuAl_2$ specimen and an intensity ratio of 0.519±0.005 obtained. The corresponding intensity ratio for Al K was found to be 0.248±0.001. The measurements were repreated using a crystal spectrometer, since this technique was expected to give the correct intensity ratios, and values of 0.485±0.005 and 0.269±0.003 were obtained for copper and aluminium respectively. The EDS data are significantly different being 7.0% higher in the case of copper and 7.8% lower in the case of aluminium (see table 1). The discrepancies are associated with dead time correction errors arising mainly from the presence of the Cu Lα peak in the x-ray spectrum. Hence when measuring the Cu Kα intensity ratio, there will be a large undercorrection for the pure copper standard and

a somewhat smaller undercorrection for the $CuAl_2$ specimen; the net result is an overestimation of the copper composition of $CuAl_2$. In the case of the Al Kα readings, the undercorrection which occurs when analysing the specimen will produce an underestimate of its aluminium content.

Table 1. Measured intensity ratios on $CuAl_2$ at 15 kV using pure standards

Analysis method	Al	Discrepancy wrt WDS	Cu	Discrepancy wrt WDS
WDS	0.269±.003		0.485±.005	
EDS	0.248±.001	-7.8%	0.519±.005	+7.0%
EDS by calibration	0.266±.001	-1.1%	0.486±.005	+0.2%

One possible solution would be to measure the real analysis time with a stop watch, calculate the actual recording rate, and use the experimental curve in figure 4.5 to determine the true input count rate. This was actually carried out in the analysis of $CuAl_2$ discussed above, and the results are shown in table 1 as 'EDS by calibration'. The new values lie, within experimental error, close to the WDS data.

4.2.2 The Covell Method

The uncorrected count rate vs. 'corrected' count rate showed that a consistent dead time correction was being applied in all cases. In this system the dead time correction is controlled by the main amplifier itself and the fast amplifier is used only for pile-up rejection. Thus this method of correcting for dead time would not be expected to suffer from the major problem experienced by the method of Barnhart. The loss of information due to rejection of pile-up pulses has been adequately covered by the modification described by Bartosek et al (1972) which is included in the LINK systems analyser.

4.2.3 Comparison of Methods

The errors experienced with the dead time correction method of Barnhart can be encountered whenever the recorded spectrum contains significant counts below $\sim$1500 eV. Elements such as magnesium, copper, nickel and zinc can produce these low energy counts even when the EDS detector has a standard beryllium window. Since these elements are common in many specimens routinely analysed with EDS systems, the probability of errors arising is large.

The use of a plastic window rather than beryllium was found to increase the problem when analysing elements with $22 \leqslant Z \leqslant 32$. When light elements alone are analysed the situation is worse because no dead time correction

at all may be applied by the system. Although only K and L x-ray emissions below $\sim$1500 eV have been considered, it is expected that low energy M emissions would also cause errors with the Barnhart method. (Elements with atomic number $51 \leq Z \leq 70$ produce M lines in the relevant range.) Errors associated with L and M radiations may be reduced by operating at higher electron accelerating voltages.

If dead time errors arise in quantitative analysis, undercorrection will occur for both specimen and standard and the net discrepancy will be somewhat reduced. In the case of a $CuAl_2$ specimen, relative errors were $\sim$10%, although in many systems they may be less than this.

The dead time correction method of Covell appears not to suffer from the above problems.

4.3 Alternative Correction Methods

It was demonstrated in the previous section, that defficiences in the Barnhart method can be overcome by using a 'calibration' curve based upon the experimental data in figure 4.5. Unfortunately a further effect within the ED electronics can alter the system response in certain conditions.

4.3.1 Dead-Time as a Function of Photon Energy

It may be deduced from descriptions of pulse-height measurement systems (Reed 1975a, Fitzgerald and Gantzel 1971) that the dead time ought to become smaller as the photon energy decreases. Clearly if this effect does occur, the calibration curve will not be generally applicable for calculating live time. The results presented in the previous section have shown that the effect is small for the spectra in question. The dead time when analysing such elements as silicon and chromium is described well by a single curve despite the fact that predominant peaks range from 1.5 to 5.5 keV. The analysis of light elements however, may produce spectra with large low energy peaks and it was therefore important to study the dead time effect further with particular attention to soft x-rays.

Since the Barnhart method does not give a true indication of system dead time when significant numbers of soft x-rays are involved it was necessary to develop an alternative technique. Curves 'A' and 'B' in figure 4.8 show the recording rate versus input count rate for dead times of 100 and 50 μs per pulse respectively. The difference in maximum recording rates when the system 'saturates' can be seen clearly. Since this maximum can be measured relatively easily for a given system and specimen, a direct indication of system dead time can be obtained; the higher the maximum recording rate the

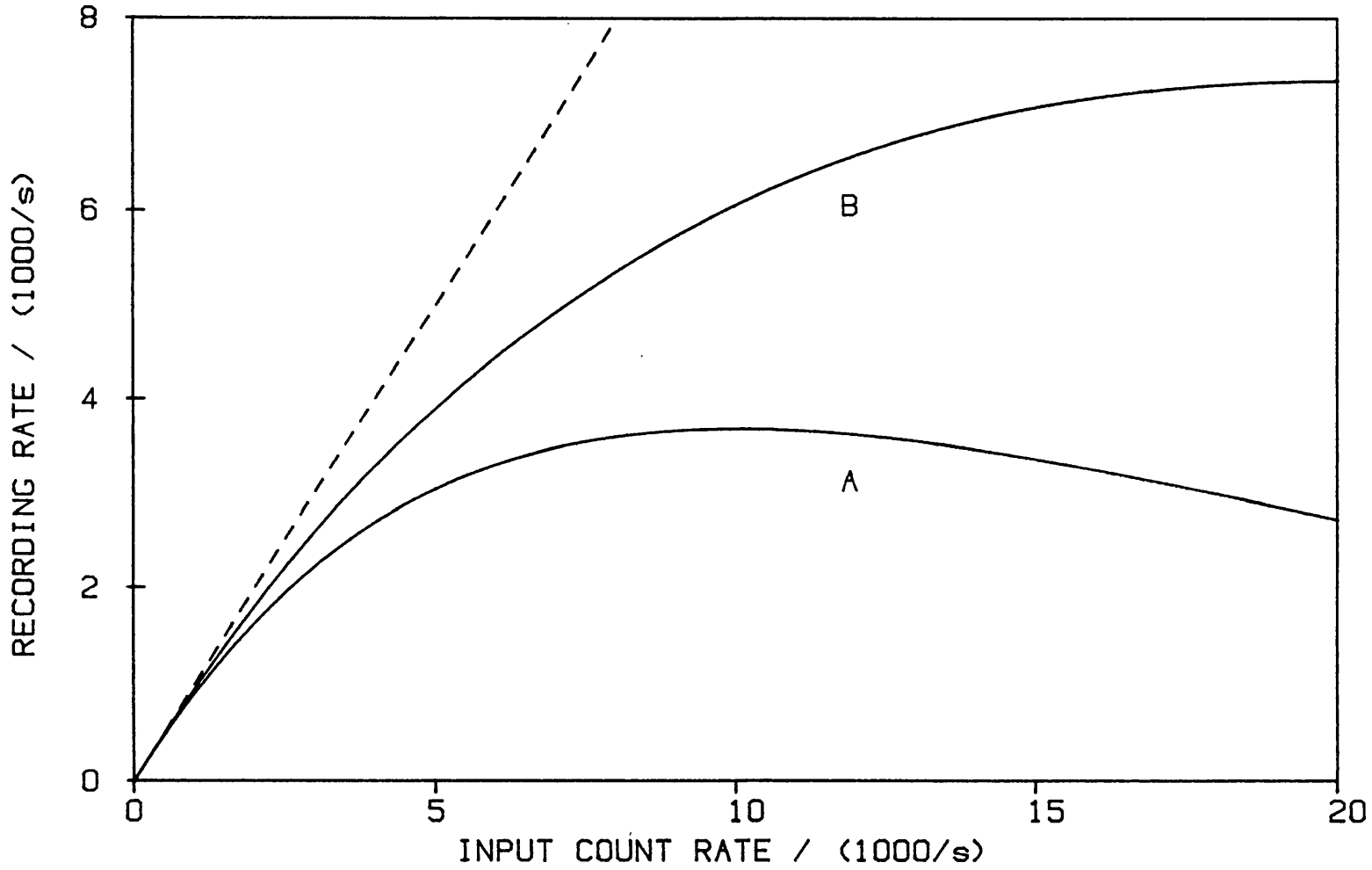

Fig. 4.8 Recording rate versus input count rate for dead times of 100 μs per pulse (curve A) and 50 μs per pulse (curve B).

shorter the dead time. Measurements on the EDAX 711 system have shown that for spectra having most of their x-rays above 1.5 keV the maximum is in the range 3550 to 3750 s^{-1} and the system response is similar to curve A. When, however, the spectrum contains a significant (10 to 20%) proportion of x-rays between 1 and 2 keV the maximum of the curve rises as high as 4000 s^{-1}. This demonstrates that dead time is affected by the energy of the incoming x-ray photon although only a very small departure from curve A is observed for recording rates most generally used (1000 s^{-1} to 2000 s^{-1}).

Specimens rarely contain light elements alone and therefore spectra containing low energy peaks usually contain high energy ones as well. The latter peaks tend to maintain the average dead time at 90 to 100 μs for the EDAX system so that curve A is only slightly in error for compound specimens. If, however, a pure light element standard such as carbon is used then a single low energy peak is produced which leads to a substantial reduction in the average dead time of the system. A maximum recording rate of 8000 s^{-1} was established for carbon, equivalent to a mean dead time of $\sim$50 μs, and indicates that curve B is appropriate in this instance.

It may be concluded therefore that for light element analysis a method of applying the dead time correction is needed which is not restricted to the use of a single

calibration curve. The mathematical procedure developed here is more generally applicable and describes a family of curves between A and B in terms of a parameter easily measured on each spectrum.

4.3.2 A New Dead Time Correction Method

Studies of randomly spaced pulses lead to a simple expression for the effect of dead time in a counting system (Beaman, Isasi, Birnbaum and Lewis 1972). The actual recording rate (n') is related to the true input count rate (n) by

$$n' = n \exp(-n\tau) \qquad (4.1)$$

where τ is the mean dead time per pulse.

An electronic counting system has various sources of dead time, each responding differently to count rate, and so the simple expression above does not necessarily predict the system response. However if it can be shown to approximate to the dead time calibration curve it can then be used to define a family of curves each with different τ.

In order to test this idea further, experimental data for silicon at 8 and 15 kV and chromium at 15 and 25 kV (previously shown in figure 4.5) were compared with equation (4.1) by calculating

$$\tau_i = \frac{1}{n_i} \ln(n_i / n_i')$$

for each pair of coordinates n_i and n_i'. The results of the comparison are shown in figure 4.9. It is evident that the equation represents the experimental results very well when τ is set equal to 110 μs. The problem remaining therefore is to formulate an expression for τ in terms of spectrum parameters which are simple to measure. This will enable the dead time to be calculated by substituting appropriate values of τ into equation (4.1).

The maximum recording rate for most spectra may be easily measured by increasing the specimen current until the measured count rate reaches saturation. This maximum occurs when

$$\frac{dn'}{dn} = 0.$$

Differentiating equation (4.1) gives

$$\frac{dn'}{dn} = \exp(-n\tau) + n(-\tau)\exp(-n\tau)$$

$$= (1-n\tau)\exp(-n\tau)$$

Hence the maximum recording rate n_m' occurs

$$\text{when } (1-n\tau) = 0 \qquad \text{i.e. } n = \frac{1}{\tau}$$

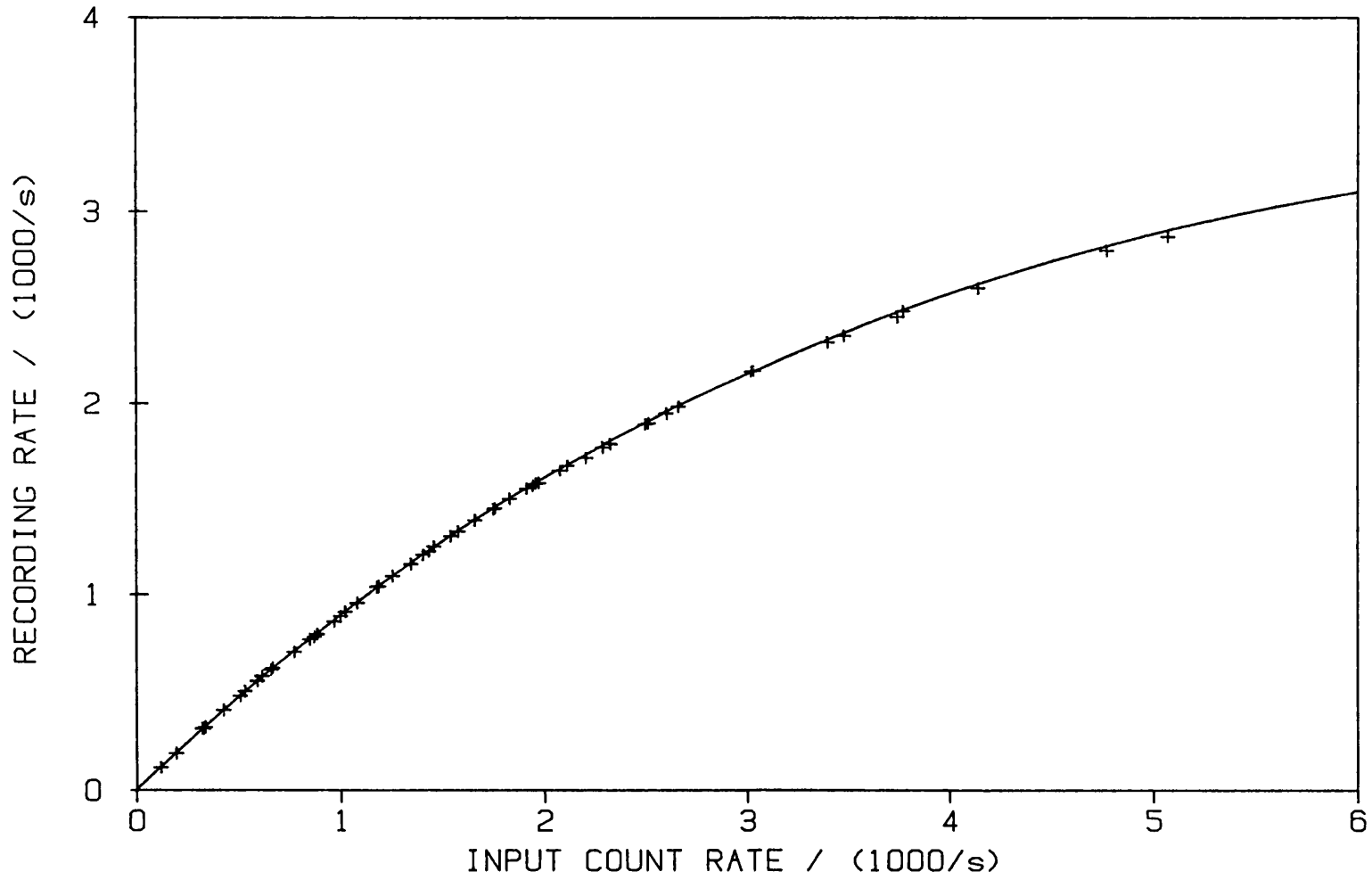

Fig. 4.9 Experimental points from silicon at 8 and 15 kV, and chromium at 15 and 25 kV, showing dead time effects; the solid curve is obtained from equation 4.1 using a dead time of 110 μs.

Subsituting for n in equation (4.1)

$$n'_m = \frac{1}{\tau} \exp(-1)$$

and re-arranging

$$\tau = \frac{1}{e\ n'_m} \qquad (4.2)$$

To implement the procedure n must be determined from equation (4.1) using appropriate values of τ and n' (the recording rate given by total counts in spectrum divided by the real analysis time). This is carried out by a simple iteration procedure as follows. Equation (4.1) may be rewritten in the general form

$$x = y \exp(-y\tau) \qquad (4.3)$$

As a starting point y is set equal to n' and x is calculated. Initially $x < n'$, so y is incremented until $x = n'$. At this point equation (4.3) corresponds to (4.1) and $y = n$. With suitable control over the incremental steps for y in relation to the difference between x and n', the iteration can be carried out extremely rapidly (in less than 1 second) on a computer.

In order to verify that the method performed satisfactorily live times calculated using the new approach were compared with values obtained from the Barnhart method. Since it was necessary to choose spectra which the

Barnhart method could deal with properly, the beryllium window was inserted to minimise the soft x-ray contribution; specimens of silicon and chromium were selected because they produce no peaks below 1.5 keV. Table 2 shows that in all cases the live time calculated from equation (4.1) agrees with the results obtained using the Barnhart method.

Finally, the new method was employed to establish the live time of the system when analysing a spectrum from pure carbon; for these measurements the formvar detector window was used. Table 3 lists the results obtained; also included are live times given by the Barnhart method and those determined from the curve in figure 4.5. The values are seen to be significantly different. The Barnhart method, as expected, gave no dead time correction at all whilst the calibration curve overestimated the dead time because no allowance was made for the shorter processing time involved in dealing with soft x-rays from carbon. Equation (4.1) used in conjunction with the appropriate value of τ was however more realistic in giving an intermediate value.

Specimen	Nominal Recording Rate (s^{-1})	Live time (s)	
		Equation 4.1	Barnhart System
Silicon	1000	89.6	89
	2000	78.9	79
	3000	65.7	66
Chromium	1000	89.5	89
	2000	76.8	77
	3000	60.8	62

Table 2. Comparison of live time obtained using equation 4.1 with that given by the Barnhart system for specimens of silicon and chromium and real time of 100 s.

Probe Voltage (kV)	Nominal Recording Rate (s^{-1})	Live time (s)		
		Barnhart System	Equation 4.1	Single Calibration Curve
7	1600	100	93.2	81
15	1350	100	93.9	85

Table 3 Comparison of live time obtained by the Barnhart system, use of equation 4.1 and use of a single calibration curve; pure carbon specimen, real time 100 s.

5. THE LOW ENERGY SPECTRUM IN EDS

When developing or assessing techniques for ED analysis it is essential to understand the nature of the recorded spectra. These spectra consist of characteristic peaks and x-ray continuum, but may also include undesirable artefacts such as escape peaks and low energy tailing. Additional effects which may occur can be related to count rate, discriminator levels and calibration settings. Most of these effects have been described in previous sections and methods have been developed for dealing with them in conventional spectra, (Fiori and Newbury 1978, Williams and Goldstein 1981). Unfortunately very little information has been presented concerning the nature of ED spectra below 1 keV. Consequently a thorough examination of this low energy region was found essential in this work. The most important results, which are discussed in the following sections, concern; the noise counts, a new artefact termed the 'spur' and the effects of different types of signal discrimination.

5.1 Effect of the Location of the Low Energy Discriminator

In pulse-height analysis some mode of energy discrimination must be employed to determine whether a particular pulse is the result of a genuine signal or whether it arises from a random fluctuation due to noise. Hence a voltage

threshold is set so that signals falling below this level are ignored and those above it are accepted for processing. When analysing for boron and carbon x-rays the threshold must be set as low as possible to maximise detection efficiency which in turn means that it will lie close to the noise level of the system.

The appearance of the recorded spectrum in the low energy region depends upon how the signal/noise discriminator is incorporated in the system. Most commonly the threshold is positioned at the input (A in figure 5.1) of the analogue-to-digital converter (ADC). An alternative method employs an auxiliary amplifier and control circuit and has the threshold at position B. To explain the operation of these systems it is helpful to consider a monochromatic source of low energy ($\sim$250 eV) x-rays incident upon the detector. Figure 5.2b shows the energy distribution of the x-ray counts after pre-amplification. The x-ray line is broadened slightly due to ionisation statistics in the detector and pre-amplifier noise. The distribution of noise counts at this stage is illustrated in figure 5.2a. The appearance of the recorded spectrum will now be considered for two different situations.

5.1.1 Discriminator on the ADC Input

This is the arrangement adopted by EDAX with their 711 and 9100 analysers. Figure 5.3b shows the effective

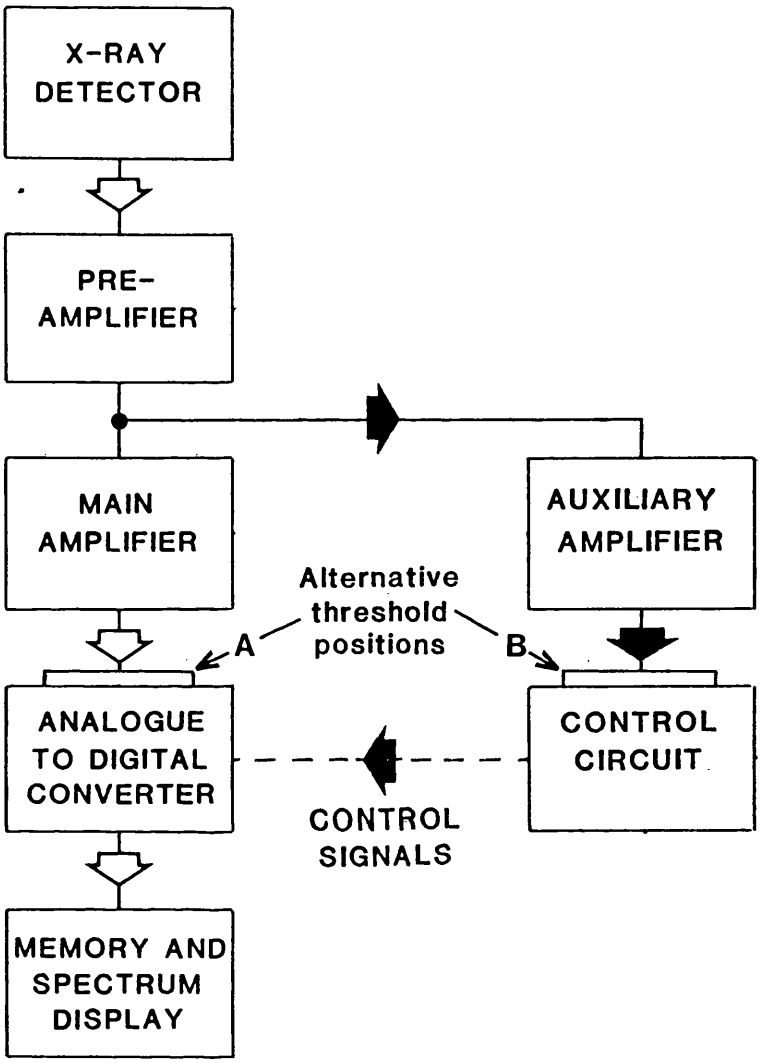

Fig. 5.1 Block diagram of an ED system showing alternative threshold positions at A and B;

A is in the main processing route (⇨)

B is in the auxiliary processing route (➡)

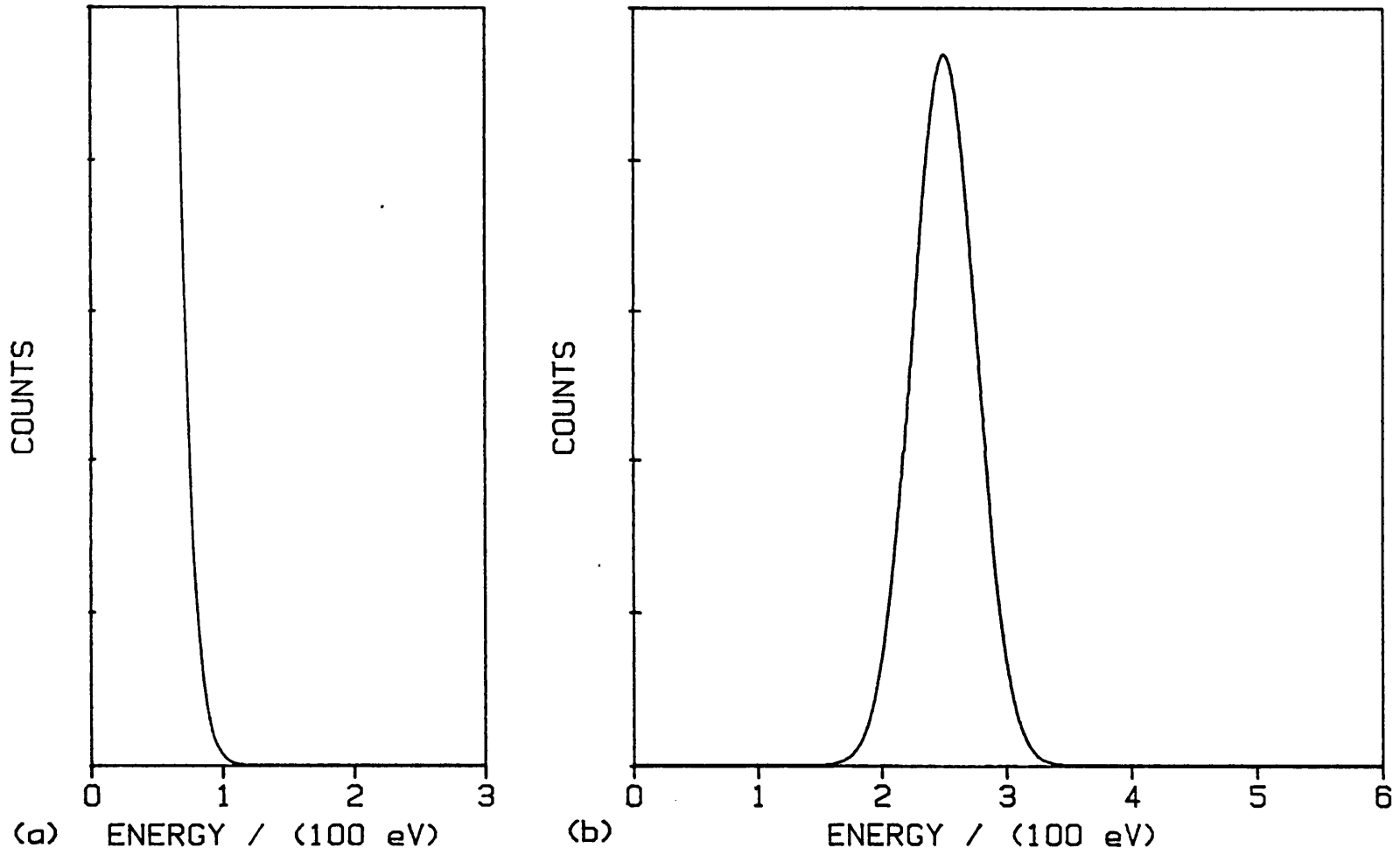

Fig. 5.2 Energy distribution of (a) noise counts and (b) x-ray counts after pre-amplification.

energy distribution of the x-ray counts after passing through the main amplifier; the corresponding noise distribution at A is illustrated in figure 5.3a. Compared with figure 5.2 both distributions are broadened by the addition of noise in the main amplifier. The threshold level at A, (figure 5.1), is indicated by dotted lines in figure 5.3. Signals represented by the shaded regions pass the threshold, are measured by the ADC and appear in the final spectrum as in figure 5.3. This results in peak shapes being largely unaffected by the threshold setting, but there is a sharp cut off at the low energy end of the spectrum.

5.1.2 Discriminator Incorporated in Auxiliary Circuit

The effective energy distribution of the counts and noise leaving the auxiliary amplifier (figure 5.1) will be virtually the same as for the main amplifier (see figure 5.3) provided that the time constants of both amplifiers are similar. The signals represented by the shaded area in figure 5.3 are not now passed onto the ADC for measurement but instead are used to trigger control circuits such that the ADC measures corresponding signals received by the main amplifier. These signals, however, suffer different noise fluctuations in the main amplifier compared with the auxiliary amplifier. Consequently, a pulse exceeding the threshold of the auxiliary amplifier may appear in the spectrum below the threshold energy; conversely, a pulse stopped by the

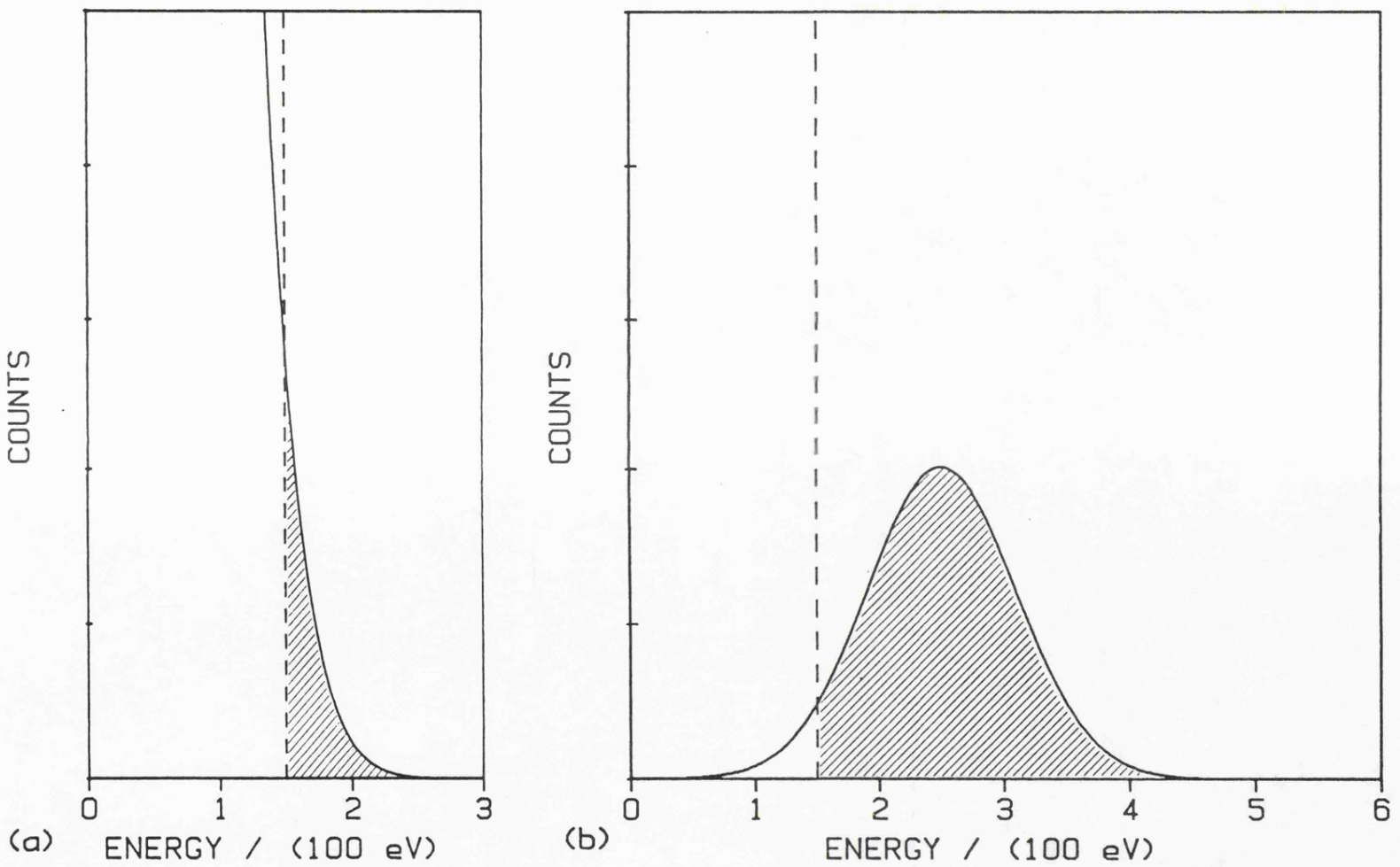

Fig. 5.3 Energy distribution of (a) noise counts and (b) x-ray counts after main amplification. The dotted lines indicate the threshold level.

threshold at B might have appeared in the spectrum above the threshold energy had the ADC been allowed to measure it. It follows that the counts missed when signals fail to cross the threshold at B are lost from a broad region, mainly on the low energy side of the peak, thereby changing the peak shape as illustrated in figure 5.4b. Similarly, the noise pulses recorded by the ADC will have preamplifier noise plus an independent contribution from the main amplifier and these will appear as a low energy peak in the spectrum (figure 5.4a).

The principal reason for including auxiliary amplifiers in ED systems is to deal with pulse pile-up, i.e. to detect closely spaced signals which cannot be separated by the main amplifier. Thus the auxiliary circuit used for pulse recognition will often share the short time constant amplifier used for pile-up rejection. When, in this type of system, monochromatic x-rays and noise signals reach the threshold, they do not possess the pulse height distribution shown in figure 5.3. Instead the higher noise level of the short time constant amplifier produces much broader distributions, see figure 5.5. More noise counts and less x-rays are thus recorded, resulting in the spectrum illustrated in figure 5.6. The noise peak is increased compared with that shown in figure 5.4 and the x-ray peak is not only reduced in size but appears shifted to higher energy.

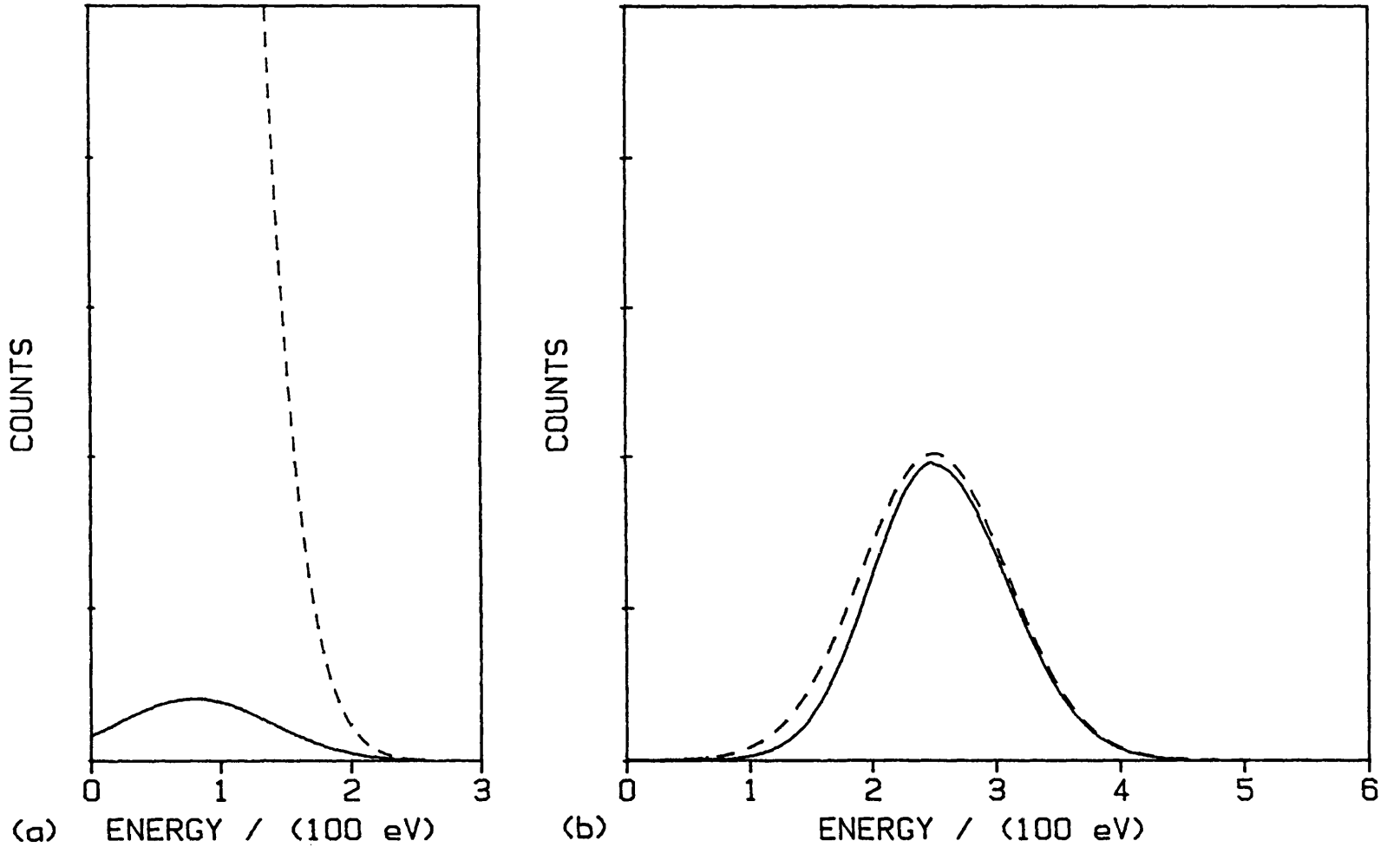

Fig. 5.4 Spectrum of (a) noise counts and (b) x-ray line, with the threshold at B (see fig. 5.1): time constant of auxiliary amplifier same as that of main amplifier. Original distributions (see fig. 5.3) are given by the dotted lines.

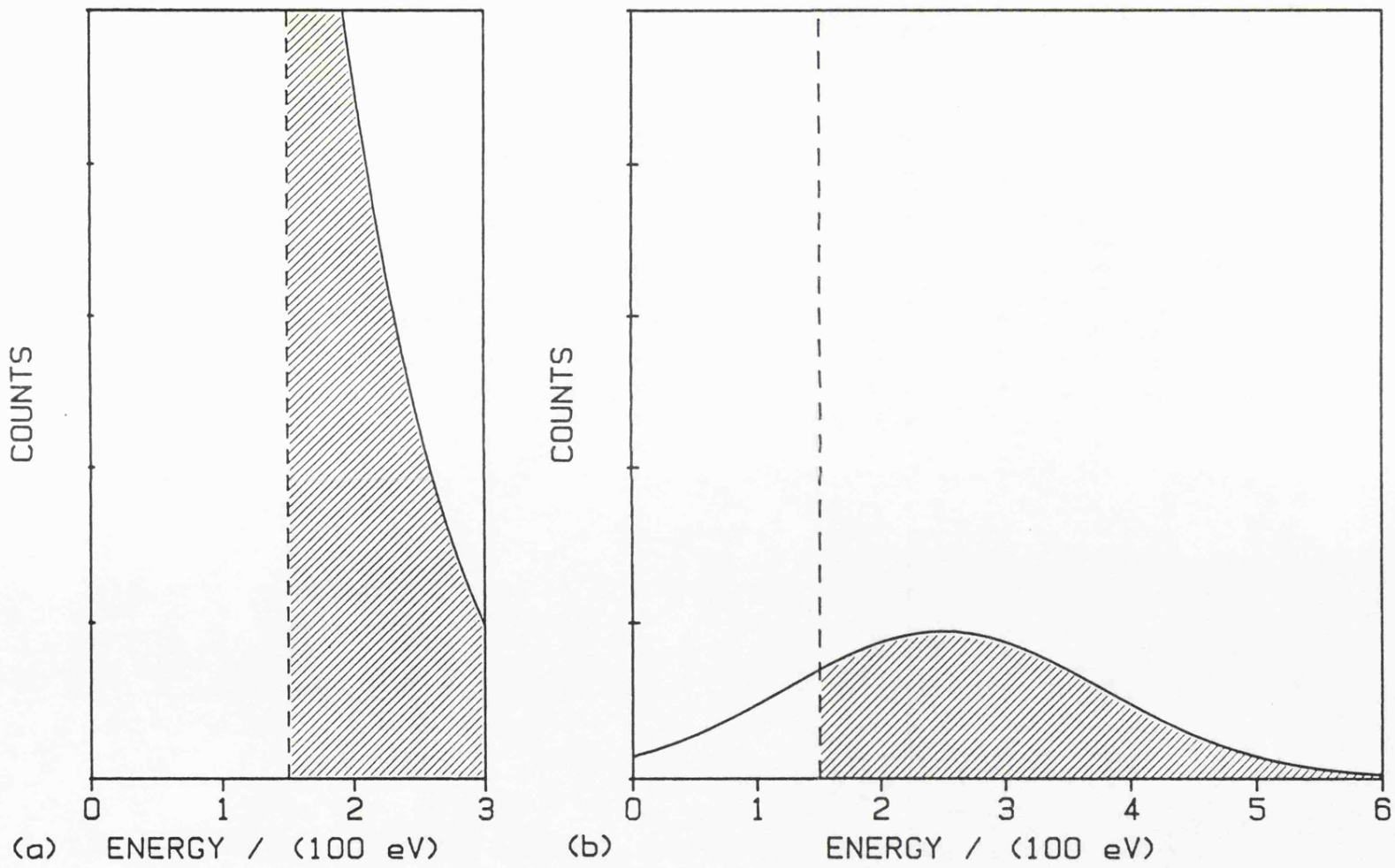

Fig. 5.5 Energy distribution of (a) noise counts and (b) x-ray counts after passing through short time constant auxiliary amplifier. The dotted lines indicate the threshold level.

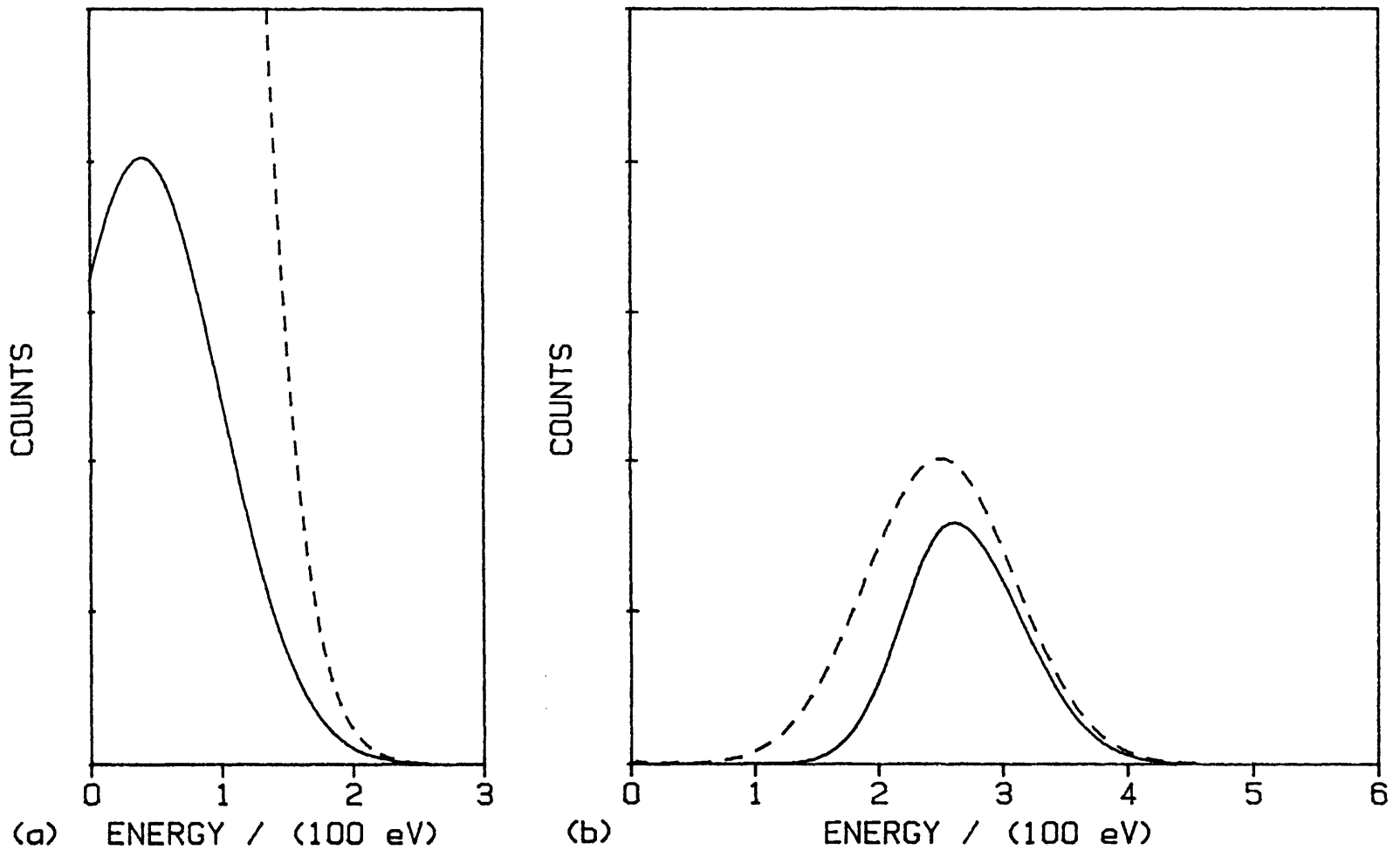

Fig. 5.6 Spectrum of (a) noise counts and (b) x-ray line, with the threshold at B (see fig. 5.1); time constant of auxiliary amplifier shorter than that of main amplifier. Original distributions (see fig. 5.3) are given by the dotted lines.

5.1.3 Comparison of Systems

The more common arrangement of positioning the threshold level on the main measurement channel suffers from the disadvantage that the tail of the noise peak overlaps low energy peaks as illustrated by the spectrum from silicon carbide (figure 5.7). The low-energy cut off is clearly visible whilst the reduced detection efficiency for soft x-rays is manifest by loss of the low energy tail of the peak, i.e. that part falling below the threshold level. Adjustments to the threshold setting do not affect the height of the nearby peak but as shown by the dotted lines in figure 5.7, simply alter the proportion of tail which is cut-off.

The use of an auxiliary recognition circuit allows some additional discrimination so that noise counts appear at a low energy. This is superficially appealing but, unfortunately, the effect on the spectrum of altering the threshold level is not now so obvious. Clearly the detection efficiency for a low energy peak is influenced by the threshold setting and changing its value results in an alteration of the height, shape and position of the peak in the spectrum. Such effects are illustrated in figure 5.8 by spectra obtained from a carbon sample using a LINK windowless detector and analyser. The measurements have been recorded for constant electron beam current and equal counting times but different threshold levels have been used. As the threshold is

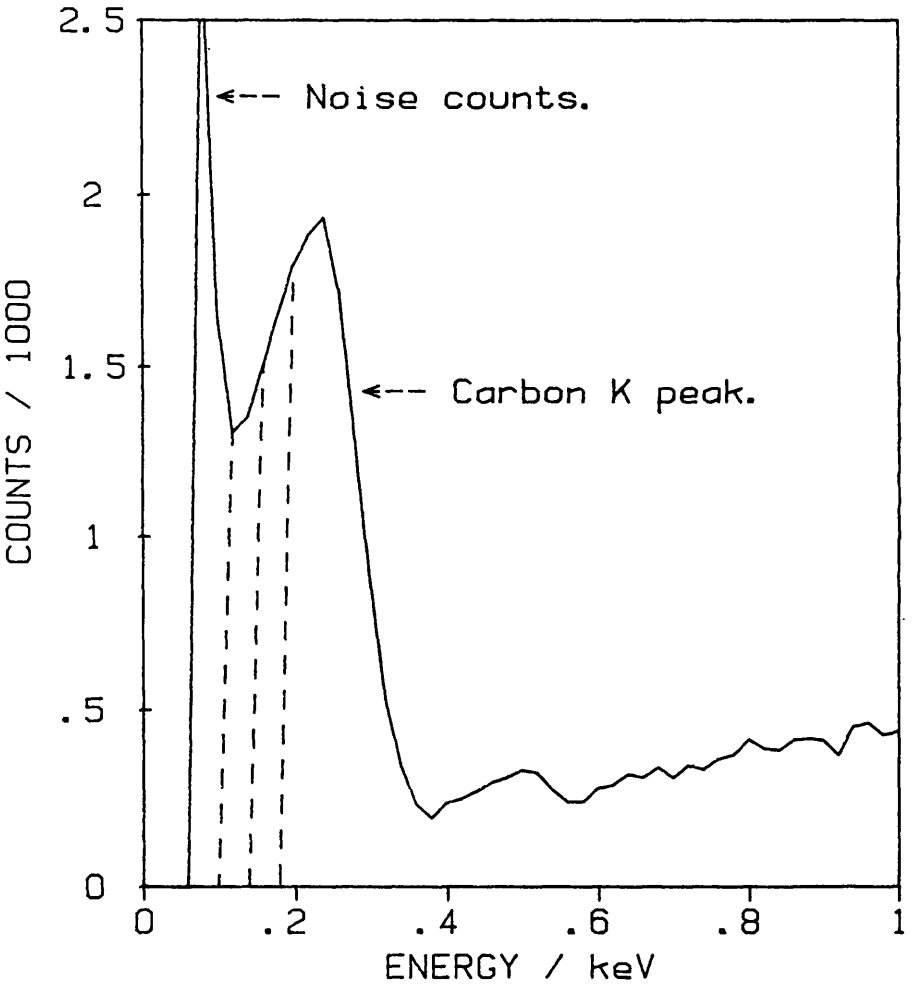

Fig. 5.7 Threshold at position A (see fig. 5.1) dotted lines indicating the cut-off position for different threshold settings: silicon carbide specimen, 7 kV probe, formvar window.

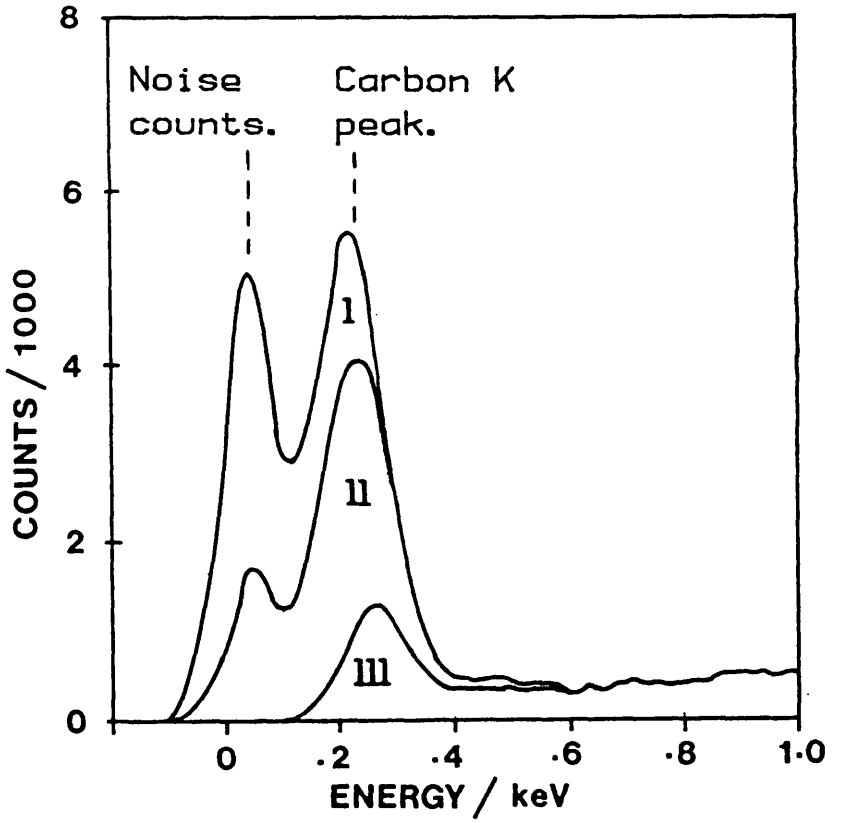

Fig. 5.8 Threshold at B (see fig. 5.1) for three different energy settings: carbon specimen, 15 kV probe, carbon window.

increased from a level which allows substantial noise to be recorded (curve I) to one where noise is virtually excluded (curve III), the carbon peak is reduced by a factor of ∿4 and shifted by ∿50 eV; an intermediate case (curve II) is also included in the figure. Because the threshold level may drift, be moved inadvertently or require adjustment to give satisfactory peak-to-background ratios on different specimens, problems will occur unless it can be reset precisely. In practice this is not easy to achieve and therefore intensity ratios obtained from specimen and standards tend to be meaningful only if the measurements are carried out within a relatively short period of time.

Systems which have the energy discriminator in the main measurement channel do not suffer from the above limitation although a way of removing the noise tail is still required before reliable measurements of carbon and boron peak intenstities can be made. Fortunately the absence of spectrum distortion means that it is possible to investigate fully, noise subtraction and the presence of artefacts in the soft x-ray spectrum.

5.2 Electronic Noise

5.2.1 Noise in the Spectrum

When carrying out analysis of, for example, carbon x-rays (277 eV) the threshold setting should be reduced to ∿80 eV to achieve maximum detection efficiency. ED

systems used for soft x-ray work are specially selected for their low noise properties but even these will have a noise level extending up to ∿200 eV. Consequently some noise counts will inevitably be introduced into the spectrum and a method of removing them must be found.

The extent of noise in a typical low energy spectrum obtained with the'threshold A' position as in the EDAX system, has been referred to earlier, see figure 5.7. Low x-ray counting rates produce proportionally large noise contributions but, if counting rates are high, dead time corrections and pulse pile-up effects become large. Hence a compromise is necessary whereby the noise level does not overwhelm the actual x-ray counts. For example with x-ray recording rates between 1000 and 2000 s^{-1} a noise level of 100 to 200 s^{-1} is acceptable. The threshold setting selected in the present investigations was 60 eV giving a noise count rate of ∿180 s^{-1}.

5.2.2 Study of the Noise Peak

Measurements were carried out at 15 keV on copper with the beryllium detector window in place. Spectra were recorded with the specimen current adjusted to give counting rates of 500, 1000, 1500, 2000 and 2500 s^{-1}, the analysis time being controlled in each case to give a total count of 200,000 over the energy range 0.2 to 16 keV. The composite figure 5.9a shows the region below 0.3 keV and it will be noticed that although as

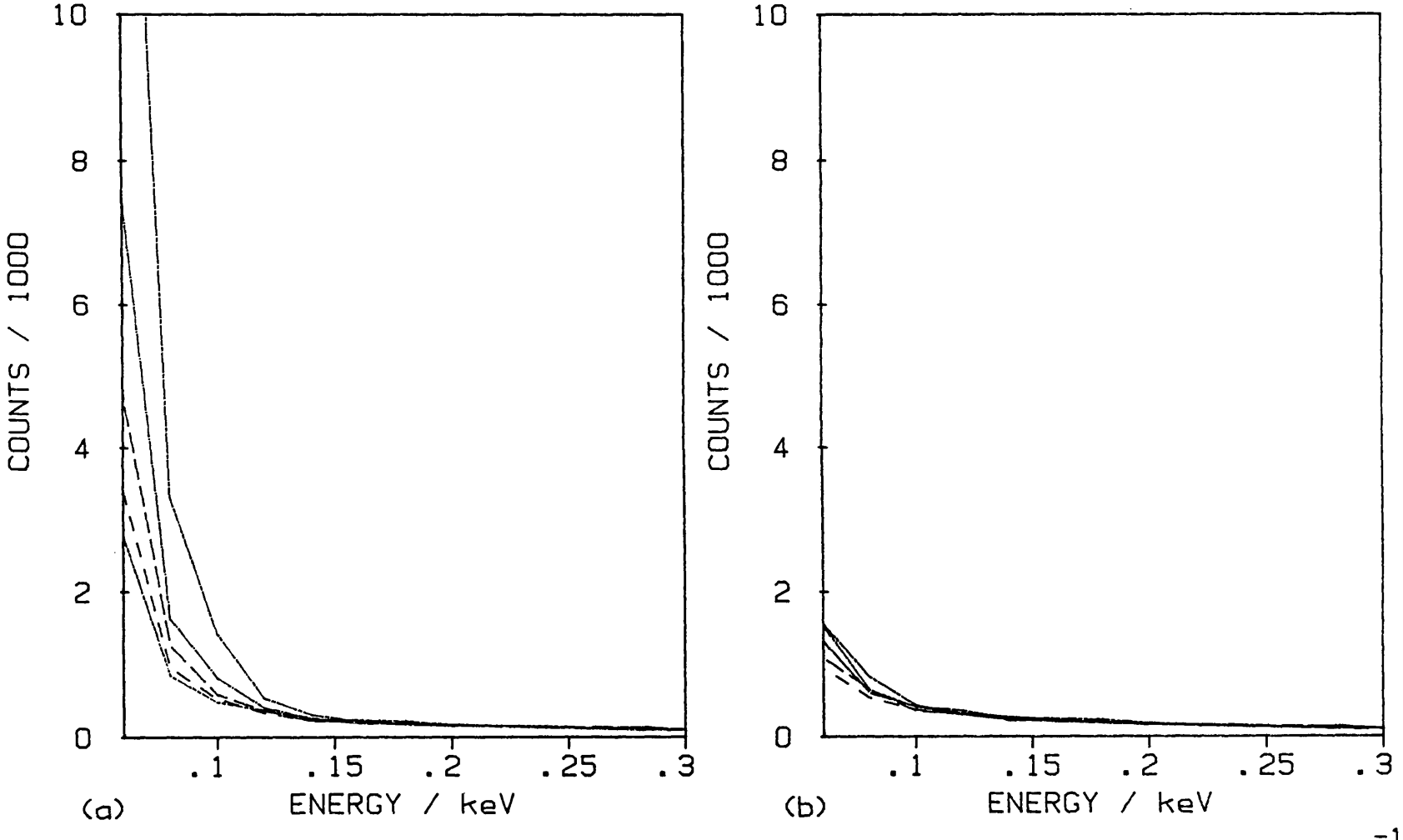

Fig. 5.9. Spectra obtained at different counting rates (500, 1000, 1500, 2000 and 2500 s^{-1}) but with the same total integrated counts of 200,000 ; copper specimen, 15 kV probe, beryllium window. (a) Original spectra. (b) Spectra after subtraction of noise counts.

expected the backgrounds are virtually identical, the number of noise counts increases with length of analysis time. The live time of every copper spectrum was next calculated (using the new method described in section 4) and by switching off the electron beam a noise spectrum was recorded for a period of 100 seconds. Finally the noise spectrum was scaled to match the live time of the respective copper spectra and subtracted channel by channel from each. Figure 5.9b, the copper spectra after subtraction, shows there is good agreement between residual backgrounds in every case. Hence it may be concluded that this background is independent of analysis time and is not produced by noise counts. Consequently, the method of live-time scaling of an independently measured noise peak has been adopted for noise removal in the present soft x-ray studies.

5.3 An Additional Component of the Background

5.3.1 Identification of a 'Spur'

Although the continuum would be expected to tail off towards zero energy because of the high absorption suffered by soft x-rays in both specimen and detector (detector window, gold coating and silicon dead layer), this is not evident from figure 5.9b. In fact there is an upturn in the spectrum at low energies which will be referred to as the 'spur'. The spur is independent of analysis time and count rate and cannot be attributed

to low energy characteristic x-rays because the beryllium window was in position when the data shown in figure 5.9b was obtained.

5.3.2 Characterisation of the Spur

In order to study the spur in more detail a wide range of electron accelerating voltages and specimens was used to determine whether they affected its shape and size. Figure 5.10a shows spectra after removal of noise, obtained from titanium at accelerating voltages of 7, 11, 15, 20 and 25 kV with the beryllium detector window in position. A recording rate of 2000 s^{-1} was used and, as before, a total of 200,000 counts was accumulated. It is evident from figure 5.10a that although the background level between 0.6 and 1 keV is markedly affected by probe voltage there is little systematic variation in the size and shape of the spur. Next a range of elements between atomic number 12 and 79 was analysed at 15 kV using the experimental conditions described above. After removal of noise the spur again appeared to be similar in all cases (figure 5.10b), suggesting that it is independent of specimen composition. A common factor with these spectra is that they were all of the same size (200,000 counts), which leads to the conclusion that the magnitude of the spur is directly proportional to the total number of counts in the spectrum.

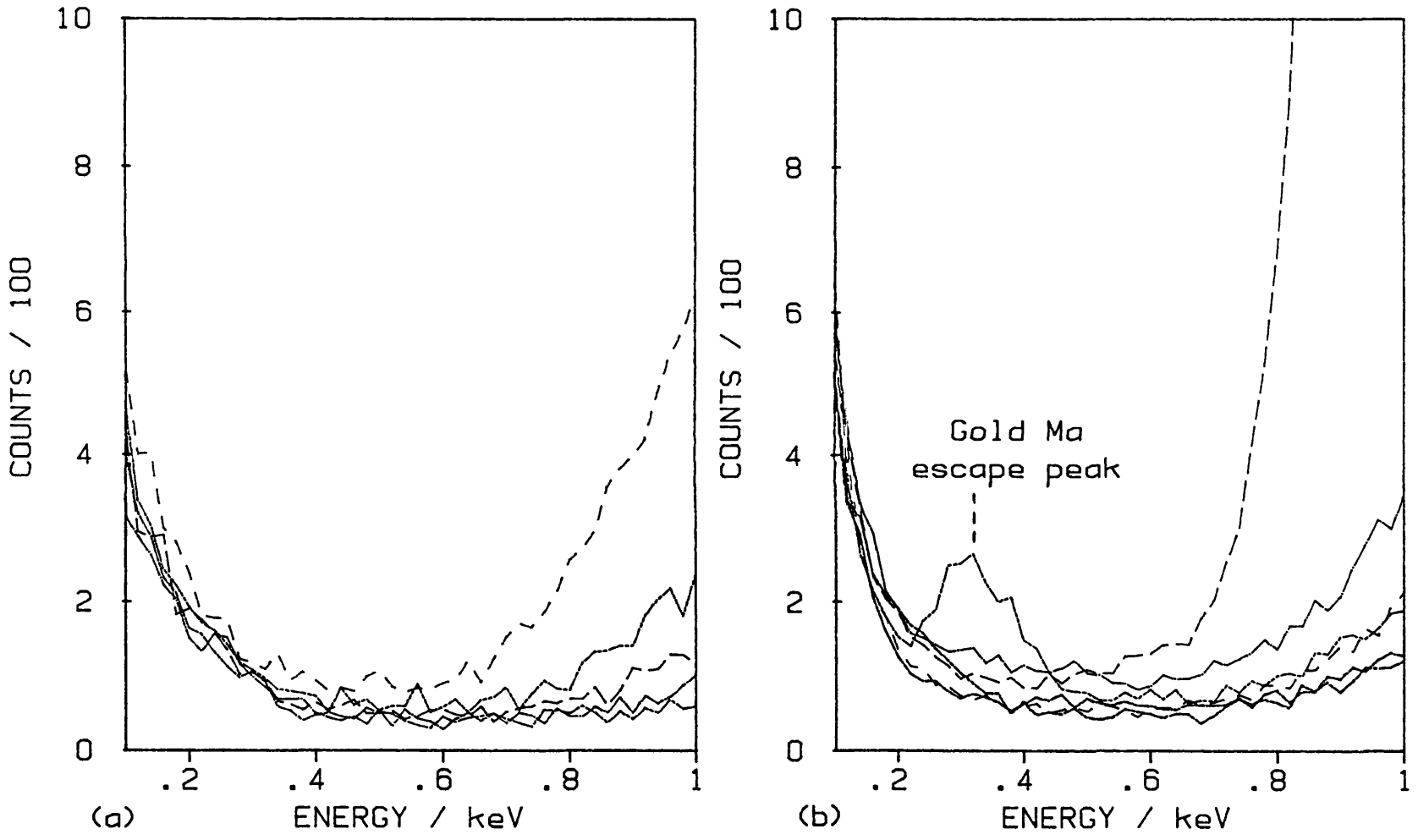

Fig. 5.10 Spectra after removal of noise counts; constant recording rate of 2000 s^{-1}, total integrated counts of 200,000, beryllium window. (a) Titanium at a range of kV (7, 11 15, 20 and 25). (b) Range of elements (Z= 12, 14, 22, 29, 74 and 79) with 15 kV probe.

5.3.3. Dealing with the Spur

The fact that the shape of the spur is virtually the same for a wide range of analysis conditions suggests that a mathematical curve might be used to model the spur and remove it from the spectrum. Because the spur increases at low energy, expressions of the form $y = aE^{-b}$ were compared with spectra over the energy range 0 to 250 eV where the contribution from continuum radiation was expected to be extremely low. The mathematical model was assessed by subtracting the computed spur from the spectrum and then looking for a smooth tail-off in the continuum over the energy range 1 to 0 keV. Figure 5.11 shows the final choice together with a typical spectrum obtained when using the beryllium window. The curve is $y = aE^{-1.5}$ where 'a' is a scaling factor which depends upon units of E. The results of subtracting the spur (scaled in terms of total x-ray counts) from the spectra shown in figures 5.9b, 5.10a and 5.10b are illustrated in figures 5.12a, b and c respectively. Now removal of both noise and spur produces a smooth tail-off in the background in accord with the theoretically predicted continuum distribution.

So far studies of the spur shape have been confined to spectra recorded with the beryllium window in place. When a formvar window is used instead or the window is removed altogether it is possible that the above equation may be inapplicable. Unfortunately under these conditions it is more difficult to examine the

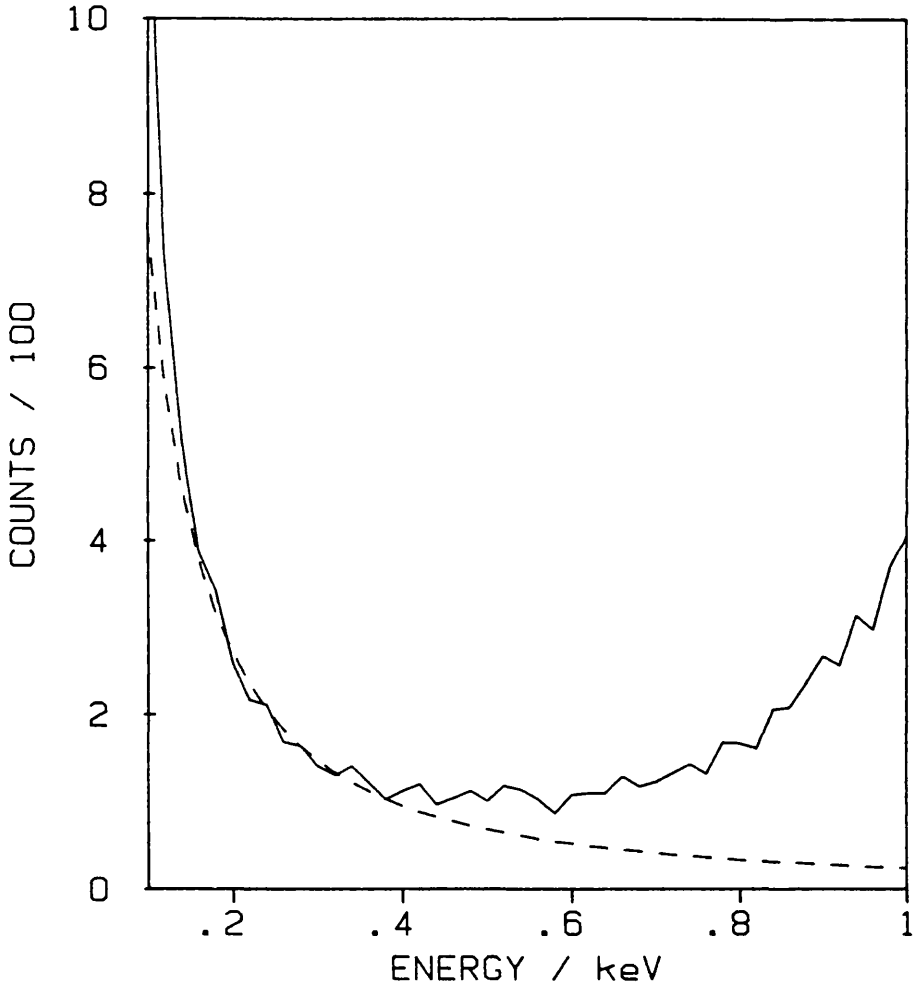

Fig. 5.11 Comparison of mathematical model for spur removal (dotted line) with typical spectrum (solid line). The difference between the two curves above 400 eV is due to continuum.

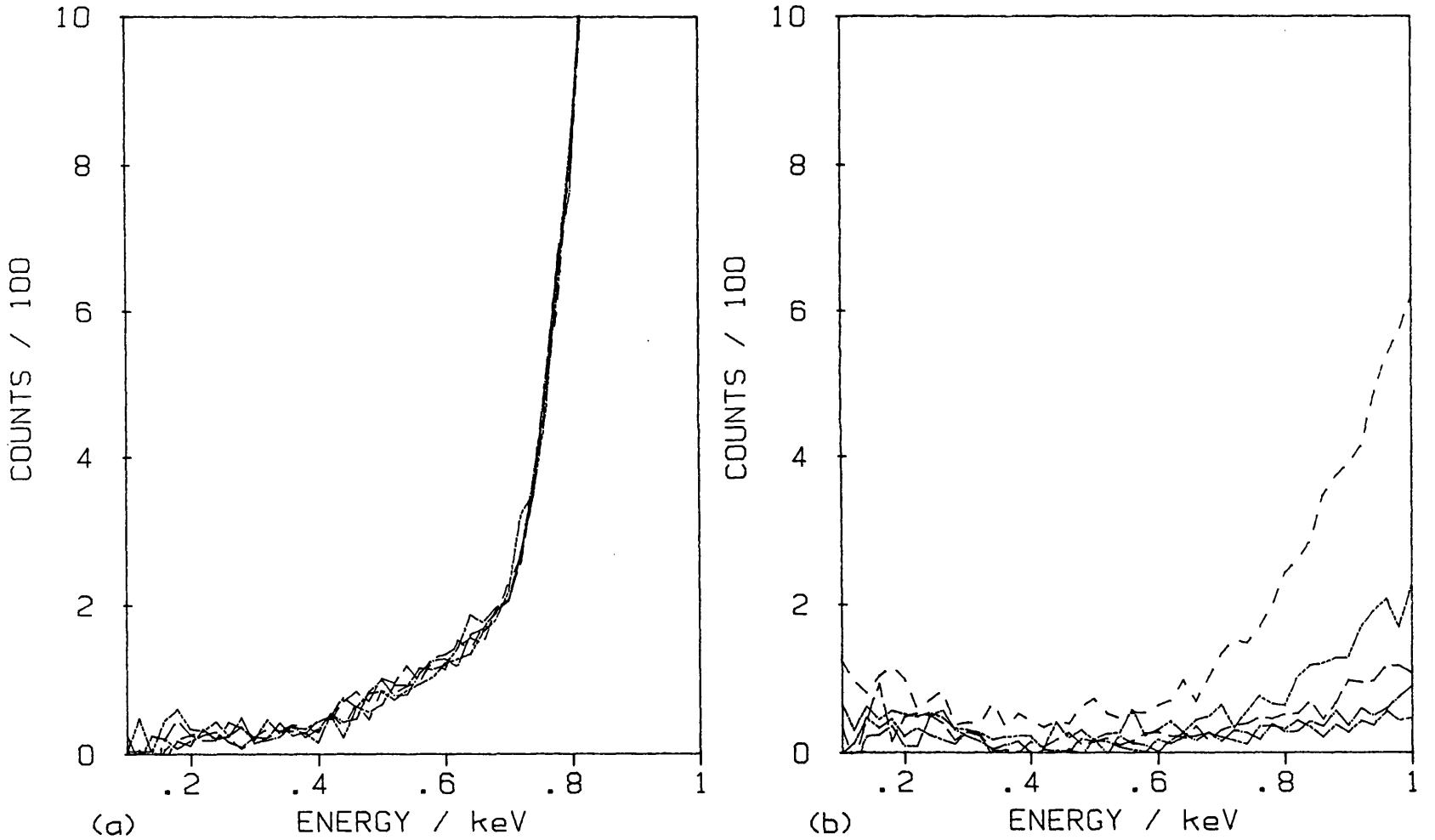

Fig. 5.12 Smooth continuum tail-off which remains after removing spur from (a) spectra in fig. 5.9b (different count rates), (b) spectra in fig. 5.10a (different probe voltages), and (c) spectra in fig. 5.10b (specimens with different atomic number).

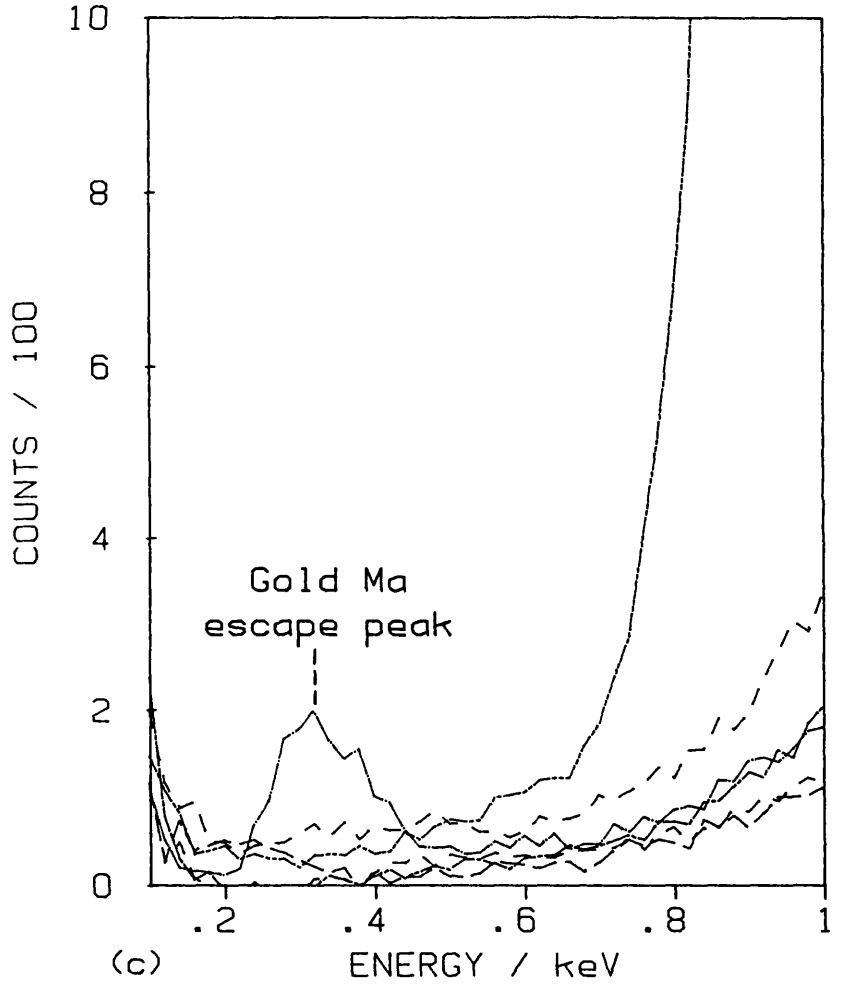

Fig. 5. 12 continued from previous page.

spur since it tends to become obscured not only by the consequent higher level of continuum but also by any small peaks of oxygen and carbon which may arise from contamination of the specimen.

However, figure 5.13a, the low energy portion of a silicon spectrum, reveals no evidence of contamination effects. Curve II was produced by subtracting noise and spur from curve I and indicates from the way the spectrum decays smoothly towards 0 keV that the equation still works satisfactorily. Figure 5.13b, a spectrum obtained from aluminium, shows the peaks from carbon and oxygen contaminants. It should be noted that after noise and spur removal the small carbon peak is much more clearly revealed. The figure also illustrates the need to use appropriate subtraction methods in order to establish peak intensities; obviously reliable intensity measurements could not be obtained prior to noise and spur removal.

5.3.4. Origin of the Spur

Because the artefact known as the spur occurs at low energies there is a possibility that it is associated with the dead layer of the Si(Li) detector where the charge collection efficiency is poor (Statham 1981a). Although the exact variation in efficiency (Ω) with depth (x) in the dead layer is not known it would be reasonable to assume that it varies from 1.0 in bulk

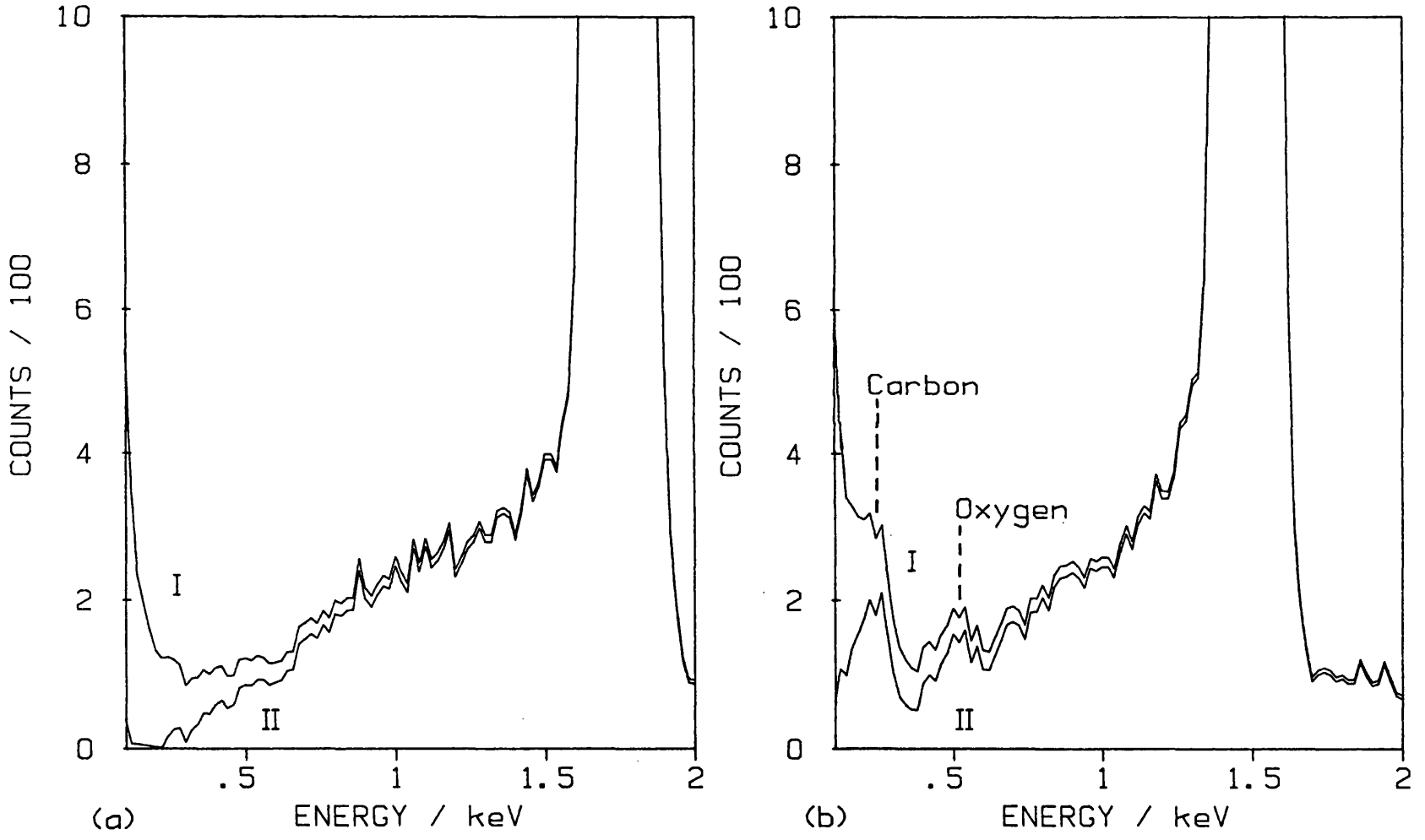

Fig. 5.13 Spectra before (curve I) and after removal of noise counts and spur (curve II) : 15 kV probe, formvar window, (a) silicon specimen and (b) aluminium specimen.

silicon to zero at the surface in a manner similar to that illustrated in figure 5.14a. To explain how absorption of x-rays in the dead layer affects the recorded x-ray energy it is helpful to consider the case of a mono-energetic beam incident on the detector. For convenience its energy is taken to be E_n, the energy of the n^{th} channel in the spectrum (figure 5.14c). The exponential curve in figure 5.14b describes the number of x-rays absorbed (N_x) as a function of depth (x) in the silicon. Most of the x-rays will be absorbed at depths greater than 0.22 μm and this number is represented by area A_n, in figure 5.14b. Because the efficiency of the detector is $\sim$ 100% here, these x-rays will be stored in the correct energy channel E_n of the multichannel analyser as shown in figure 5.14c. However when mono-energetic x-rays are absorbed at depths between 0.18 and 0.22 μm where the charge collection efficiency is significantly less than 1, counts will be stored in the lower energy channel E_{n-1} rather than E_n. The number of counts in the channels adjacent to E_n (E_{n-1}, E_{n-2} etc) are given by areas A_{n-1}, A_{n-2} etc. and each of these areas is successively smaller than the previous one. The counts in these channels are responsible for the low energy tails observed on x-ray peaks from light elements (B,C,N,O and F) and other x-ray lines which are strongly absorbed in silicon (e.g. S_k, P_k and Cl_k). Because efficiency of charge collection varies rapidly with depth between 0.08 and 0.12 μm the x-rays absorbed in this layer are

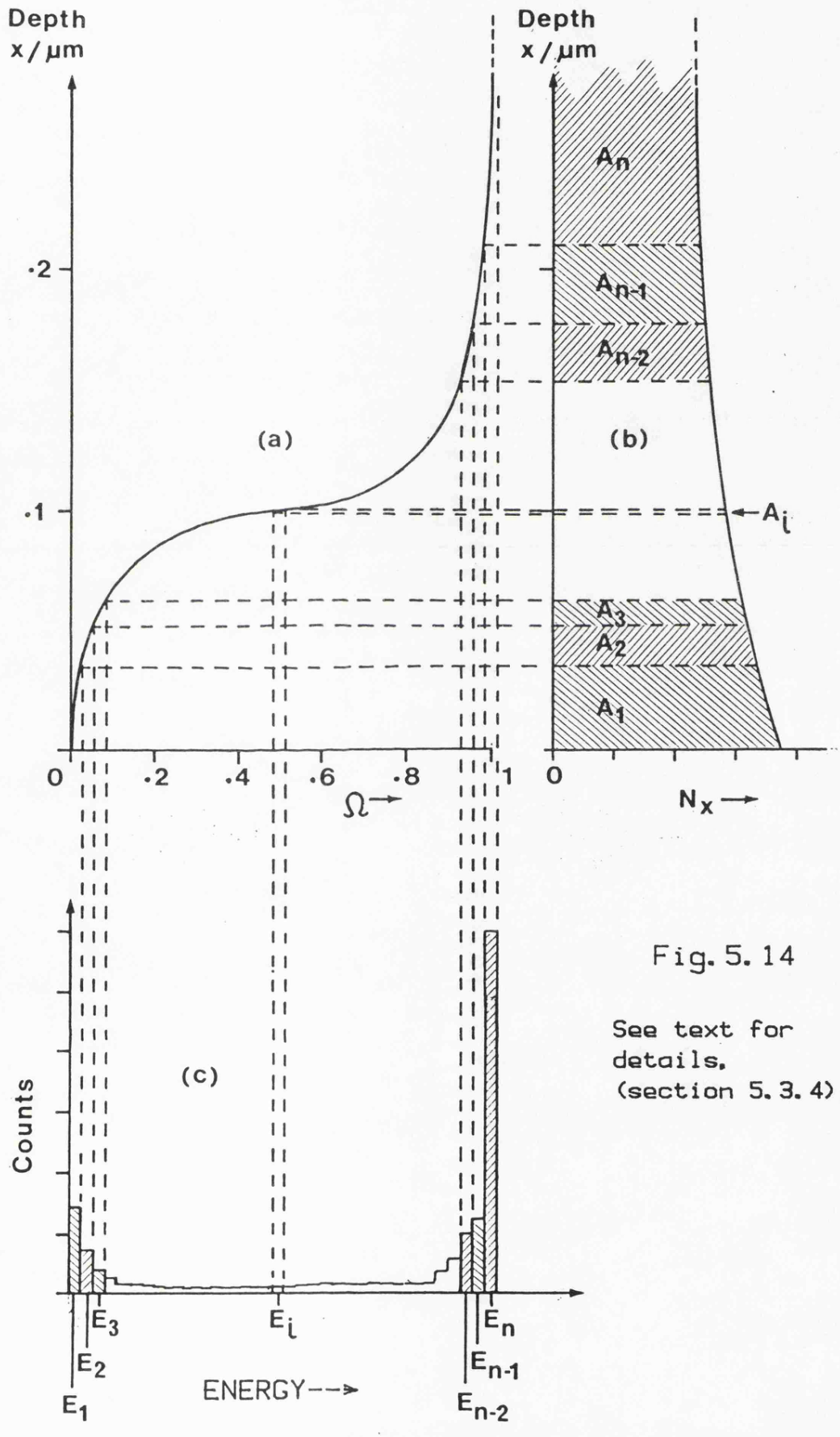

Fig. 5.14

See text for details, (section 5.3.4)

distributed over a wide range of spectrum channels although the number of counts in each channel is small (e.g. E_i in figure 5.14c). Finally, when the charge collection efficiency becomes less than 0.1 it changes more slowly with depth and x-rays absorbed in outermost regions of the dead layer ($x < 0.08$ μm) cause a rise in the recorded spectrum at low energies (channels E_1, E_2, E_3 etc in figure 5.14c).

Thus the hypothetical charge collection efficiency curve illustrated in figure 5.14a would result in a spur-like artefact. However it may be shown that if the dead layer is responsible then the size of the spur should be affected by the intensity and energy of the various x-ray lines comprising the spectrum. Since no such variation has been found here an alternative explanation must be sought.

Perhaps then the most likely cause of the spur is pulse distortion or ringing effects in the amplifier. Clearly such a problem would require solution by the manufacturers of the equipment.

6. DEVELOPMENT OF A NEW CONTINUUM PREDICTION METHOD

The techniques developed in the previous section allow noise and spur artefacts to be accounted for. Thus the final background component which must be dealt with in low energy ED spectra is the x-ray continuum.

6.1 Consideration of Existing Techniques

Several methods have been discussed already and basically fall into two categories, those which use mathematical filtering and those which attempt to predict the background shape. Although problems were anticipated with both types when processing soft x-ray spectra, several aspects of the filtering approach made it unsuitable for this work. Firstly, digital filtering does not give an explicit background level and any assessment of detection sensitivity requires accurate measurement of both peak and background intensity. Secondly, if filtering is employed, it becomes impractical to obtain reliable estimates of statistical errors in overlap deconvolution, (Statham 1977). Thirdly, filtering would be difficult in the vicinity of the carbon peak where the low energy cut off introduces a discontinuity in the spectrum. Finally, it was felt that background modelling was the more flexible approach offering greater scope for development.

6.1.1 Problems at Low X-ray Energies

Since continuum radiation is the principal constituent of the background in conventional ED analysis, there has been considerable effort to represent its shape accurately. However, Russ (1977a) has examined the effectiveness of established methods of calculating the continuum and has concluded that they are inadequate below 3 keV. This view is substantiated by Statham (1976) who, despite much work on the nature of the continuum found it extremely difficult to predict in the region below 2 keV. The situation becomes worse when carrying out soft x-ray analysis (Russ 1977b) because the continuum becomes larger and its curvature more pronounced. An additional complication is that calculation of the continuum requires a knowledge of the absorption characteristics of any detector window employed and of surface layers on the Si(Li) crystal itself. Furthermore, absorption may alter if significant contamination occurs on these surfaces from condensation of vapours present in the vacuum system (Love, Scott, Dennis and Laurenson 1981) or when the thin plastic detector window is replaced by another. However, an alternative approach to background prediction, proposed by Smith, Gold and Tomlinson (1975) and Smith and Gold (1976) eliminates the need to establish the absorption characteristics of the detector.

6.1.2 Reference Standard Method of Smith et al

This technique, which was outlined in section 2.3.3 is based on the use of a continuum spectrum from a reference standard. The continuum is modified channel-by-channel, using atomic number and absoption corrections, to produce a 'normalised' continuum. (Smith et al used the term 'normalised background' whereas the more specific term 'normalised continuum' is used in this work since spectral backgrounds generally consist of x-ray continuum plus artefacts). The continuum intensity for the specimen of interest is then determined by modifying the 'normalised' continuum with corrections relevant to the specimen. An advantage of the Smith method, especially important with soft x-ray analysis, is that the detector efficiency is incorporated in the spectrum obtained from the reference specimen and therefore need not be explicitly known. Moreover, any change in detector efficiency may be easily taken into account by re-recording the reference spectrum.

In order to correct the continuum distribution for absorption effects Smith et al used a method commonly employed in ZAF programs, namely that of Philibert (1963). The absorption factor, $f(\chi)$ is given by

$$f(\chi) = \{(1 + \chi/\sigma)\ (1 + \frac{h}{1+h}\ \chi/\sigma)\}^{-1}\ ;$$

$h = 1.2\ A/Z^2$ where A and Z represent the mean atomic

weight and mean atomic number of the specimen respectively;

$\sigma = \frac{4.5 \times 10^5}{E_o^{1.65} - E_\nu^{1.65}}$ where E_o is the incident electron energy and E_ν is the energy of the continuum radiation being corrected for absoption; $\chi = (\frac{\mu}{\rho})_{E_\nu} . \text{ cosec } \theta$, where θ is the x-ray take-off angle and $(\frac{\mu}{\rho})_{E_\nu}$ is the mass absorption coefficient for x-rays of energy E_ν in the specimen.

The atomic number correction for the continuum was treated by Smith et al in two parts. Firstly losses in continuum production arising from electron backscattering were calculated using backscatter factor (R) values given by Rao-Sahib and Wittry (1974). Secondly a correction factor, analogous to the stopping power factor (S) used in the conventional ZAF correction theory for characteristic radiation, was determined. This latter factor involves the efficiency with which electrons remaining in the specimen produce x-rays and is dependent upon the energy of the electron at each point along its path and the corresponding cross section for x-ray generation. Early theoretical work by Kramers (1923) based upon the Thomson-Whiddington law for electron retardation and a mainly classical approach to the calculation of the scattering cross section led to,

$$I_\nu = KZ \frac{(E_o - E_\nu)}{E_\nu}$$

I_ν refers to the number of continuum x-rays with energy E_ν generated per second per electron, E_o is the incident beam energy and K is a constant. Smith et al found that this expression was not sufficiently accurate and investigated the use of a modified version, derived by Rao-Sahib and Wittry (1974) using the Sommerfeld cross section and Bethe retardation law;

$$I_\nu = KZ^n \left(\frac{E_o - E_\nu}{E_\nu} \right)^X \qquad (6.1)$$

with X = 1.11 and n ranging from 1.2 to 1.37 depending on Z, E_o and E_ν. Smith et al (1975) and Smith and Gold (1976) reported initially that X was close to unity and

$$n = 1.159 + (.1239 - .02857 \ln E_o)(E_\nu - 2.044) \qquad (6.2)$$

but in later work (Smith and Gold 1979) new expressions for X and n were given, both being functions of Z, E_o and E_ν.

6.2 Development of the Reference Standard Method for Soft X-rays

The method of Smith et al was felt to be the most promising for predicting continuum in low energy ED

spectra. This was partly because the detector efficiency, which is difficult to predict, is incorporated in the spectrum from the standard. But in addition, it is often possible to select a standard close in atomic number to the specimen, thereby minimising the differences in continuum shape which have to be calculated. This provides a greater degree of flexibility than methods based on explicit calculation of continuum intensity which must attempt to cover a wide range of specimens and experimental conditions with a single expression.

The reference standard method was developed by Smith et al for predicting x-ray continuum above 1.5 keV. In order to extend its range of applicability to energies below 1.5 keV, further development was carried out on absorption and atomic number corrections. The use of these corrections was then examined, with spectra from various specimens, to determine the best method for obtaining normalised continuum spectra which are independent of specimen. Finally this technique was combined with methods developed in section 5 for dealing with noise and spur artefacts, to predict complete spectral backgrounds which extend down to 0.1 keV.

6.2.1 Matrix Absorption

Instead of using the Philibert absorption correction, it was decided to adopt the method of Love and Scott (1978) since the latter should be more accurate when dealing

with low energy x-rays and large absorption effects. Here the absorption correction is given by

$$f(\chi) = \frac{1-\exp(-2\chi\overline{\rho z})}{2\chi\overline{\rho z}} \quad , \quad \text{where}$$

$\overline{\rho z}$ is the mean depth of x-ray generation and is represented in terms of the electron backscatter coefficient, the maximum path length of an electron in the specimen and the overvoltage ratio (E_o/E_ν) . As with the Philibert model, the Love-Scott absorption correction was designed to deal with characteristic radiation rather than continuum. The distribution with depth in the specimen of continuum x-rays is, however, slightly different from characteristic x-rays, the mean depth of x-ray production being a little larger for the former (Reed 1975b). Fortunately, the two distributions are of similar shape and therefore until continuum distributions are known with greater certainty the mean depth appropriate for characteristic radiation has been used in the above formula for $f(\chi)$.

In order to apply the absorption correction, the matrix mass absorption coefficient is required for each spectrum channel energy. For energies above 1.2 keV the empirical expression

$\mu/\rho = C\lambda^n$ is often used, where λ is the x-ray wavelength, n is a constant between a particular set of absorption edges and C is a function of the

absorber and the set of absorption edges bounding λ; tabulations of C and n have been produced by Heinrich (1966).

Although soft x-ray absorption coefficients for most characteristic line energies have been determined by Henke and Ebisu (1973) no expressions exist for calculating intermediate values. A non-linear regression algorithm (Ralston and Rabinowitz 1978) was therefore used to generate polynomial least-squares approximations to these data. Initial attempts using polynomials in energy (E) were found to give poor agreement with experimental results unless the order was at least as high as five. This is illustrated in plots of μ/ρ versus energy, figures 6.1 a and b, where third and fifth order polynomial expressions are compared with the absorption coefficients of silicon. RMS percentage errors are 30 and 6 respectively. Even the fifth order polynomial shows poor agreement and whilst polynomials of higher order produce less deviation they still behave erratically between data points. Clearly a different approach is required if a useful accuracy of $\sim$1% is to be achieved. The method finally adopted uses a third order polynomial in E^p rather than E. Least squares regression analysis indicated the optimum value for silicon was $p = -1.14$. Figure 6.1c, the third order polynomial fit, shows that the curve is well behaved and that there is good agreement (RMS percentage error 0.8) with the results of Henke and Ebisu. A full set of polynomial

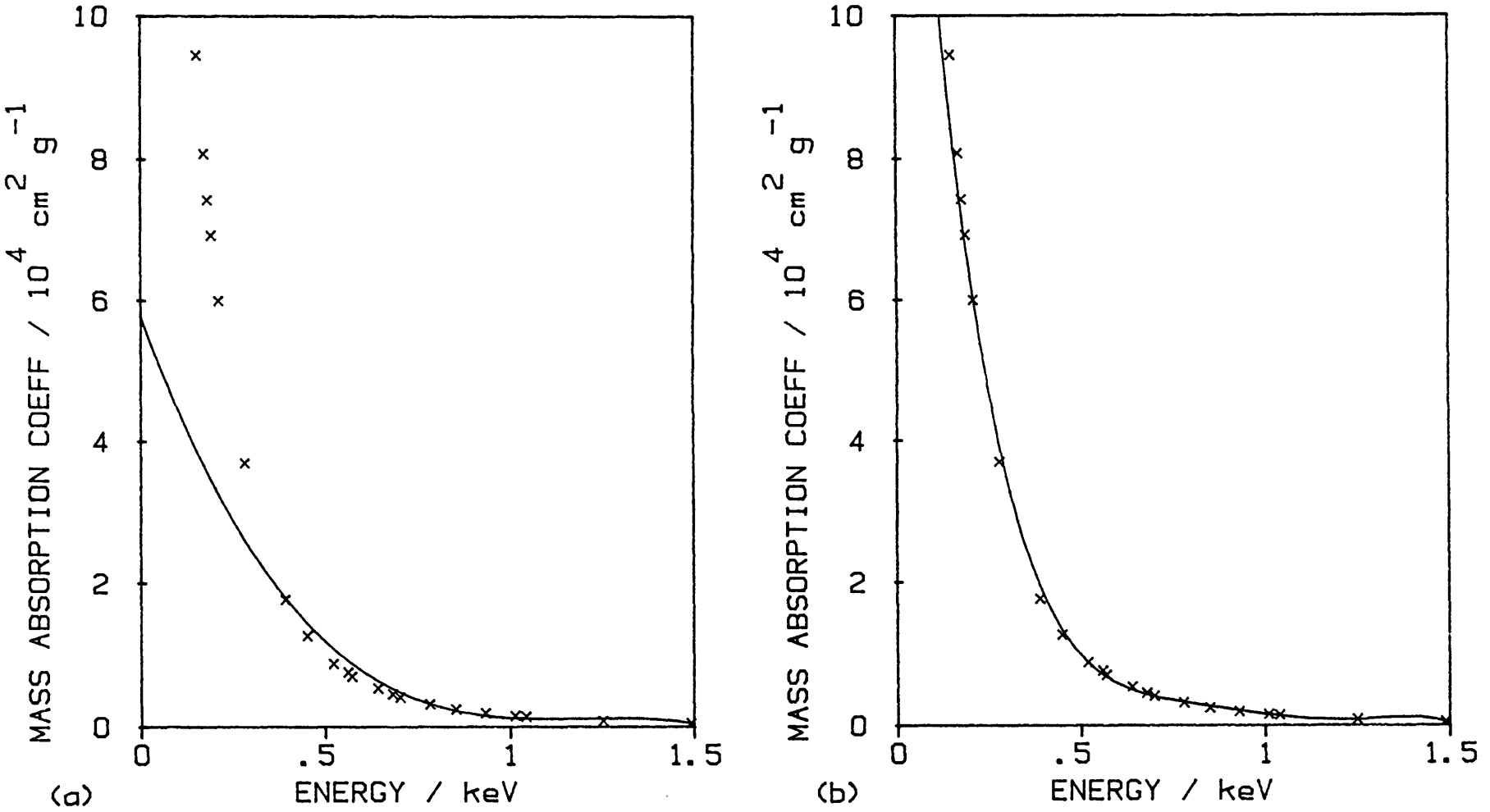

Fig. 6.1 Mass absorption coefficient for silicon absorber, showing experimental data (x) from Henke and Ebisu (1973). The curves are polynomial least squares approximations to the data; (a) third order in E, (b) fifth order in E, and (c) third order in $E^{-1.14}$.

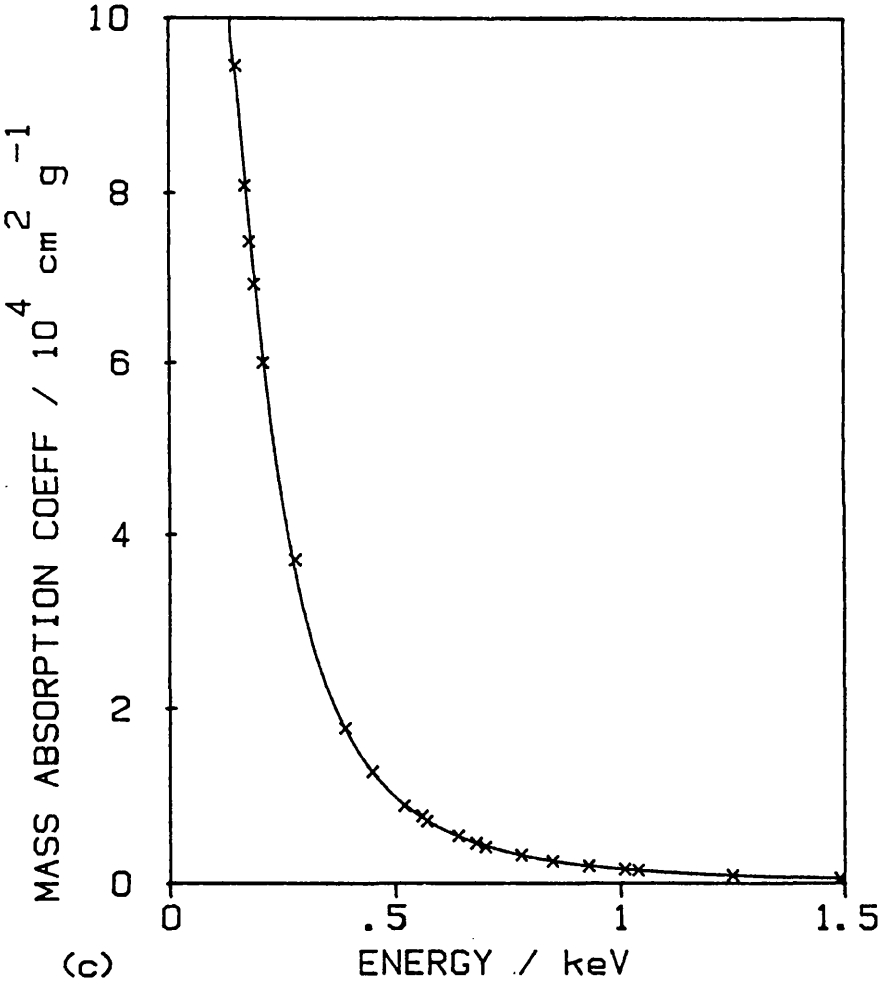

Fig. 6.1 continued from previous page.

parameters for each element was obtained in a similar manner. These data were then combined with the C and n tabulation of Heinrich (suitable for x-rays > 1.2 keV) to provide a means of rapidly calculating absorption coefficients for a range of x-ray energies from 0.1 to 25 keV in any element.

This data base for mass absorption coefficients was combined with the Love-Scott absorption model into a computer programme to correct, sequentially, each spectrum channel for the effects of absorption by the matrix.

6.2.2 Atomic Number Effects

Unlike the backscatter corrections used in conventional ZAF procedures, which relate to characteristic radiation, the R values given by Rao-Sahib and Wittry (1974) were determined specifically for continuum radiations. This suggests that they would be particularly useful in this work, but unfortunately, these R values cover a limited range of overvoltage (E_o/E_ν) from 1 to 10. Thus when working with a 15 keV probe, R values will not be available below 1.5 keV. Extrapolation to lower energies would be possible but could introduce errors when considering energies as low as 0.1 keV. The alternative was to use a backscatter factor for characteristic radiation which was applicable to the low energy region. It appears that R values given by the approach of Love, Cox and Scott (1978) and Love and Scott (1978) agree well with those

of Duncumb and Reed (1968) and are in fact very similar to those for continuum given by Rao-Sahib and Wittry (1974). It was therefore decided to use the method developed by Love et al in which R is calculated from the backscatter coefficient (η) in the expression

$$R = 1 - \eta\left[I(U_o) + \eta G(U_o)\right]^{1.67}$$

I and G are functions of overvoltage U_o ($U_o = E_o/E_\nu$) and η is determined from an expression involving Z and E_o.

Two methods of correcting for atomic number were investigated. The first was to use equation (6.1) taking X as unity, as proposed by Smith et al, giving a dependence of I_ν upon Z^n with n calculated for each channel energy from equation (6.2). The second involved setting n equal to unity which effectively assumes a dependence of I_ν on Z as given by Kramers' law.

6.2.3 Obtaining Normalised Continuum Spectra

The correction factors discussed in the two previous sections were used, individually and collectively, on continuum spectra from a range of specimens. The results indicated that because of the strong influence of absorption edges, the absorption correction was most significant in correcting the continuum shape. Spectra corrected only for absorption showed large differences in size but these were found to be very nearly

proportional to atomic number Z. Thus channel by channel division of spectra by the absorption factor and Z (equivalent to the use of Kramers' Law) appeared successful in eliminating specimen dependent effects. This is illustrated in figure 6.2a, for silicon and copper specimens, showing good agreement between the continuum levels in the corrected spectra. Figure 6.2b shows the result of a further division by backscatter factors, giving a slightly poorer agreement.

If the absorption and backscatter corrections are retained, but the Z factor replaced by the Z^n term proposed by Smith et al then good agreement is again achieved, as shown in figure 6.2c.

The corrections for backscattering would be expected to become more significant as the difference in specimen atomic number is increased. This was found to be the case. Figure 6.3a shows the result of dividing silicon and tin spectra by absorption factors and Z; it is apparent that the continuum from tin is reduced at low energies due to greater backscattering loses. Additional use of a backscatter correction for each spectrum improves the agreement as shown in figure 6.3b. If, however, the Z term is replaced by the Z^n of Smith et al the agreement becomes worse again as in figure 6.3c.

Similar results were obtained with other specimens and probe voltages. It was therefore concluded that

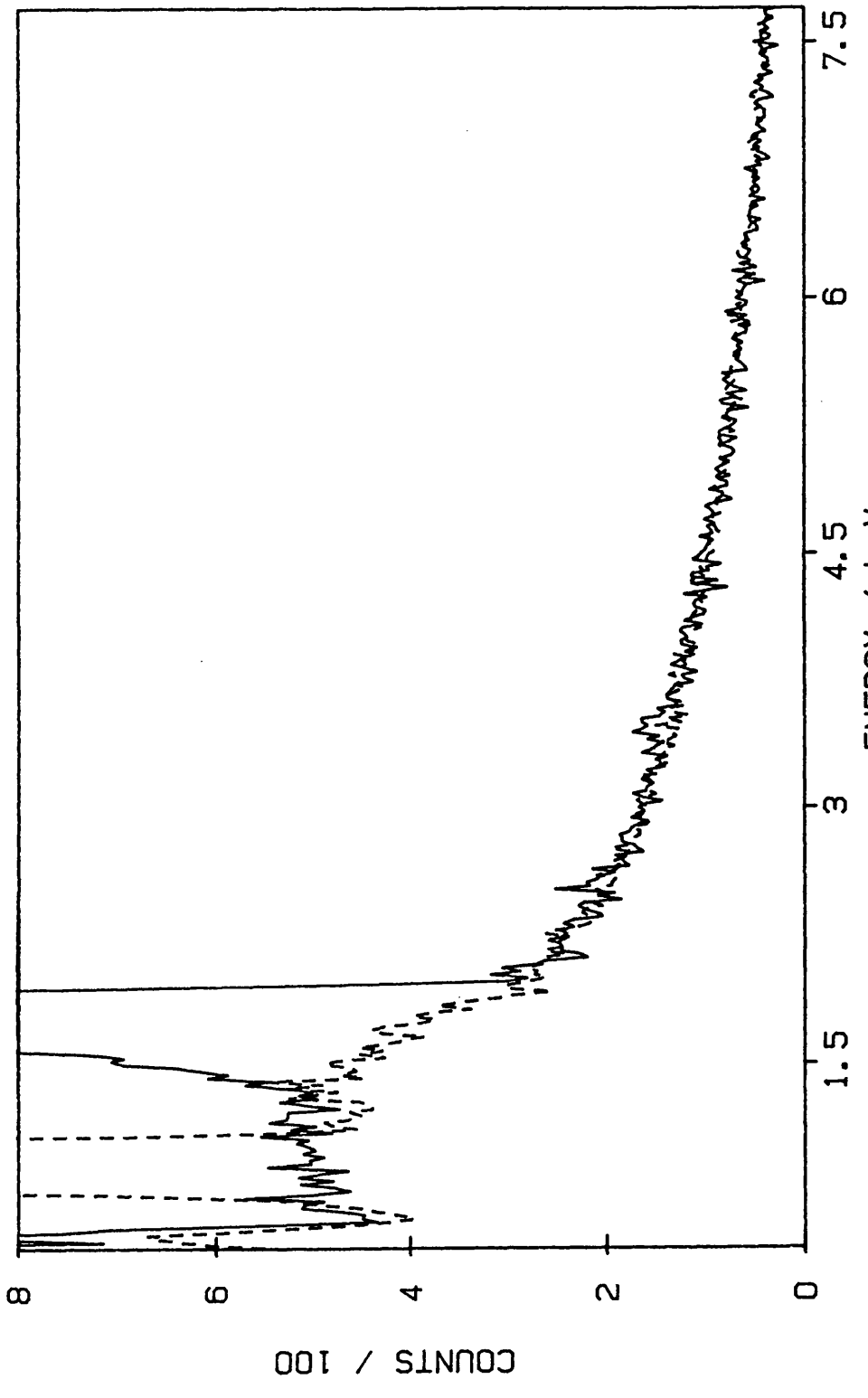

Fig. 6.2a Comparison of spectra from silicon (solid curve) and copper (dotted curve) after dividing through by absorption factor and Z. Formvar window, 15 kV probe.

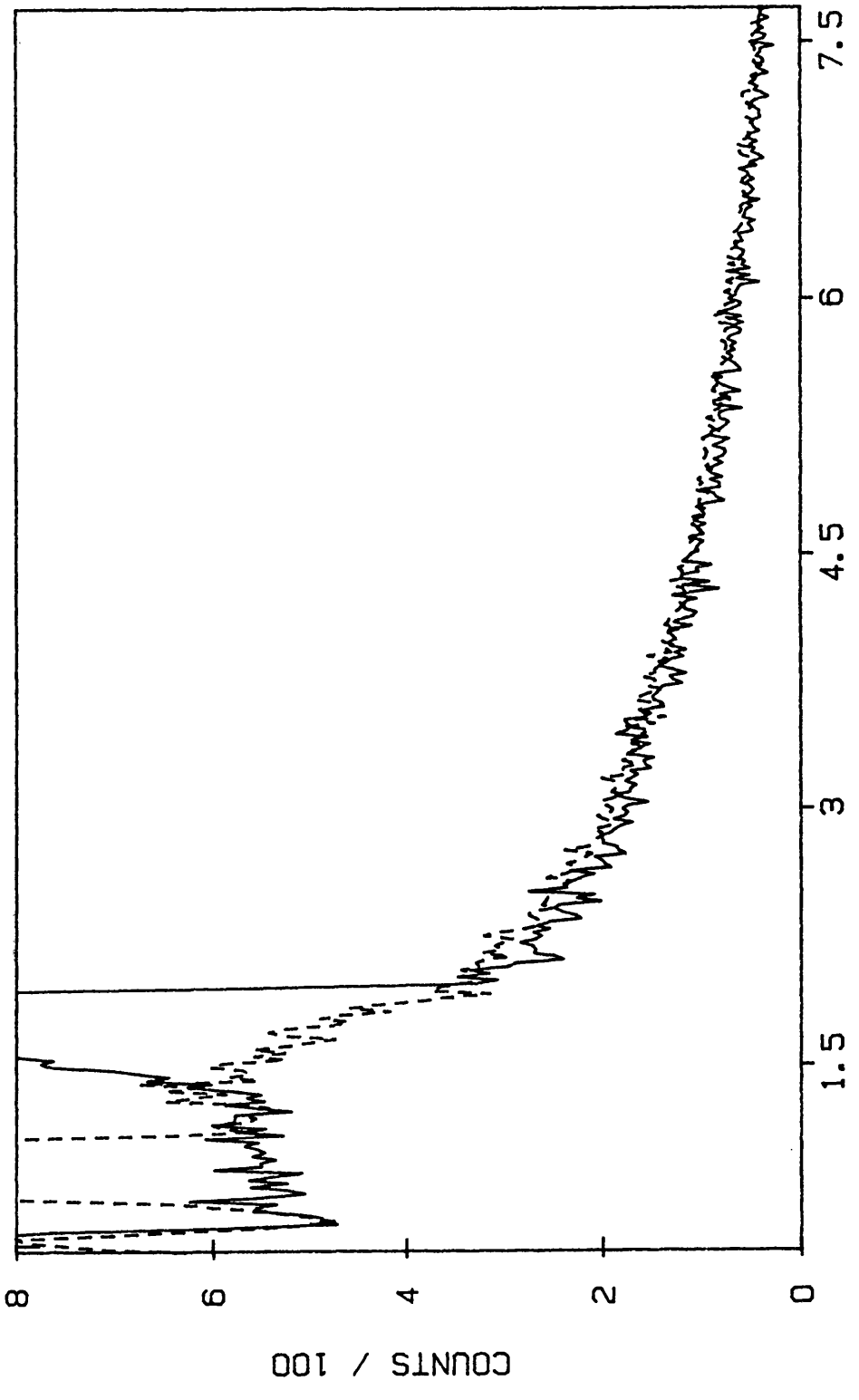

Fig. 6.2b Comparison of spectra from silicon (solid curve) and copper (dotted curve) after dividing through by absorption and backscatter factors and Z. Formvar window. 15 kV probe.

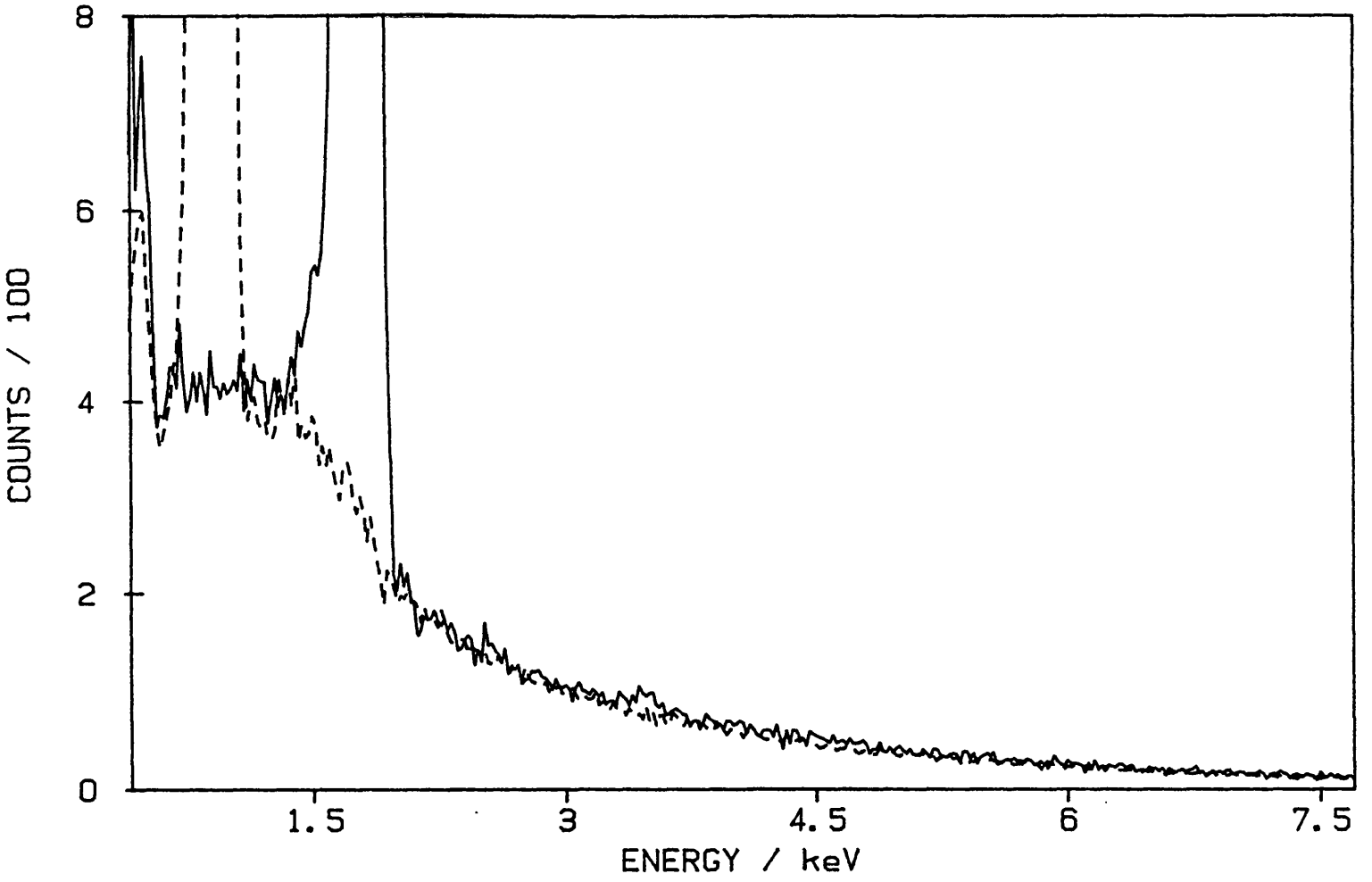

Fig. 6.2c Comparison of spectra from silicon (solid curve) and copper (dotted curve) after dividing through by absorption and backscatter factors and Smith's Z^n factor. Formvar window, 15 kV probe.

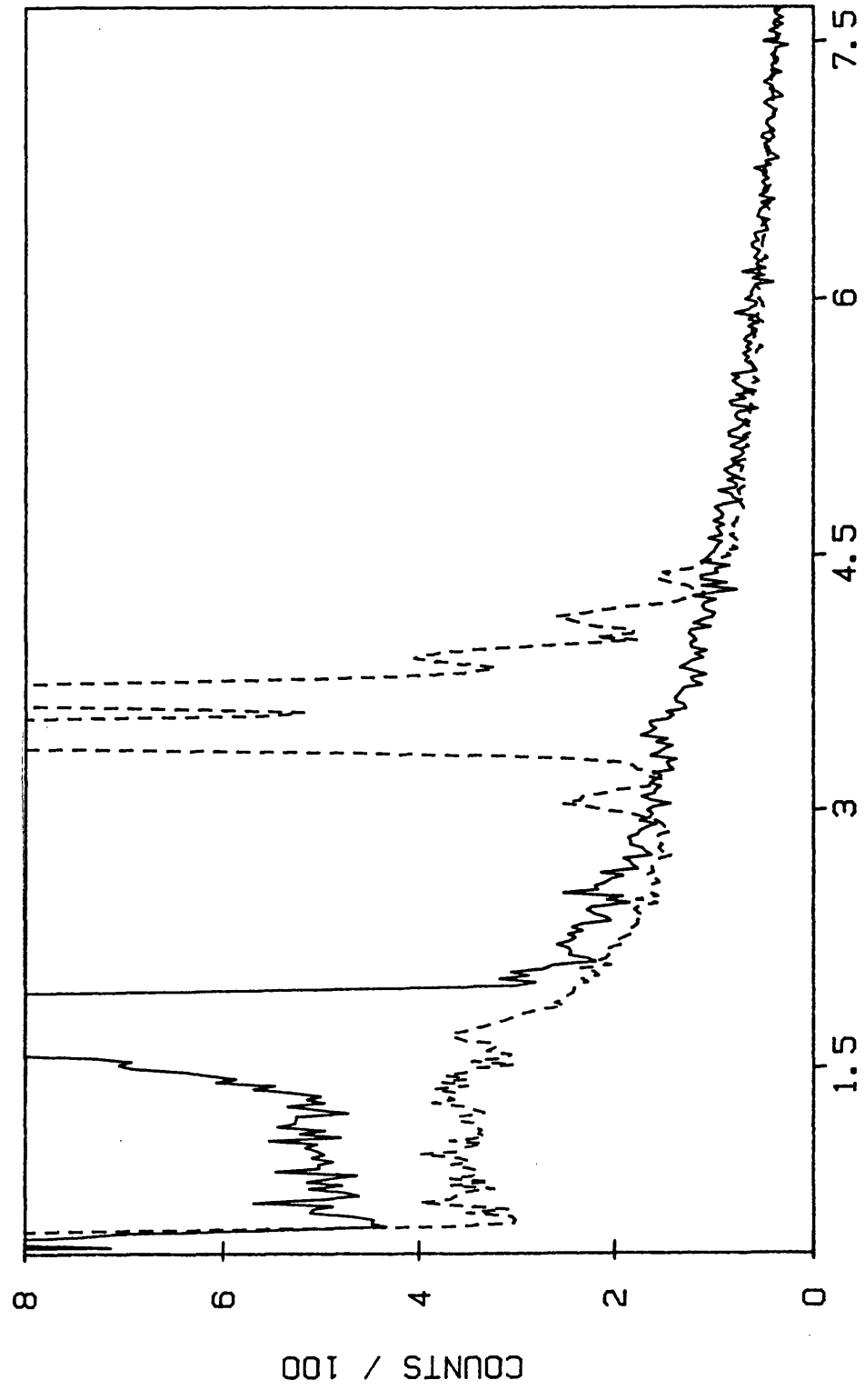

Fig. 6.3a Comparison of spectra from silicon (solid curve) and tin (dotted curve) after dividing through by absorption factor and Z. Formvar window, 15 kV probe.

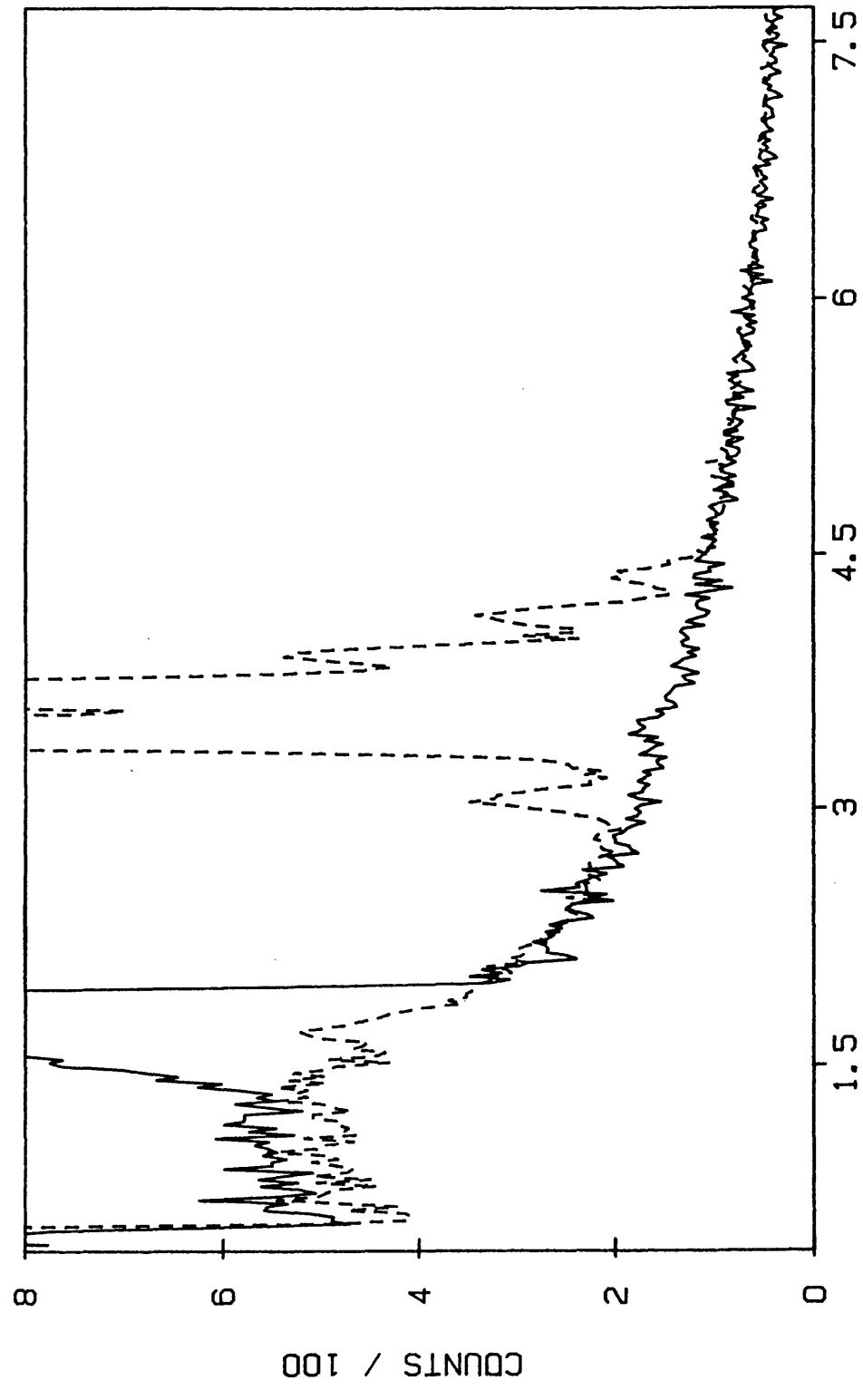

Fig. 6.3b Comparison of spectra from silicon (solid curve) and tin (dotted curve) after dividing through by absorption and backscatter factors and Z. Formvar window, 15 kV probe.

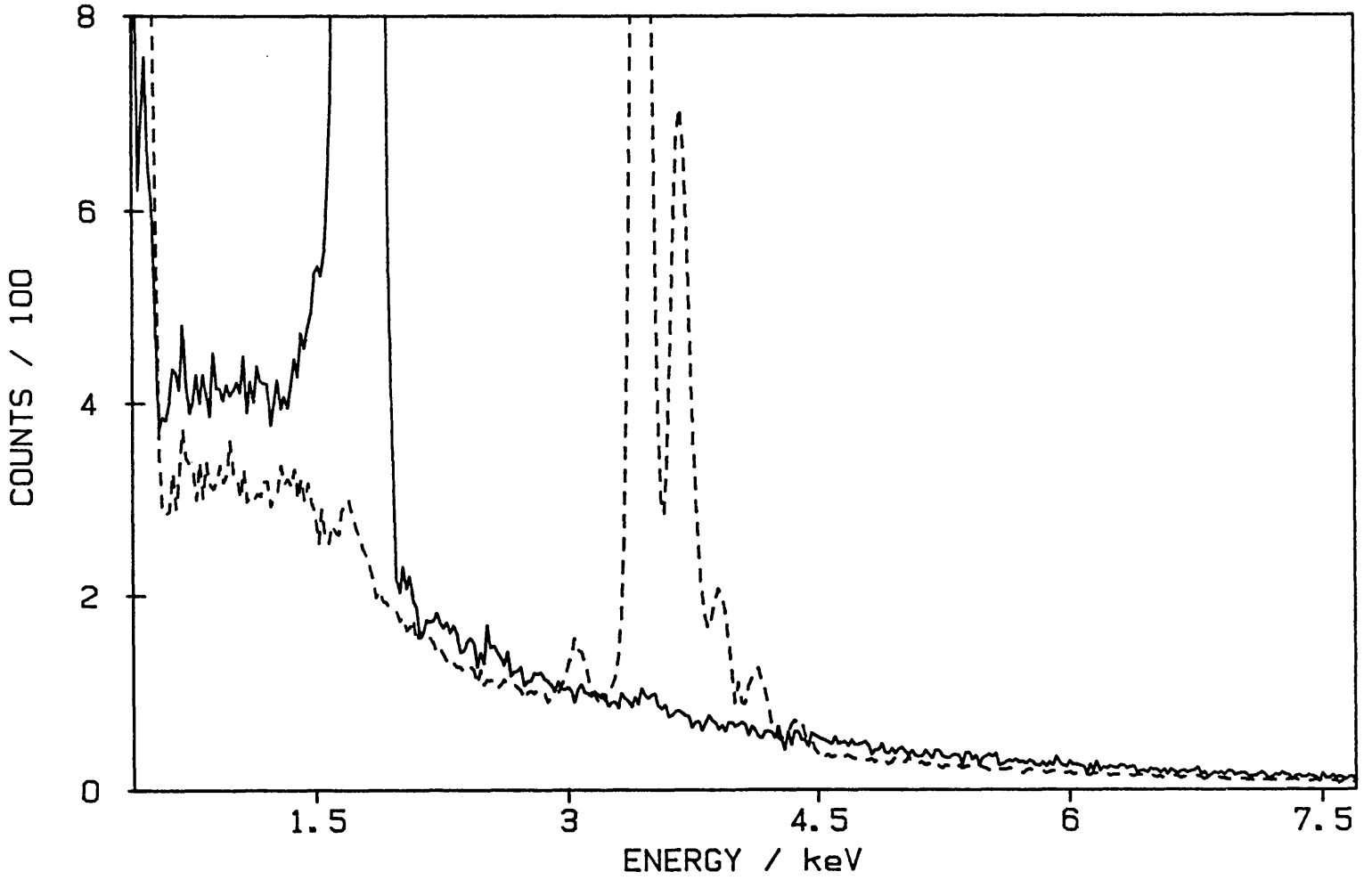

Fig. 6.3c Comparison of spectra from silicon (solid curve) and tin (dotted curve) after dividing through by absorptian and backscatter factors and Smith's Z^n factor. Formvar window, 15 kV probe.

channel by channel division by the absorption factor and Z could be used to produce a 'normalised' continuum spectrum from a given standard. This normalised spectrum would then be correct for other specimens over a useful range of atomic numbers, such as Z/2 to 2Z. Furthermore a wider range of validity can be achieved, if necessary, by use of the backscatter correction.

6.2.4 Use of the Reference Standard Method

A standard is required, to give a reference spectrum which does not contain peaks in the energy range of interest (0 to 1.0 keV in light element analysis). Silicon is a good choice although if the specimen has a high mean atomic number it may be preferable to select a heavier element in order to minimise errors in calculating the background.

The reference spectrum is obtained at the same accelerating voltage and sample inclination used when recording the spectrum from the specimen; live time is determined and both noise and spur artefacts subtracted. Next, the continuum is modified as described earlier, to take account of the different absorption and atomic number of specimen and standard. Finally, the background of the specimen is completed by adding to the continuum the appropriate contributions from noise and spur.

Backgrounds calculated using this procedure are illustrated in figures 6.4 and 6.5 for specimens of silicon and germanium respectively. The calculated backgrounds agree well with experimental data over this energy range even when the reference standard and specimen differ widely in atomic number. Figure 6.6 shows a practical example of the technique applied to a spectrum containing low concentrations of light elements, in this instance from carbon and oxygen in a contamination layer on the surface of aluminium. It should be noted that the background beneath the carbon peak (figure 6.6a) is very different from that given by linear interpolation and that after background subtraction (figure 6.6b) both carbon and oxygen peaks are clearly resolved.

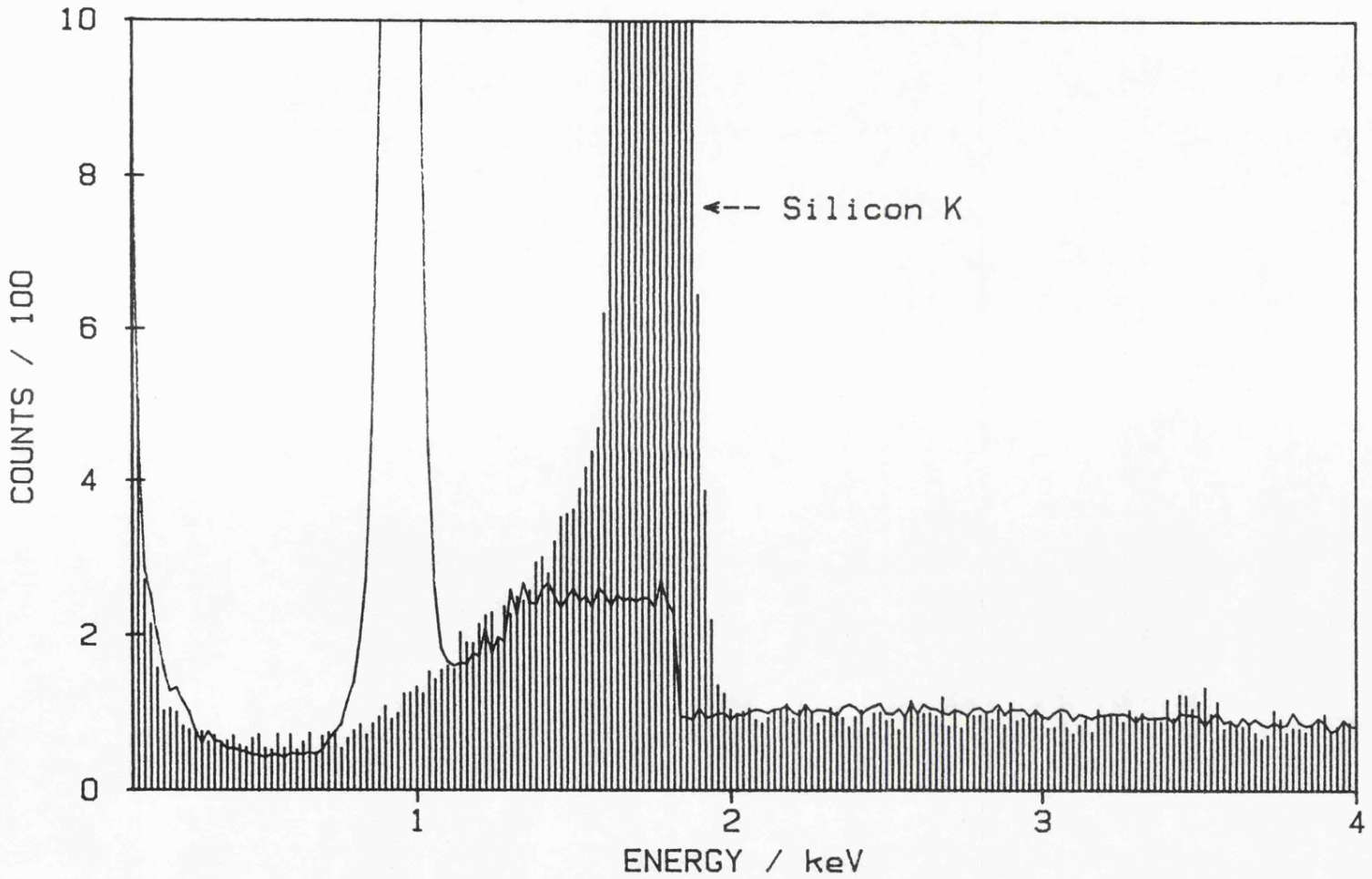

Fig. 6.4 Calculated background (continuous line) based on the continuum reference method. Silicon specimen and copper reference standard; beryllium window. 15 kV probe.

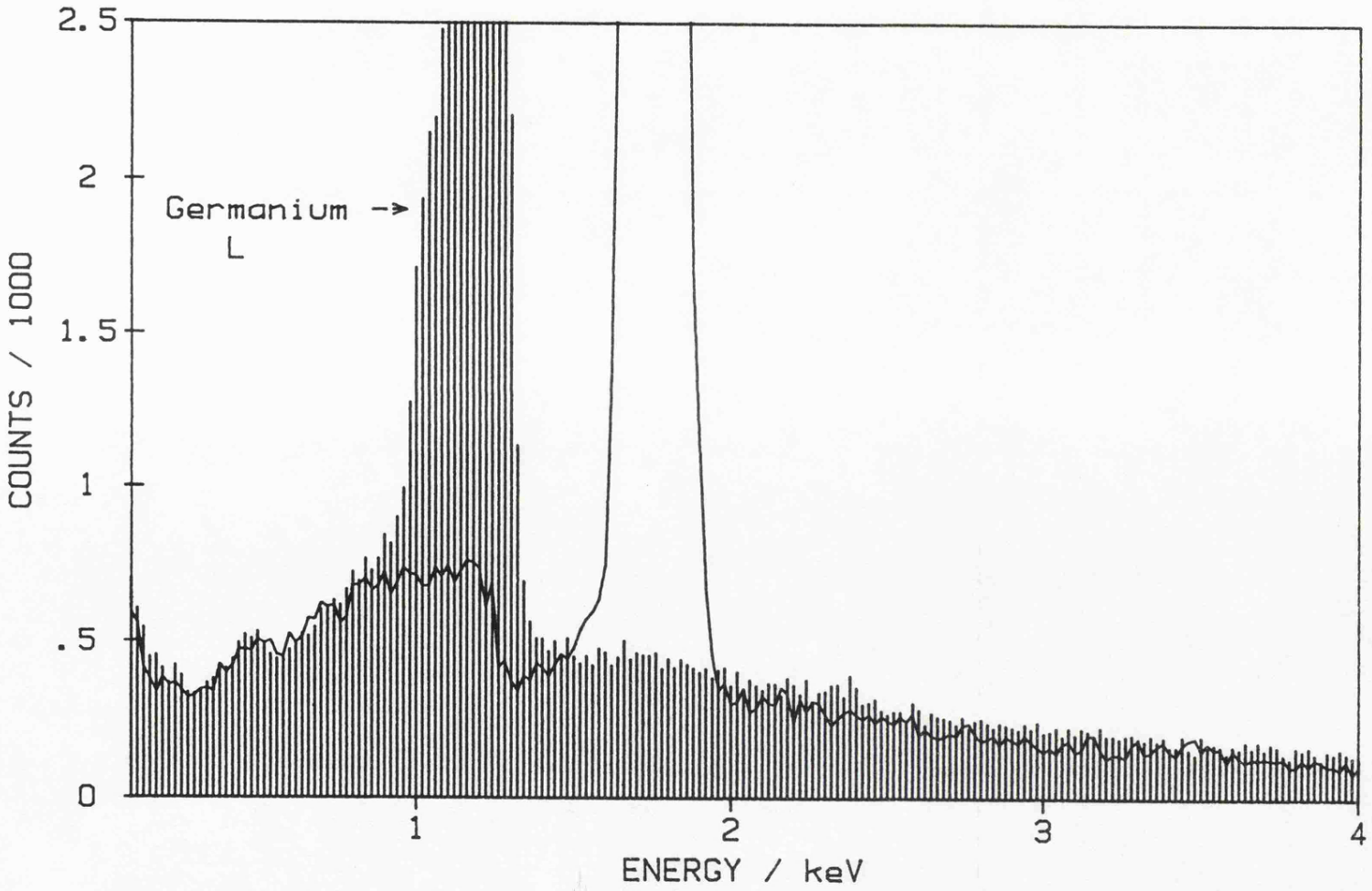

Fig. 6.5 Calculated background (continuous line) based on the continuum reference method. Germanium specimen and silicon reference standard ; beryllium window. 7 kV probe.

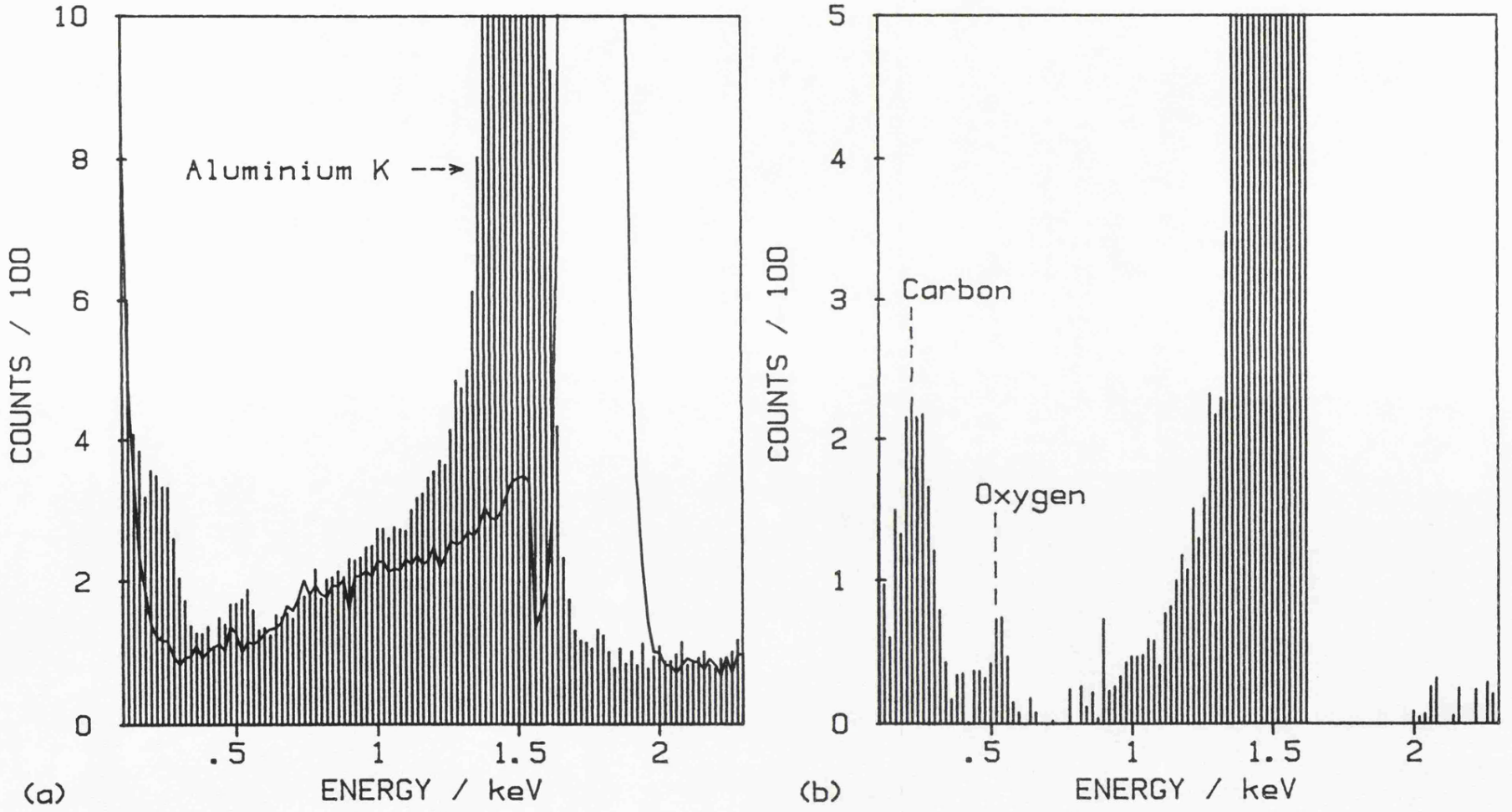

Fig. 6.6 Spectrum from contaminated aluminium specimen ; formvar window, 15 kV probe.
(a) Continuous line shows background calculated using a silicon reference standard.
(b) Spectrum with background removed.

7. OVERLAP DECONVOLUTION

Techniques developed in previous sections should allow accurate separation of soft x-ray peaks from background in ED spectra. The final goal however is accurate peak intensity measurement, and this will be rendered particularly difficult when peaks overlap. The problem presented by overlapping peaks is not unique to soft x-ray analysis and therefore deconvolution techniques which have been applied to the analysis of hard x-rays (discussed in section 2.3.4) may be applicable here. Unfortunately as figure 7.1 shows, there are a great many lines with energy between 0 and 2 keV and the possibility of overlap is high. Furthermore the proximity of these lines in relation to the energy resolution of the ED system (about 120 eV FWHM below 1 keV) means that overlaps will often be severe in practical light element analysis. Deconvolution was therefore examined in detail to assess the merits and limitations of different techniques. In addition methods were developed to determine the statistical accuracy of the final results. This is obviously important in practical analysis, but also made it possible to determine the theoretical accuracy which could be expected for differing degrees of overlap.

Although the principles of the most commonly used techniques, 'overlap factors' and 'least squares fitting' have been discussed (see section 2.3.4),

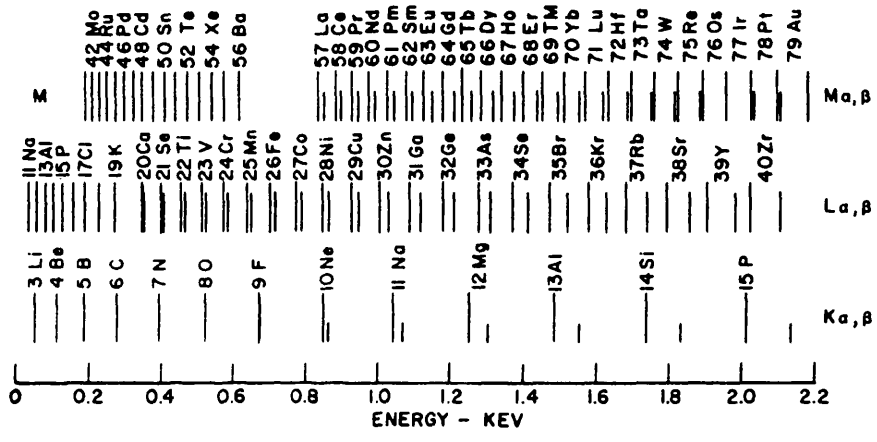

Fig. 7.1 Principal low energy emission lines showing potential inter-element interferences.
(From Russ 1971)

they are both studied more fully in this section to emphasis the relationship between them.

7.1 Overlap Factors

Overlap factors represent the fraction of integrated peak intensity from one element which appears in the region over which the neighbouring peak is integrated. For example in fig 7.2 the factor describing the overlap of peak A into the integration region of B (denoted ab) is given by Y/X. If these are known, true peak intensities may be established from uncorrected intensities by mean of an iterative procedure. When, however, three or more peaks are involved the situation becomes complicated and is more easily solved by using a set of simultaneous equations

$$\begin{aligned} A. \quad &+ B.ba + C.ca = S_1 \\ A.ab &+ B. \quad + C.cb = S_2 \\ A.ac &+ B.bc + C. \quad = S_3 \end{aligned}$$

where S_1, S_2, and S_3 are the measured integrals at peak positions and A, B and C are the unknown peak integrals. These equations can be expressed in matrix notation as follows

$$\begin{bmatrix} 1 & ba & ca \\ ab & 1 & cb \\ ac & bc & 1 \end{bmatrix} \times \begin{bmatrix} A \\ B \\ C \end{bmatrix} = \begin{bmatrix} S_1 \\ S_2 \\ S_3 \end{bmatrix}$$

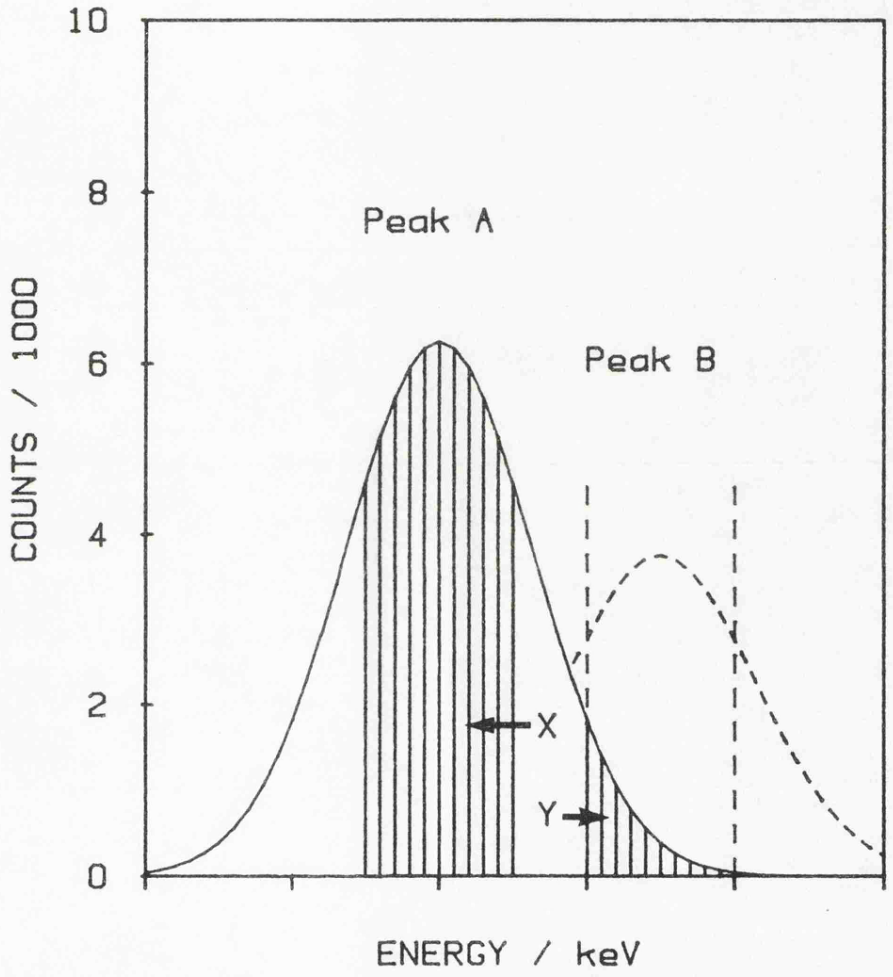

Fig.7.2 Schematic diagram showing the integration region (X) of peak A and the overlap (Y) of A into the integration region of peak B.

or rewritten in the more general form

$$P_{ij}\ I_i = S_j \qquad (7.1)$$

where $1 \leqslant i \leqslant 3$ and $1 \leqslant j \leqslant 3$. Now a solution may be obtained by, for example, inversion of the P matrix in equation (7.1).

7.2 Peak Fitting

The treatment outlined above may be extended by increasing the size of the matrix so that $1 \leqslant i \leqslant n$ and $1 \leqslant j \leqslant m$, then a complete band of the spectrum (after background removal) may be represented as the sum of a series of characteristic peaks. Equation (7.1) is still applicable but now S_j is a portion of spectrum containing m channels and the n columns of P_{ij} are the various components of the spectrum, the size of each component being I_i. Thus the count S_j in the jth channel of the spectrum is given by

$$S_j = \sum_{i=1}^{n} \{P_{ij}\ I_i\}$$

It follows that the method of overlap factors is merely a simplified version of this more general treatment. When overlap factors are employed P_{ij} represents counts integrated over a number of channels of the spectrum, the integration bands being centred at the position of each peak. In this case P_{ij} is a square matrix and equation (7.1) has a unique solution. Since statistical errors affect results directly, those associated with

the spectral background are minimised by keeping the integration bands narrow ($\sim \frac{1}{2}$ FWHM). In the general treatment the actual components of spectrum P_{ij} are not simply overlap values but representations of peak shapes. Approximations of these shapes can be obtained from experimental or model peak shapes, M_{ij}. Equation (7.1) then becomes

$$M_{ij} \, I_i \simeq S_j \qquad (7.2)$$

which consists of m equations in n unknowns. This has many possible solutions but the one generally chosen is that which minimises the sum of the squared errors for each j, i.e. the least squares fit of M_{ij} to S_j. Channel counts from tails of peaks may be included for fitting purposes since despite poor statistics they provide additional information. Thus, the general approach is capable of treating peaks over their full width, thereby offering potentially greater accuracy than the method of overlap factors. An additional advantage is that the results of the fit, $M_{ij} \times I_i$ can be calculated and compared directly with the original spectrum S_j.

Fitting requires a knowledge of peak shapes and this is most easily attained by storing relevant spectra (with background removed) from standard specimens. It would be possible to use mathematically generated Gaussian shapes, but these have to be compared with experimental

peaks at some stage to ensure that they provide a sufficiently accurate representation. Also, in the low energy region below 1 keV peaks tend to be asymmetrical and difficult to model; consequently use of experimentally recorded spectra is recommended for deconvolution purposes.

7.2.1 The Least Squares Solution

One way of solving equation (7.2) is to multiply both sides by an m × n matrix, Q_{ji} giving,

$$Q_{ji}\ M_{ij}\ I_i = Q_{ji}\ S_j \qquad (7.3)$$

Q.M is an n × n matrix and so the above expression represents n equations in n unknowns and generally has a unique solution. The choice of Q_{ji} is, however, arbitrary and each Q_{ji} matrix will result in a different solution. The least squares solution (I_i) to equation (7.3) is the one which minimises

$$\Sigma_j\{S_j - \Sigma_i(M_{ij}\ I_i)\}^2 \qquad (7.4)$$

This result will be obtained from equation (7.3) if $Q_{ji} = M_{ij}^T$, where M_{ij}^T is the transpose of matrix M_{ij} (see Ralston and Rabinowitz 1978). Since $M^T.M$ is a n × n matrix it generally has an inverse, in which case the solution can be expressed

$$I = \{M^T.M\}^{-1}.\ M^T.S \qquad (7.5)$$

This inverse matrix may be calculated in various ways (Westlake 1968) but it is generally accepted that inversion is prone to computational errors in certain situations (Ralston and Rabinowitz 1978).

A more reliable method for solving equation (7.2) is to use singular value decomposition (SVD) which generates a pseudo inverse M^+ such that

$$I = M^+.S \qquad (7.6)$$

gives the least squares solution I. The SVD method can be implemented in various ways (Nash 1979) to suit the requirements of speed and available computer memory.

As well as computational accuracy there are two other requirements to be taken into account when choosing an algorithm for solving equation (7.2). Firstly, statistical variations in the number of counts in each energy are not constant but have standard deviations given by $\sigma_j^S \simeq \sqrt{S_j}$ (see section 1.3.2) where S_j is the count in the jth channel. Hence, it is more appropriate to use a modified form of expression

(7.4) and minimise

$$\Sigma_j \left(\frac{S_j - \Sigma_i M_{ij} . I_i}{\sigma_j^S} \right)^2$$

Secondly, it is important to calculate the statistical accuracy of the resulting fit. This depends on counting statistics in the ED spectrum and the mathematical operations used to calculate the results. For example in equations (7.5) and (7.6) the solution can be written as

$$I_i = X_{ji} S_j$$

where X_{ji} is derived in some manner from the standard or model peak shapes M_{ij}. If statistical errors in M_{ij} are small compared with those in the spectrum S_j then errors σ_i^I in I_i can be calculated as

$$(\sigma_i^I)^2 = \Sigma_j (X_{ji}\ \sigma_j^S)^2$$

Furthermore, if σ_j^S is approximated by $\sqrt{S}_j$,

$$(\sigma_i^I)^2 = \Sigma_j (X_{ji}^2\ S_j)$$

7.2.2. Assessment of Peak Deconvolution by Least Squares Fitting

Matrix inversion and SVD methods of solving equation

(7.2) were examined by use of simple Gaussian shapes added together in known proportions to simulate a variety of overlap situations. Computer programs were written to calculate least squares fits of the original Gaussian shapes to the overlap. Options to apply the necessary weighting and to calculate statistical errors in the final results were incorporated in both matrix inversion and SVD programs. Computational accuracy was also checked by comparing the results of the fit with the known sizes of the original Gaussian shapes.

In all cases, the simple matrix inversion and SVD method gave similar predictions of statistical error, but the SVD approach incurred consistently lower computational errors. Nevertheless statistical errors were always at least 100 times greater than the computational ones, so the matrix inversion technique is still perfectly adequate in this type of application. The choice of which technique to use therefore depends largely upon which is most convenient to implement. Matrix inversion was selected here because matrix handling routines were already available on the Data General computer used in this work.

Statistical errors arising from the deconvolution of two peaks with centroids separated by varying amounts were then evaluated. Matrix inversion was used to deconvolute a Gaussian peak with 10,000 counts and a full width half maximum of 120 eV from (a) a neighbouring peak of the same magnitude (b) a peak of 250,000 counts

and (c) a peak of 250,000 counts and a background of 15,000 counts per 20 eV channel. The relative sizes of these peaks and the background are illustrated in figure 7.3. The results of the deconvolution are shown in figure 7.4 plotted as percentage statistical error versus peak separation. It is evident that a 10,000 count peak which is overlapped by a similar size peak can be resolved with only 5% error when the separation is as little as 20 eV provided that the background is low. In extremely difficult situations when a large neighbouring peak and high background level are present, the statistical errors are greater, being 10% for a peak separation of 50 eV.

Non-linear fitting

The results presented above represent the limit of accuracy that can be achieved under ideal conditions, in practice changes in resolution or peak position will cause additional errors. Non-linear fitting techniques which compensate for such changes have been described (Fiori, Myklebust and Gorlen 1981), they search for progressive improvements in the fit by adjusting the peak parameters until the optimum positions, widths and sizes are found. Whilst this is most directly applicable when fitting mathematical peak models a certain amount of 'peak shape manipulation' is possible even when experimental spectra from standards are used. In

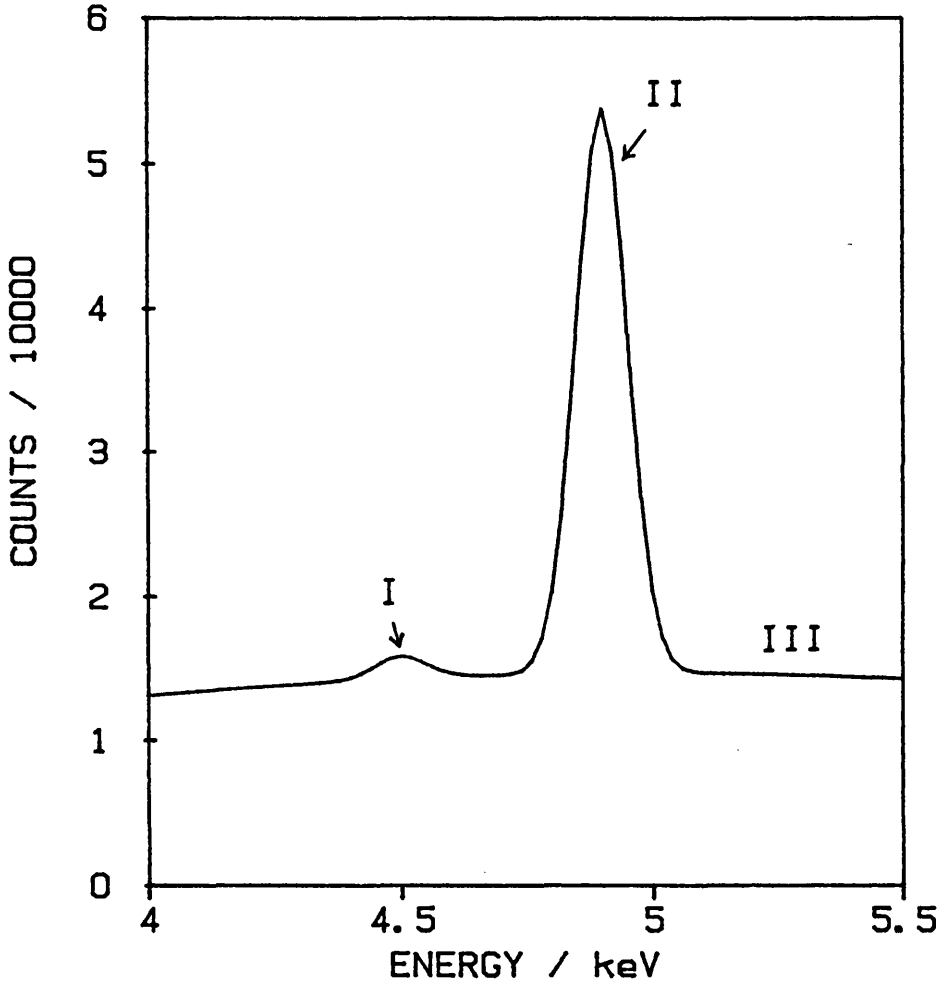

Fig. 7.3 Relative sizes of peaks (FWHM 120 eV) with; 10,000 integrated counts (I), 250,000 integrated counts (II) and a background level (III) of 15,000 counts. 20 eV per channel.

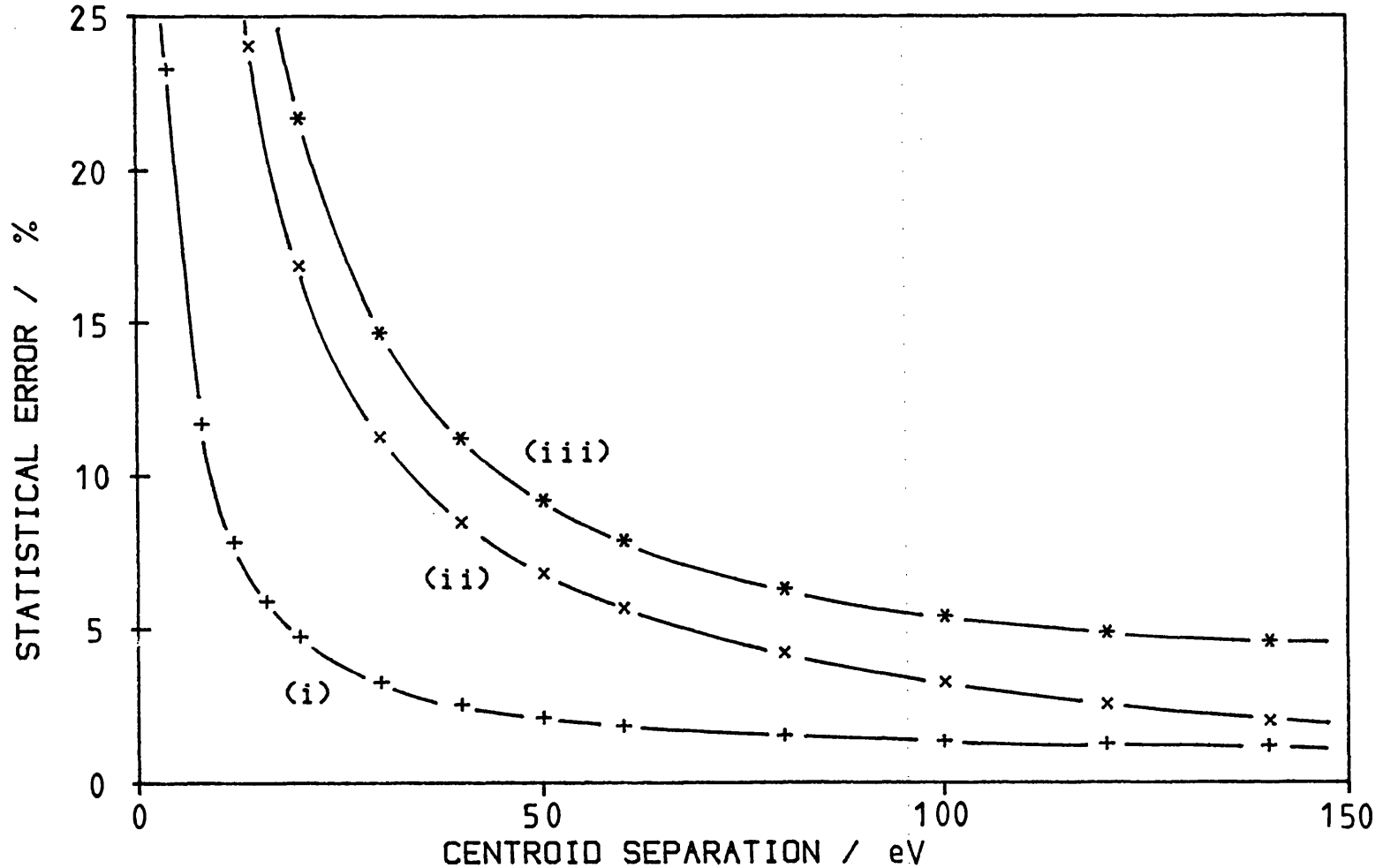

Fig. 7.4 Statistical error versus peak separation for deconvolution of the small peak I in fig. 7.3 from ; (i) a peak of the same size, (ii) the large peak II in fig. 7.3 and (iii) peak II with a high background level III.

simple overlap situations, the ability to correct for a change in peak position would be useful but Statham (1978) has shown that in severe overlaps the non-linear approach can sometimes produce large errors. Further investigation (Schamber 1981) has shown that although the occurance of such errors is unlikely it remains difficult to assure the reliability of non-linear fitting. Furthermore, changes in resolution and peak position are not inherent in the analysis technique but depend upon the stability of the electronic equipment. Non-linear fitting has not been studied further in this work owing to its lack of reliability. In practical situations the emphasis will be placed on careful calibration of the system and analysis of specimen and standards within short time periods to minimise any changes in resolution and peak position.

8. PRACTICAL ASSESSMENT OF ACCURACY AND SENSITIVITY

In previous sections techniques were developed for applying an accurate dead time correction and dealing with spur and noise counts. It was then demonstrated (in section 6.2.4), that these could be combined with a new method of predicting x-ray continuum to allow background prediction for energies as low as 0.1 keV. In addition, ways of deconvoluting overlapping peaks were discussed and a least squares fitting procedure adopted. It remains to determine the accuracy of the background prediction method and the effectiveness of deconvolution for soft x-ray work. This has been done by first using WD analysis to obtain specimen-to-standard peak intensity ratios for light element K lines and heavy element L lines in the low energy region. Then equivalent measurements were made with the ED system to allow direct comparison of the quantitative results.

Two probe voltages were selected, to be representative of those used in practical ED analysis. When low voltages are used many of the high energy x-ray lines are not excited and the proportion of soft x-rays in the spectrum is enhanced. Thus a low voltage, 7 kV, was chosen to provide conditions favouring analysis of light elements. In some work however, the ability to analysis for heavier elements as well as light ones is desirable and the second voltage, 15 kV, represents a more general purpose operating level.

In addition to the quantitative study the new processing technique was also used to provide estimates of the sensitivity which can be expected in ED analysis of light elements. Here measurements were made at 4,7,11, 15 and 20 kV to determine the dependence of light element sensitivity on probe voltage.

Conventional processing methods are inappropriate for use in low energy ED spectra, but the inherent simplicity of linear interpolation of background made it useful in this work. It was used, when there were no problems from overlapping peaks, as a simple means of illustrating the magnitude of any improvements offered by the newly developed method.

The ED work was carried out using an EDAX 711 analyser with an ECON detector attached to a JEOL 35C scanning electron microscope. A JEOL JXA 50A was used for the comparative WD measurements; this instrument was fitted with a cold finger which was employed throughout the analyses to minimise contamination of the specimen. The x-ray take-off angle was 35 degrees for both ED detector and WD spectrometer. Light element analysis with the ECON detector was carried out using a thin formvar window rather than in windowless mode for reasons discussed in section 3.1.2.

8.1 Specimens and Preparation

Table 4 lists the first series of specimens and standards used and the soft x-ray lines which where measured; these specimens where selected so that no overlap problems should arise in ED analysis. A second series of specimens listed in table 5 was likely to present overlap problems in EDS; the standards used therefore included the elements involved in the overlaps to allow deconvolution by use of standard peak shapes. Pure silicon was used to provide a continuum reference for the new background calculation method.

The specimens were prepared in groups; carbides, nitrides, oxides and fluorides each with their respective standards. This allowed each analysis to be carried out using a single specimen block with the following benefits.

(i) When a conductive coating was required it could be applied to all specimens and related standards in one operation giving a single uniform coating.

(ii) Specimen and standards never become separated between analyses thus reducing the risk of differential contamination, loss or mix-up.

X-rays analysed	Specimen	Standard
Fluorine K	Lead fluoride (PbF_2)	Magnesium fluoride (MgF_2)
Oxygen K	Nickel oxide (NiO)	Alumina (Al_2O_3)
Carbon K	Silicon carbide (SiC)	Carbon
Carbon K	Cementite (Fe_3C) in cast iron	Carbon

Table 4. X-ray lines analysed by WDS and EDS showing the specimens and standards used.; Light element peaks are free from overlap in the ED spectra.

X-rays analysed	Specimen	Standards
Fluorine K and manganese L	Manganese fluoride (MnF_2)	Magnesium fluoride (MgF_2) and manganese
Oxygen K, iron L and titanium L	Iron titanate (Fe_2TiO_5)	Alumina (Al_2O_3) and titanium
Oxygen K and chromium L	Magnesium chromate ($MgCr_2O_4$)	Alumina (Al_2O_3) and chromium
Nitrogen K, iron L chromium L and nickel L	Nitrided steel (Fe,Cr,Ni, and N)	Nickel, iron, chromium, silicon nitride (Si_3N_4)

Table 5. X-ray lines analysed by WDS and EDS showing specimens and standards used. Light element K peaks are overlapped by L lines from the heavy elements in the ED spectra.

(iii) The time between measurements on specimen and standard could be minimised, reducing any effects of calibration changes in the instruments.

All specimens were polished, finishing with 1 μm grade diamond or alumina paste, whichever was appropriate. To avoid charging effects, specimen blocks containing poorly conducting materials such as oxides and nitrides were coated with a thin layer of gold after polishing. Sputter coating for 30 seconds at 10 mA and 1.4 kV was found adequate, even for the specimen currents of about 50 nA required in WD analysis. The coating produced in this way gave only minor gold peaks in the ED spectra which did not interfere with any of the x-ray lines of interest.

8.2. WD Measurements

Specimen-to-standard peak ratios were obtained by WD analysis of the specimens and standards listed in tables 4 and 5 using diffraction crystals RAP and STE. The choice of probe voltages 7 and 15 kV for the quantitative work has already been discussed. Specimen currents of between 40 and 80 nA were used and soft x-ray count rates were typically in the range from 50 to several hundred s^{-1}. The aim was to achieve a peak count in excess of 10,000 (giving a standard deviation of less than 1%) and analysis times between 100 and 200 s were generally used. In cases where the x-ray

intensity was much lower, such as nitrogen in nitrided steel which gave 10 s^{-1} at 15 kV, the analysis time was not extended beyond 500 s. A low peak count was accepted to avoid excessive build-up of contamination on the specimen or changes in the electron beam intensity.

The WD technique gives better resolution and higher peak-to-background ratios than EDS so there were no difficulties in resolving closely spaced lines and background removal was usually trivial. There were however, several problems which required special attention in the WD analysis of soft x-rays; and these will now be discussed.

High order diffractions

Figure 8.1 illustrates the problems of overlap from high order diffraction, for oxygen in alumina. In some cases the situation was much worse, nitrogen in silicon nitride for example, being entirely swamped by high order lines. It was possible to eliminate the interfering lines by careful use of the pulse height analyser on the WD system. But this entailed scanning the spectrometer across the peak being analysed several times, initially to check for any possible interference and subsequently to ensure the interfering lines had been removed. Background positions either side of the peaks had to be selected with care when adjacent lines were present, such that the level of

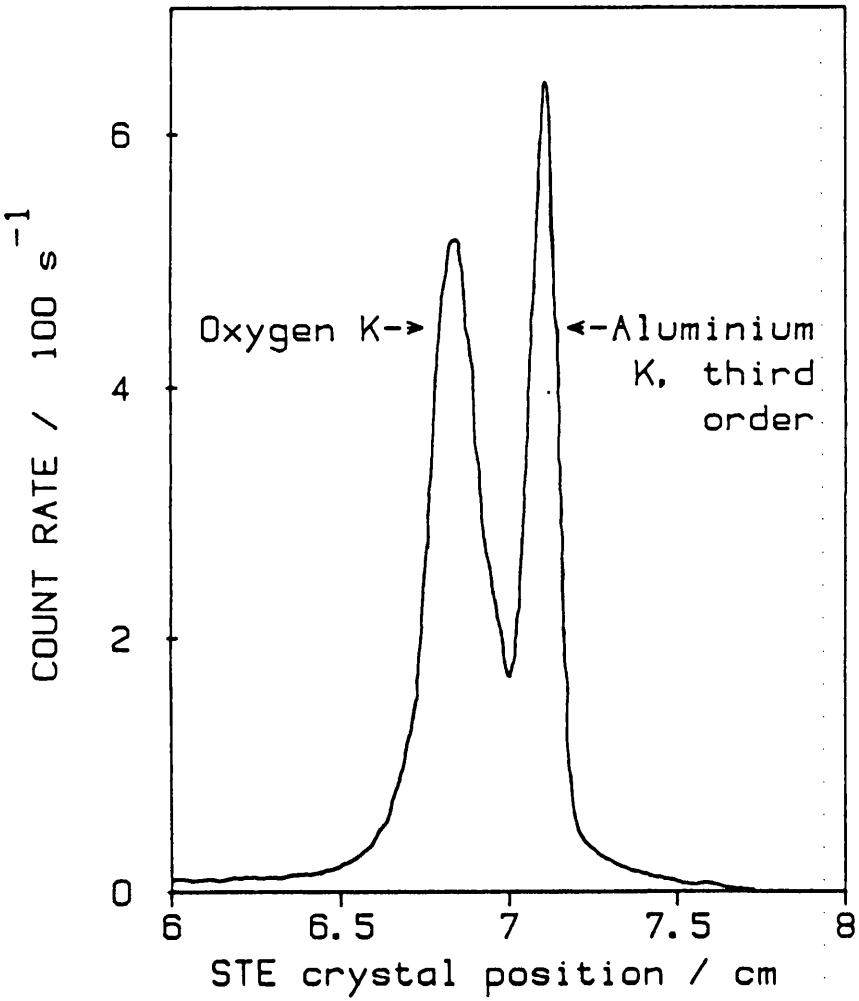

Fig. 8.1 WD spectrum from alumina (Al_2O_3) showing oxygen K line and interference from a high order diffraction of aluminium K. 7 kV probe.

continuum radiation recorded was representative of the background at the peak position.

Line shape

Figure 8.2 shows the carbon peaks obtained by WD analysis of (a) silicon carbide and (b) a carbon standard; there is significant difference in peak widths, presumably due to bonding effects which have been reported in earlier work (e.g. Love, Cox and Scott 1974). Differences are also found in the fluorine peaks from magnesium, lead and manganese fluorides due to varying size of a satellite line. In these cases measurement of peak height is inadequate and it is necessary to integrate the WD intensity across the peak to provide an accurate quantitative result.

L emission spectra

Figures 8.3 and 8.4 show the main lines in the manganese L series from the pure element and manganese fluoride respectively. The difference in the relative heights of the lines indicates, once again, that integration would be required for comparison with quantitative ED measurements. However the lines are well separated by the WD spectrometer and integration across the entire series is impractical. Similar problems were found with other specimens and measurements of L line intensities were generally limited to integration of only the major peaks.

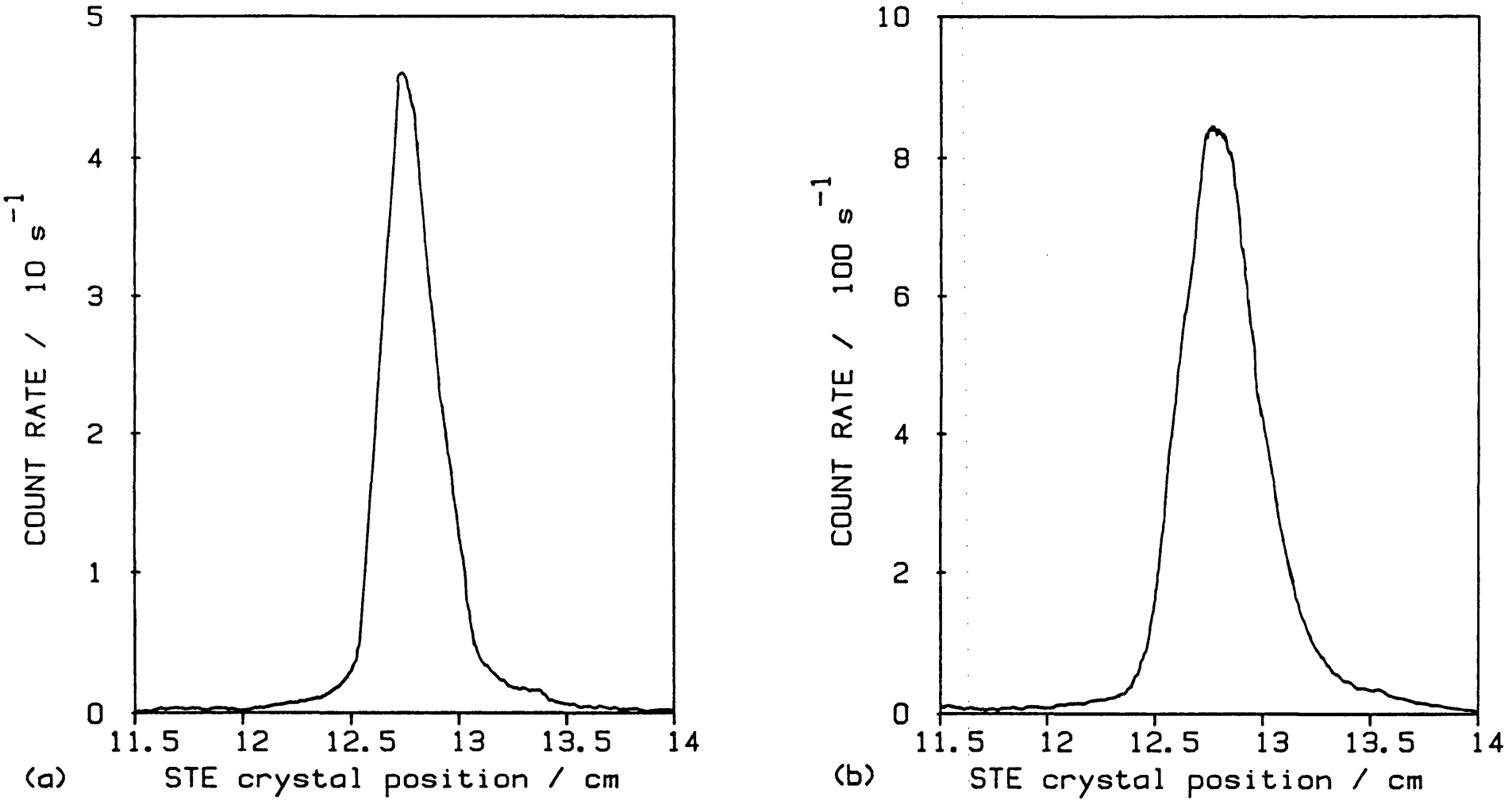

Fig. 8.2 Carbon peaks obtained by WD analysis of (a) silicon carbide (SiC) and (b) pure carbon (graphite). 15 kV probe.

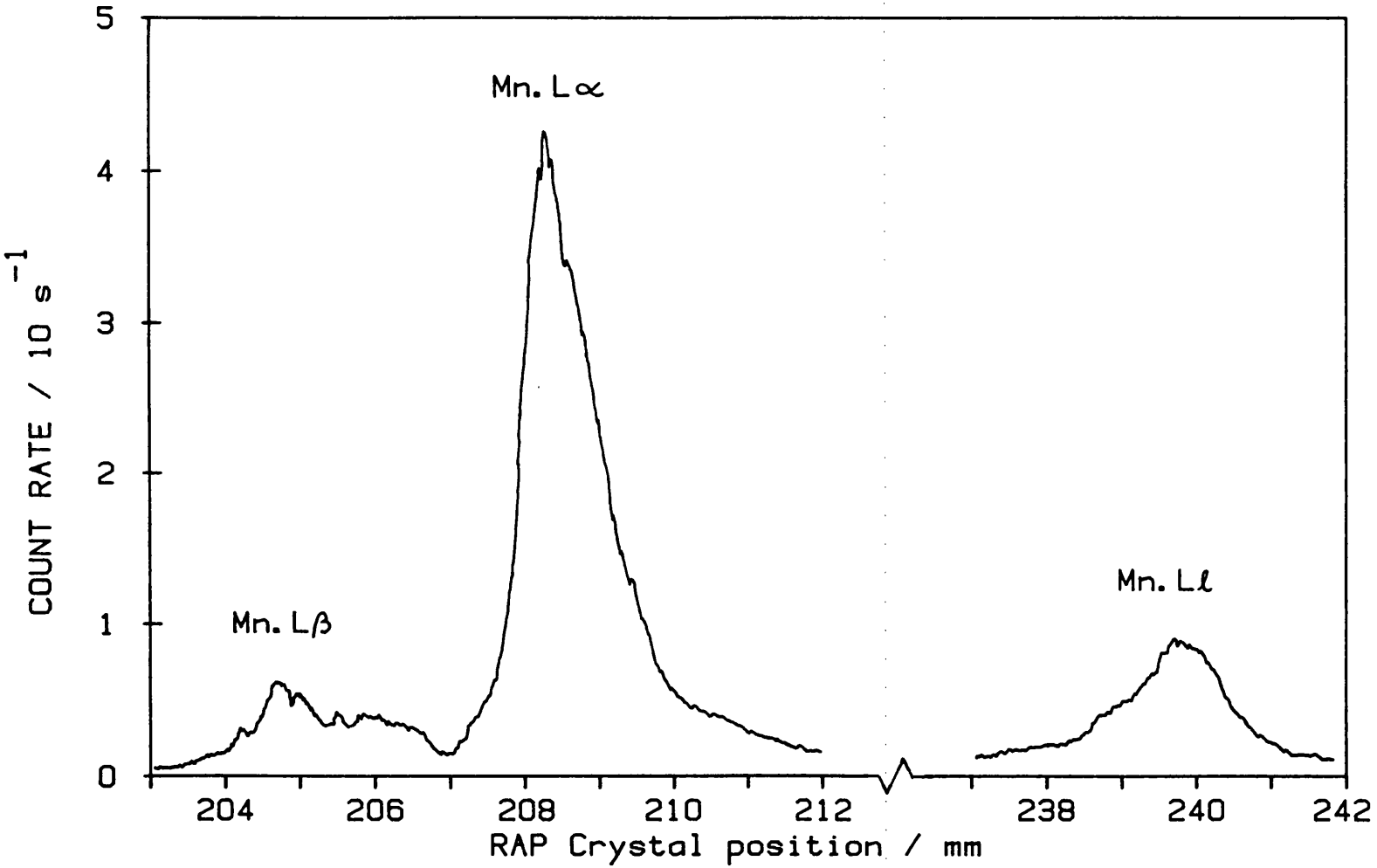

Fig. 8.3 WD spectrum from a pure manganese specimen, obtained with 7 kV probe.

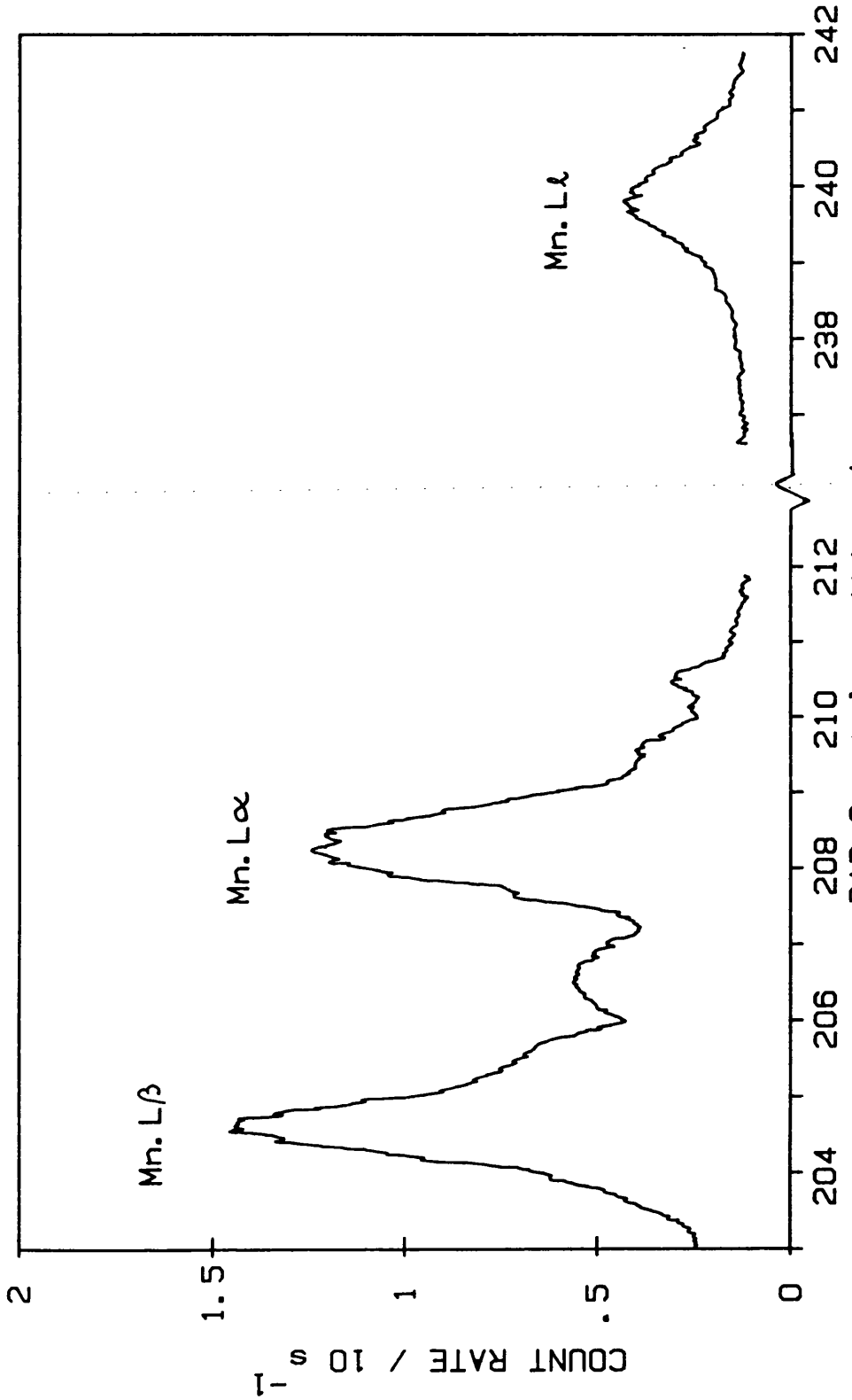

Fig. 8.4 WD spectrum from manganese fluoride (MnF_2), obtained with 7 kV probe.

8.3. ED Measurements

8.3.1 Experimental Method

The ED system was set up whilst recording a copper spectrum at about 2000 s^{-1} with a 15 kV probe, the energy calibration controls being adjusted until the copper L and K peaks appeared at the correct energies. The low energy discriminator was set at 60 eV giving a noise count rate of about 120 s^{-1} and the formvar window was used on the ED detector.

As described in section 4.3.2 the new correction for dead time is based upon measurement of the maximum recording rate which can be achieved with the specimen concerned. It was most convenient to make these measurements for all specimens and standards before starting the actual analyses. This also provided a useful opportunity to note changes in specimen current between the different materials, and the currents required to give moderate count rates. In this way a suitable beam strength could be selected for the analysis work, giving count rates in the range 1000 to 2000 s^{-1} for all specimens and standards.

Spectra used for the comparison with WDS results were recorded under constant electron beam conditions, from each of the specimen and standard combinations listed in tables 4 and 5. Probe voltages of 7 and 15 kV were used as in the WD work and specimen currents were about

0.4 nA at 15 kV and 0.9 nA at 7 KV. Analysis times of up to 400 seconds (real time) were used providing, in most cases, low energy peaks in excess of 10,000 counts (the nominal level required for a standard deviation of less than 1% in the peak size).

The spectra for sensitivity measurement were recorded from the silicon carbide, silicon nitride and alumina specimens at 4, 7, 11, 15 and 20 kV. Constant specimen currents of 0.5 nA were used and all analyses were carried out for 200 seconds (real time), this being more representative of analysis times used in practice.

The live time for each analysis was calculated by use of the new correction method developed in section 4 and each spectrum was stored on computer disc for subsequent processing.

After every two or three analyses the electron beam was temporarily switched off so that noise spectra could be recorded and saved on disc. Silicon standards were used to provide continuum reference spectra at each probe voltage.

8.3.2. Spectrum Processing

Single peaks

Figure 8.5 shows the spectra obtained from silicon carbide,

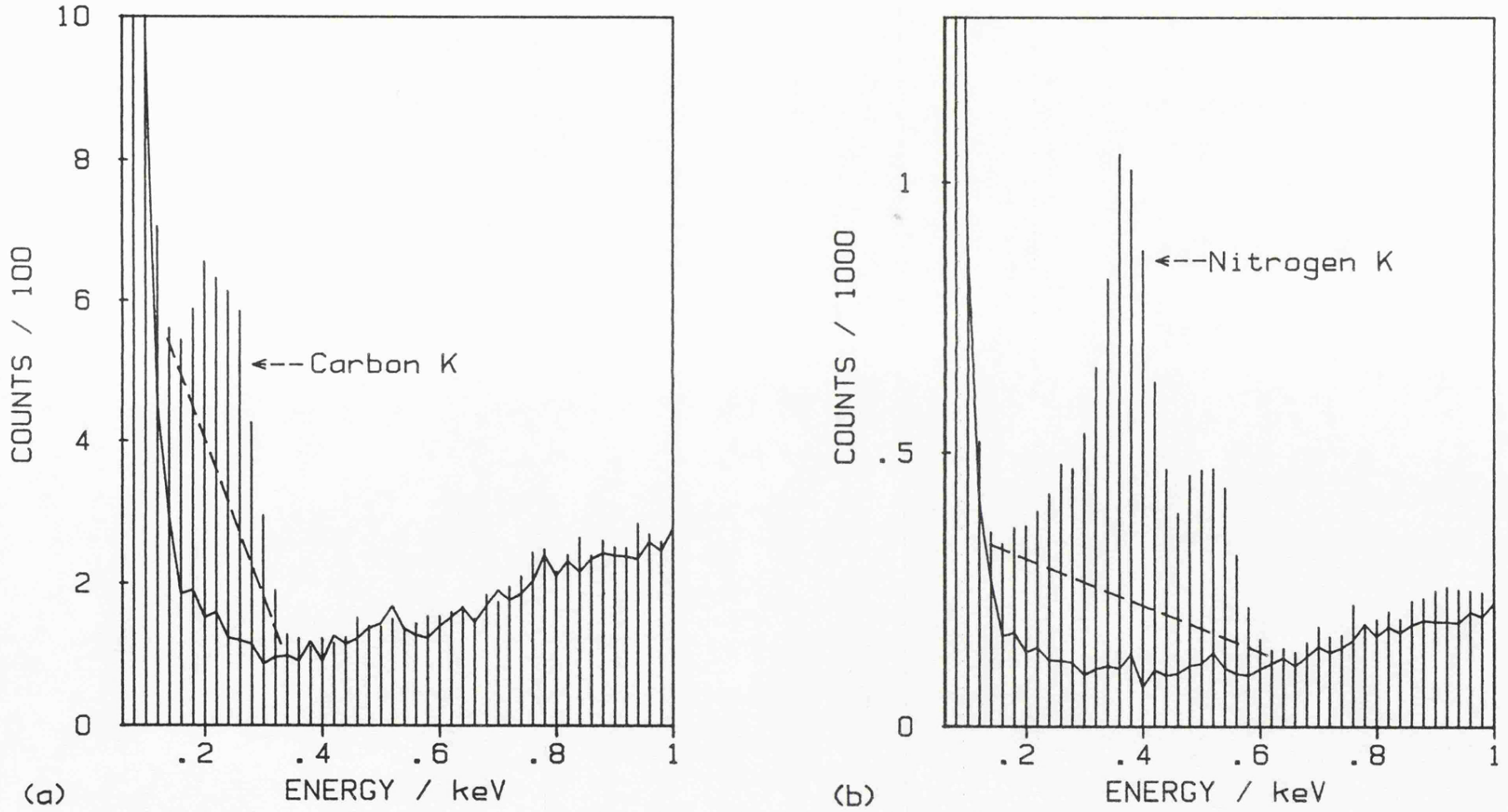

Fig. 8.5 ED spectra from (a) silicon carbide, (b) silicon nitride and (c) alumina, showing background levels given by linear interpolation (dotted lines) and by calculation using a silicon reference standard (solid curves). Formvar window, 11 kV probe.

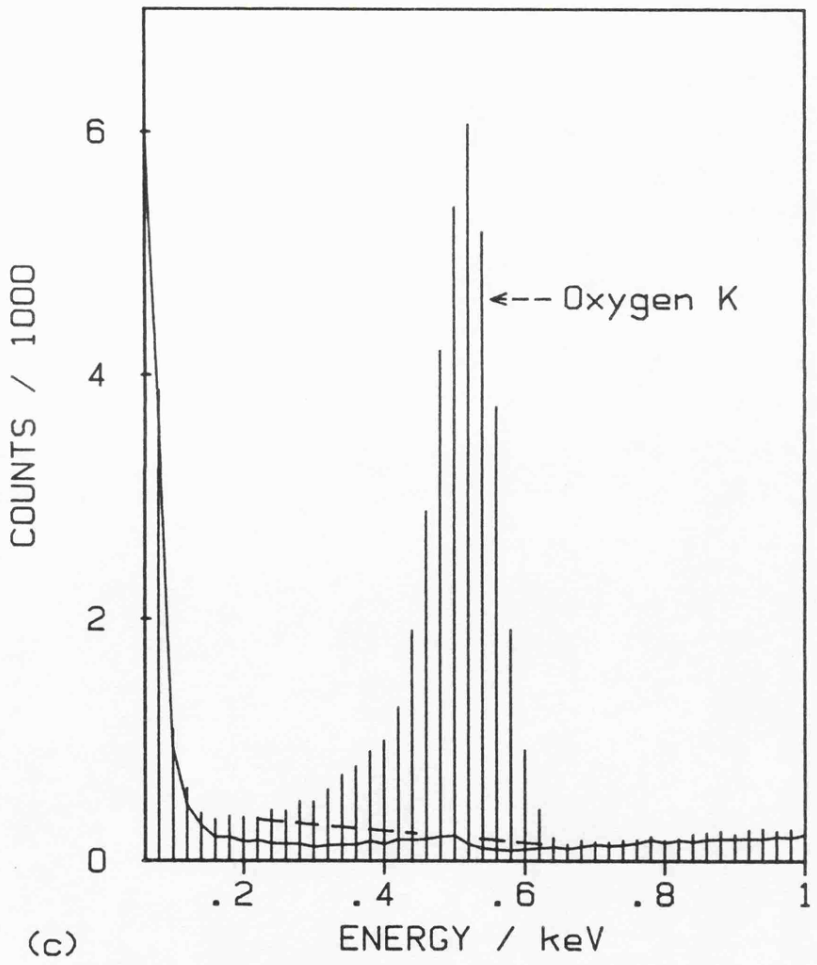

Fig. 8.5 continued from previous page.

silicon nitride and alumina with an 11 kV probe. The background level was first measured by linear interpolation, indicated by the dotted lines in figure 8.5. Background counts were integrated over a range of 140 eV, centred on the peak position, and subtracted from the equivalent integral of counts beneath the peak to give the net peak intensity.

Backgrounds were then calculated by the new procedure developed in this work, (summarised in section 6.2.4.) and are illustrated by the continuous lines in figure 8.5. These backgrounds were also used to measure peak integrals over a range of 140 eV by the subtraction method described above.

The peak intensities measured by the linear interpolation and calculation of background were used to determine specimen-to-standard ratios for the analyses listed in table 4 and to determine sensitivity values for the elements carbon, nitrogen and oxygen.

Overlapping peaks

Figure 8.6a shows the low energy spectrum from iron titanate obtained with a 7 kV probe. Deconvolution was carried out by use of the least squares fitting technique developed in section 7 which makes use of standard peak shapes. The statistical information given by this technique is valid only if the deconvolution is carried

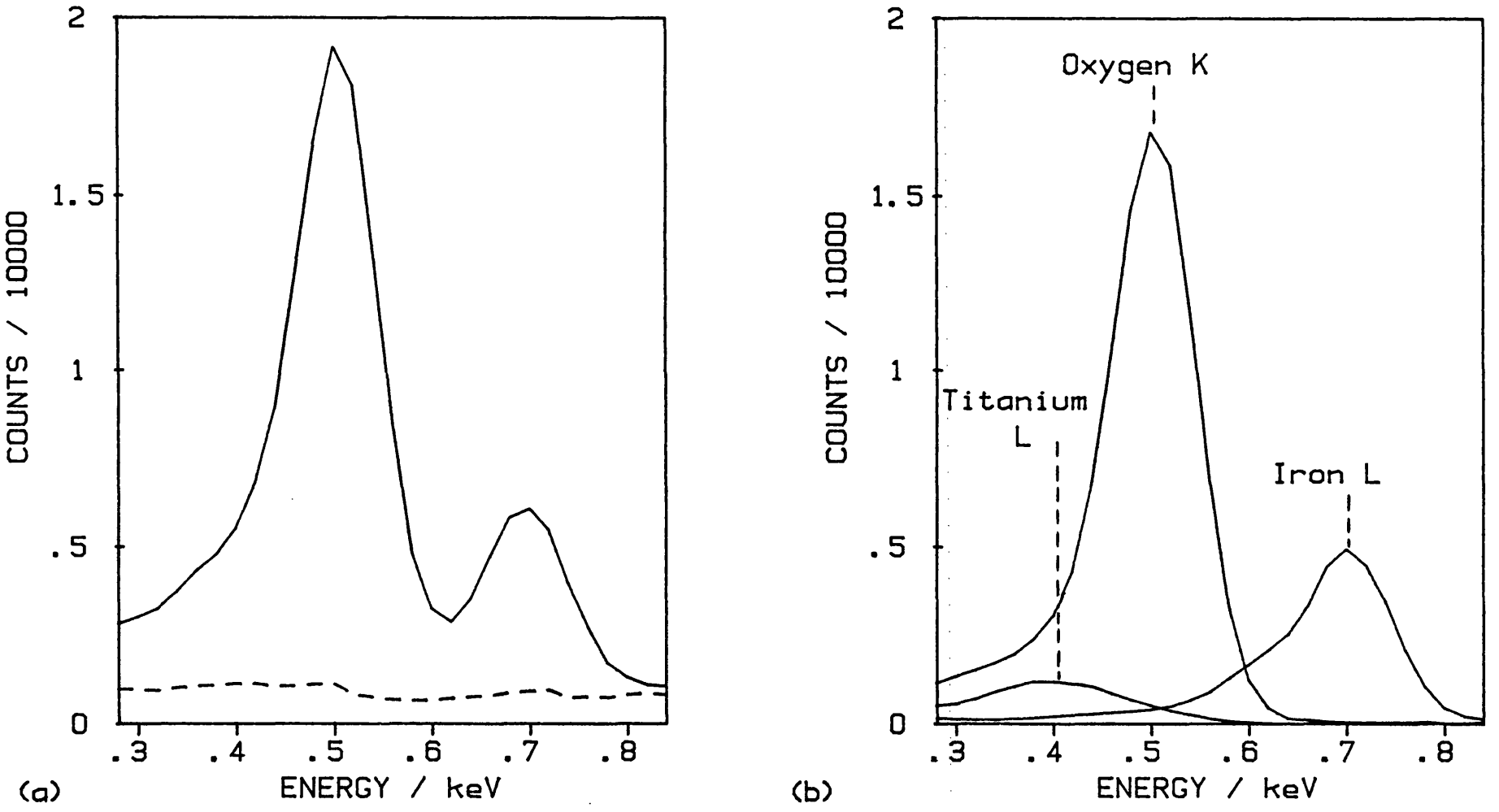

Fig. 8.6 (a) Low energy ED spectrum from iron titanate (Fe_2TiO_5), and the background (dotted line) calculated using a silicon reference standard. Formvar window, 7 kV probe.
(b) The result of deconvolution, showing the individual peaks present in the overlap.

out on the original spectrum rather than after background removal. This was achieved by including the specimen background as one of the components of the least squares fit, along with the standard peaks. Thus the first step was to calculate the background (using the silicon reference spectrum) for the specimen concerned, and here the specimen composition must usually be estimated and improved by iteration. The dotted line shows the background calculated by the new procedure and small discontinuities can be seen, associated with the K absorption edge for oxygen and the L edge for iron. Backgrounds were then determined for each standard in turn and subtracted to give the standard peak shapes. Finally the specimen background and standard peaks were fitted to the original spectrum giving the specimen-to-standard ratios for peaks in the overlap. This was repeated for each of the analyses listed in table 5.

The result of deconvoluting the low energy region of the iron titanate spectrum is illustrated in figure 8.6b, where the titaniuim L, oxygen K and iron L peaks present in the overlap are shown individually. A similar example is shown in figure 8.7, in this case for the manganese fluoride specimen were the fluorine K (677 eV) and maganese L (637 eV) lines are separated by only 40 eV. The final example in figure 8.8 is for magnesium chromate where the chromium L line appears directly below the oxygen peak.

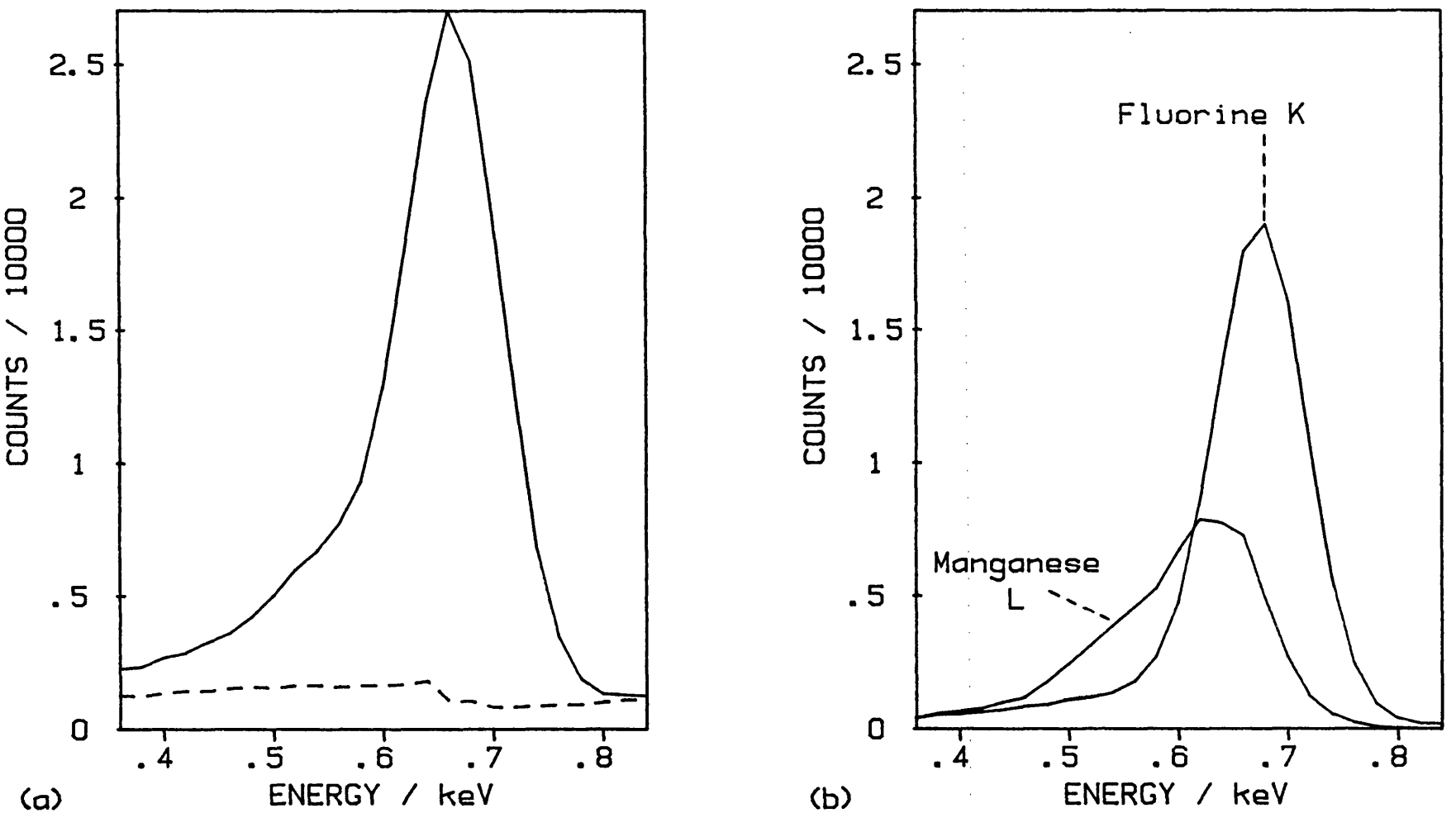

Fig. 8.7 (a) Low energy ED spectrum from manganese fluoride (MnF_2), and the background (dotted line) calculated using a silicon reference standard. Formvar window, 7 kV probe. (b) The result of deconvolution showing the individual peaks present in the overlap.

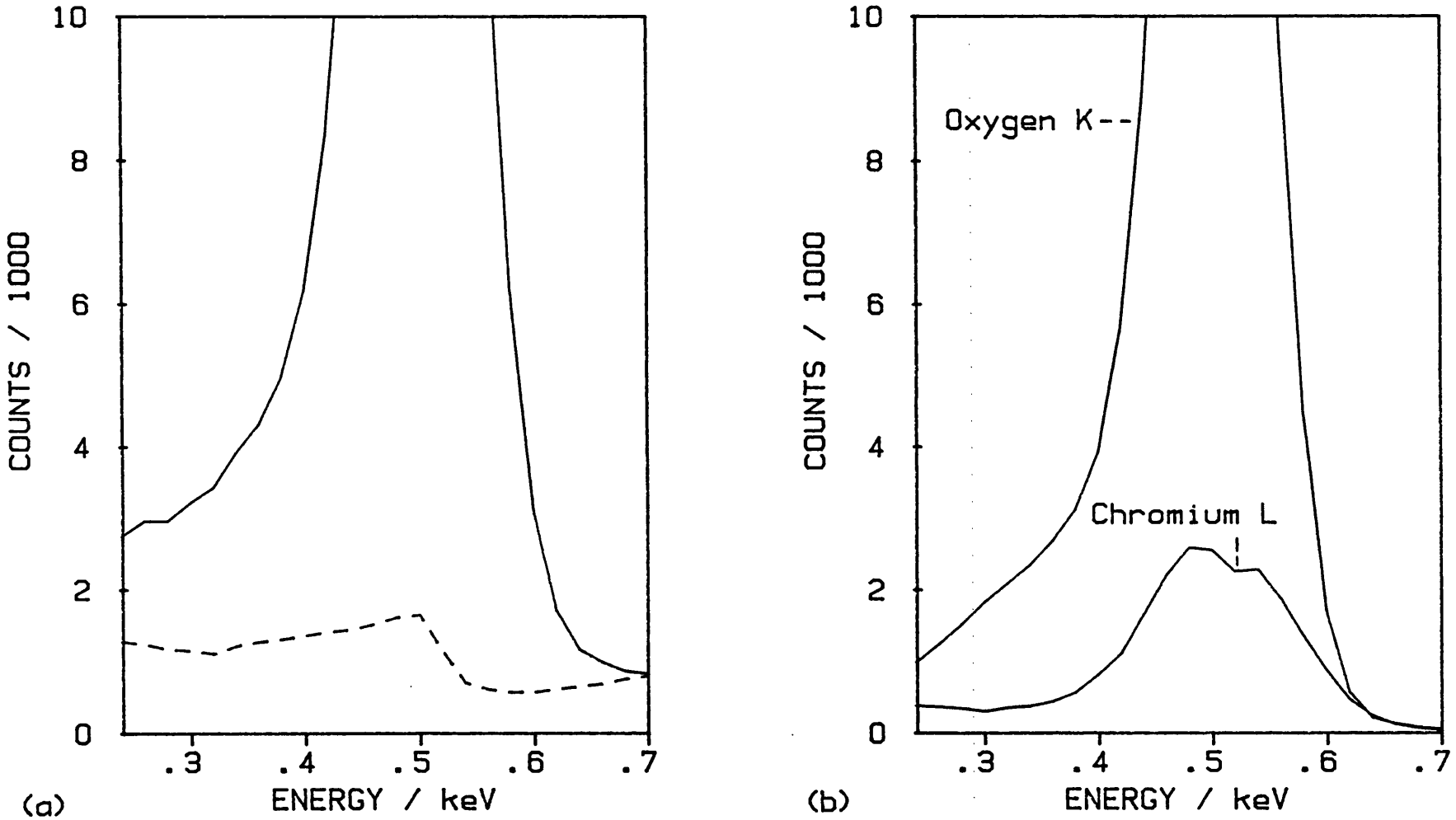

Fig. 8.8 (a) Low energy ED spectrum from magnesium chromate ($MgCr_2O_4$), and the background (dotted line) calculated using a silicon reference standard. Formvar window, 7 kV probe.
(b) The result of deconvolution showing the individual peaks present in the overlap.

8.4 Comparison of Quantitative Results

8.4.1 Single Light Element ED Peaks

The specimen-to-standard ratios determined by EDS and WDS for the systems listed in figure 8.9a are compared in figure 8.9b for 7 kV probe and in figure 8.9c for 15 kV. Each set of ED and WD measurements is normalised with respect to the mean WD value and the results are presented on a common scale allowing analysis of different elements to be compared on an equal basis. The 95% confidence intervals, based on count statistics are indicated to compare the accuracy of ED measurements with the statistical errors in both ED and WD results. The WD results are shown with shading, centered on 1.0 as a result of normalisation and the dotted outlines are the values obtained by EDS using linear interpolation of background. It can be seen that this technique gives reasonable accuracy for fluorine but agreement becomes progressively worse with decreasing atomic number irrespective of whether a 7 or 15 kV probe is used.

The solid outlines in figure 8.9 are the values obtained by EDS using the new background calculation method and it may be seen that close correspondence is achieved with the WD data. Differences are in the region of 1 or 2% in most cases and all are within the range expected due to count statistics. This indicates that the new approach gives an accurate representation of the background levels at low energies and allows sensible

	X-rays analysed	Specimen	Standard
A	Fluorine K	Lead fluoride (PbF_2)	Magnesium fluoride (MgF_2)
B	Oxygen K	Nickel oxide (NiO)	Alumina (Al_2O_3)
C	Carbon K	Silicon carbide (SiC)	Carbon
D	Carbon K	Cementite (Fe_3C) in cast iron	Carbon

(a)

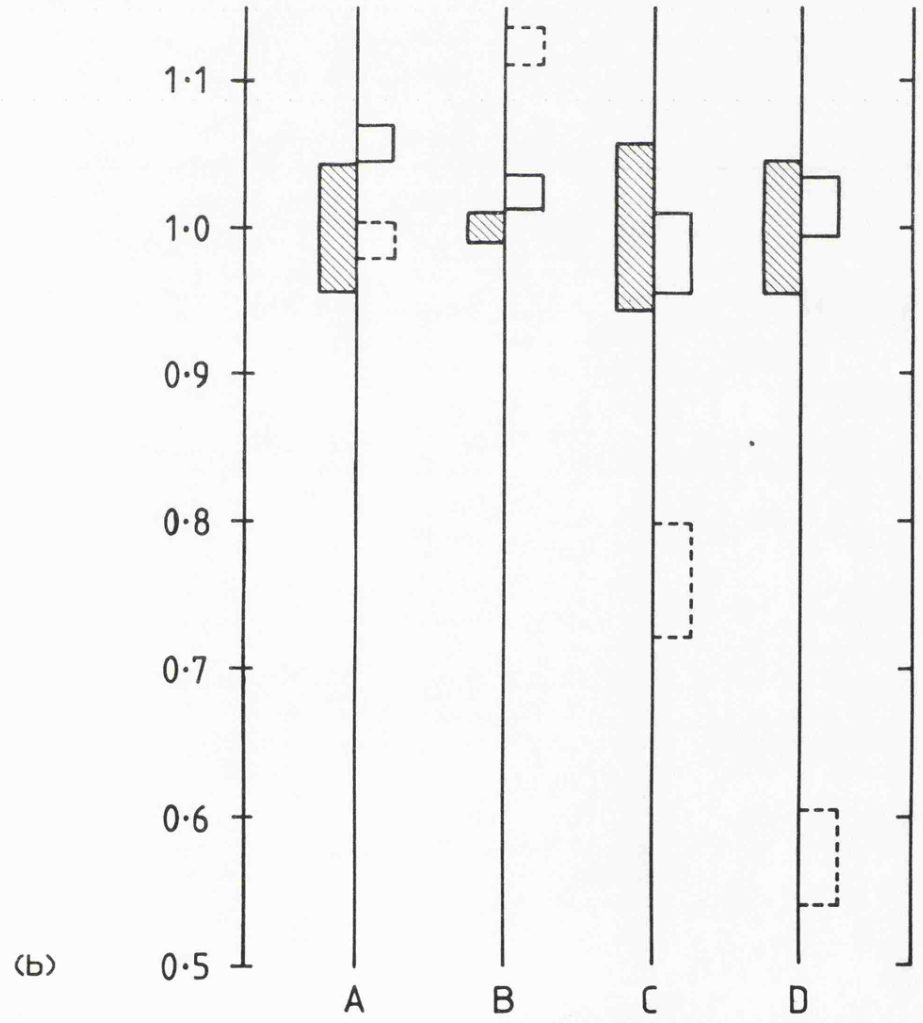

Fig. 8.9 Results for analysis of the systems listed in (a) at 7 kV (b) and 15 kV (c) by: WDS (shaded), EDS with linear interpolation of background (dotted outline) and EDS using the new background calculation method (solid outline).

(continued overleaf)

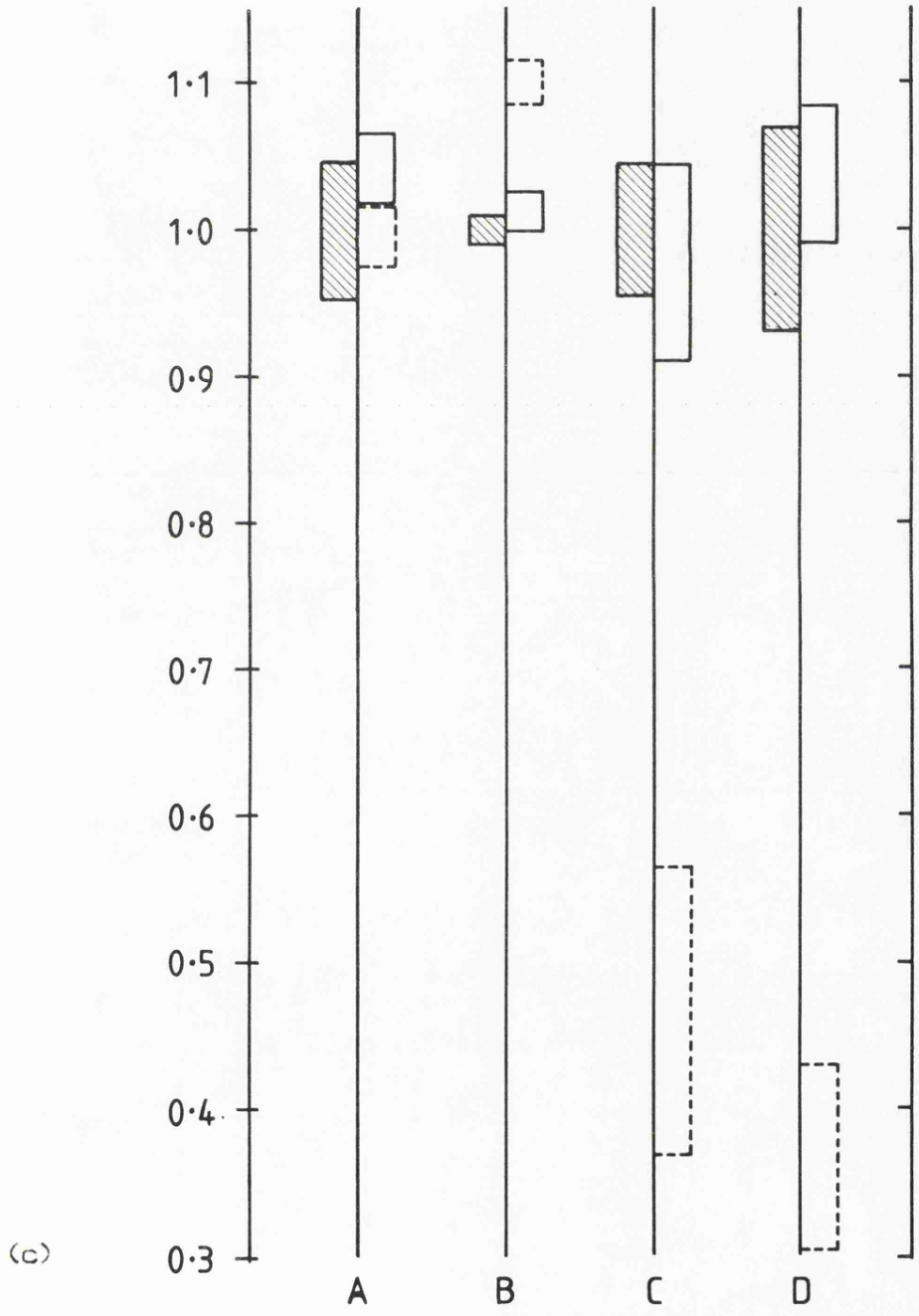

Fig. 8.9 (continued from previous page.) The results are normalised with respect to the WD values and show the 95% confidence interval based on counting statistics.

quantitative ED data to be obtained in light element work.

8.4.2 Overlapping Peaks in EDS

The results of the analyses involving peak overlap in EDS are presented in figure 8.10. The data are again normalised with respect to the WD values to allow comparison of relative accuracy of the ED measurements for the different systems. The poor result for nitrogen at 15 kV may be due to a low peak-to-background ratio which would cause small errors in the calculated background to have a large effect on the measured peak intensity.

The 7% error in the case of fluorine analysis at 7 kV may be attributed to the interfering manganese peak. WD analysis (see figures 8.3 and 8.4) indicated that the proportions of individual lines in the manganese L series change significantly from specimen to standard. Although the ED system does not resolve these differences there will be in changes in peak shape leading to a less accurate deconvolution of the overlap. Furthermore the manganese L peak represents a large proportion of the ED overlap (see figure 8.7b) and could therefore give rise to errors in the measured fluorine intensity.

Nevertheless most of the ED results differ by only a few percent from the WD values showing that the deconvolution

	X-rays analysed	Specimen	Standards
A	Fluorine K	Manganese fluoride (MnF_2)	Magnesium fluoride (MgF_2) and manganese
B	Oxygen K	Iron titanate (Fe_2TiO_5)	Alumina (Al_2O_3) and titanium
C	Oxygen K	Magnesium chromate ($MgCr_2O_4$)	Alumina (Al_2O_3) and chromium
D	Nitrogen K	Nitrided steel (Fe,Cr,Ni, and N)	Nickel, iron, chromium, silicon nitride (Si_3N_4)

(a)

(b)

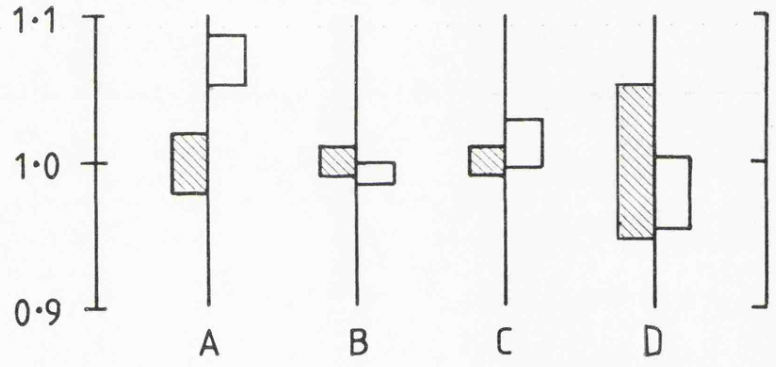

(c)

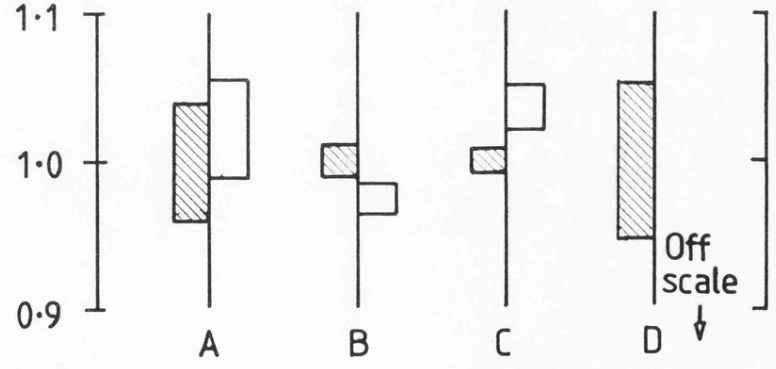

Fig. 8.10 Results for analysis of systems listed in (a) at 7 kV (b) and 15 kV (c) by: WDS (shaded), and EDS using the new background calculation method (solid outline). Each set of results is normalised with respect to the WD value and 95% confidence intervals are shown based on counting statistics.

technique is able to deal well with overlap situations in light element analysis.

Comparisons of WD and ED data for L lines showed generally poorer agreement with discrepancies in the region of 20 to 30%. This indicates that the problems of obtaining intensity measurements for L lines (discussed in section 8.2) do impose a severe limitation on their use for quantitative analysis.

8.5 Light Element Sensitivity with EDS

The new method of calculating background (section 6.2.4) was shown in the previous section to be accurate even at low energies in ED spectra. It therefore allows ED sensitivity for light elements to be measured more accurately than in previous work where little attempt has been made to deal properly with the low energy background.

The basic assumptions made when determining sensitivity are as follows. If a weight concentration C of an element produces a peak of size P counts in the ED spectrum then a smaller peak p, indicates the presence of a lower concentration c, where c=p.C/P. This method effectively ignores the conventional ZAF correction factors relating concentrations to peak size. However, for light elements ZAF factors are not well proven and the assumption gives a useful estimate of sensitivity. This is in fact adequate since sensitivity itself will often depend significantly

upon the particular system being examined.

The minimum detectable peak size is about three times the standard deviation σ_B of the background B beneath the peak which is $3\sigma_B$ or approximately $3\sqrt{B}$. Inserting this as a value for p into the above equation we have the minimum detectable concentration given by,

$$c = 3\sqrt{B}\ C/P \qquad (8.1)$$

The peak intensities (P) and backgrounds (B) for carbon, nitrogen and oxygen were determined in section 8.3.2 by use of linear interpolation of background and also by the new calculation technique. These values were used in equation (8.1) with the known concentrations (C) to determine the sensitivities for each element at different probe voltages and the results are shown in figures 8.11, 8.12 and 8.13. It can be seen that the new method for predicting background allows distinct improvements in sensitivity compared with linear interpolation. These improvements are more significant for low energy peaks such as carbon and nitrogen which suffer more interference from the spur and noise counts.

The sensitivity for each element appears worse at both high and low voltages, with an optimum in between. When high voltages are used the x-rays are generated at greater depths and the soft x-rays from light elements suffer from the increased absorption paths in the specimens. Reducing

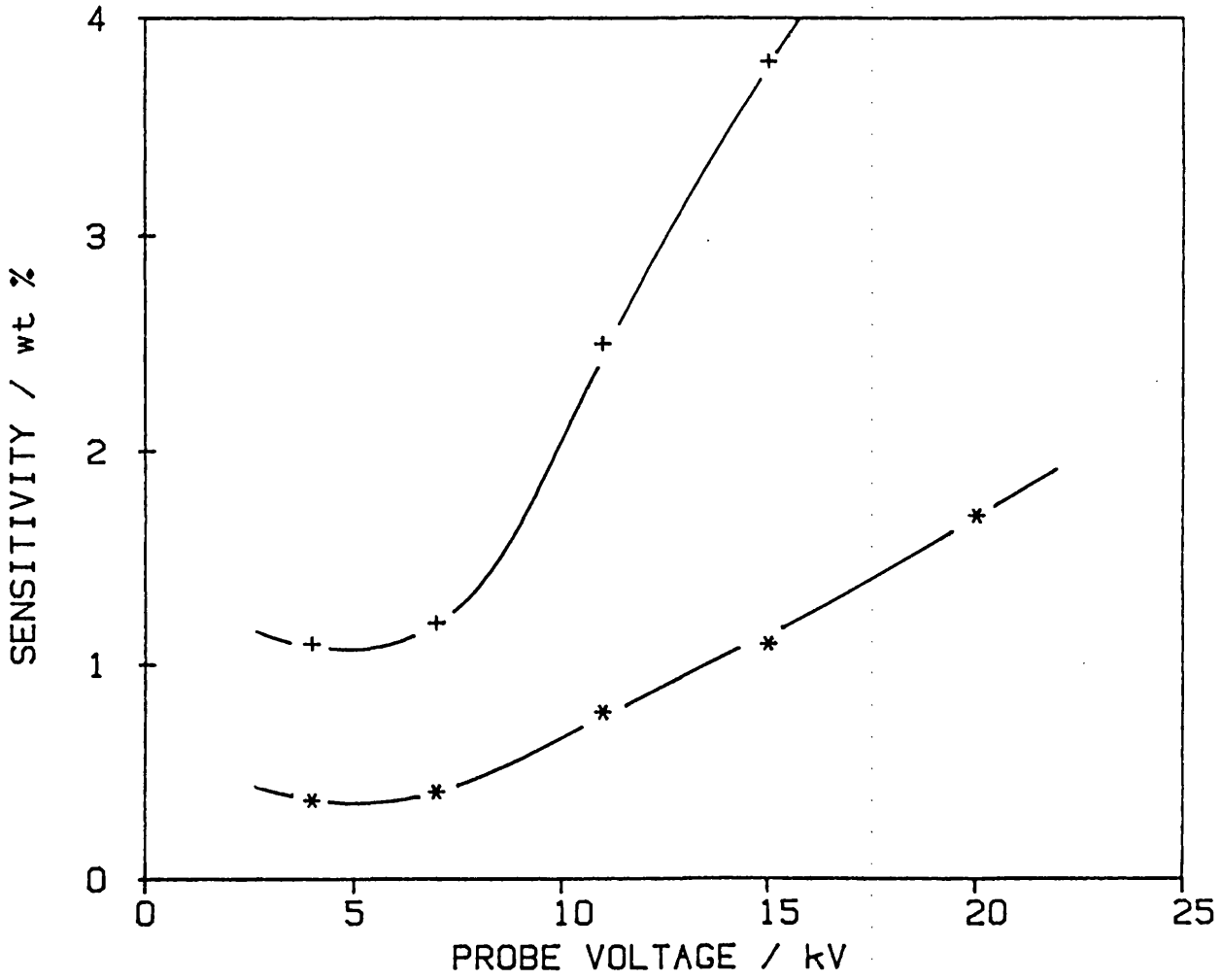

Fig. 8.11 Sensitivity of ED analysis for carbon, measured using silicon carbide (SiC) with background removal by ; linear interpolation (+) and calculation using a reference standard (*). Formvar window.

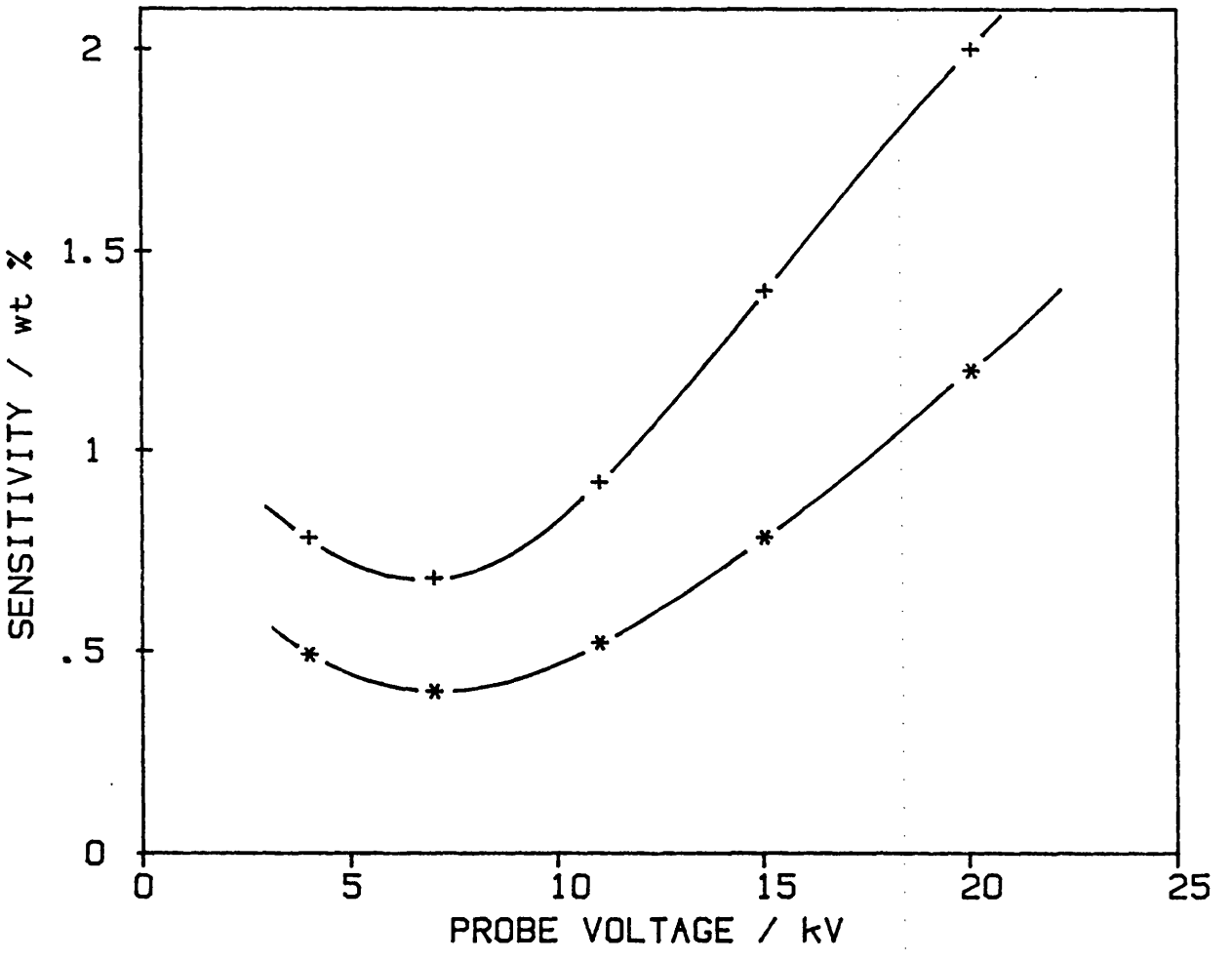

Fig. 8.12 Sensitivity of ED analysis for nitrogen, measured using silicon nitride (Si_3N_4) with background removal by ; linear interpolation (+) and calculation using a reference standard (*). Formvar window.

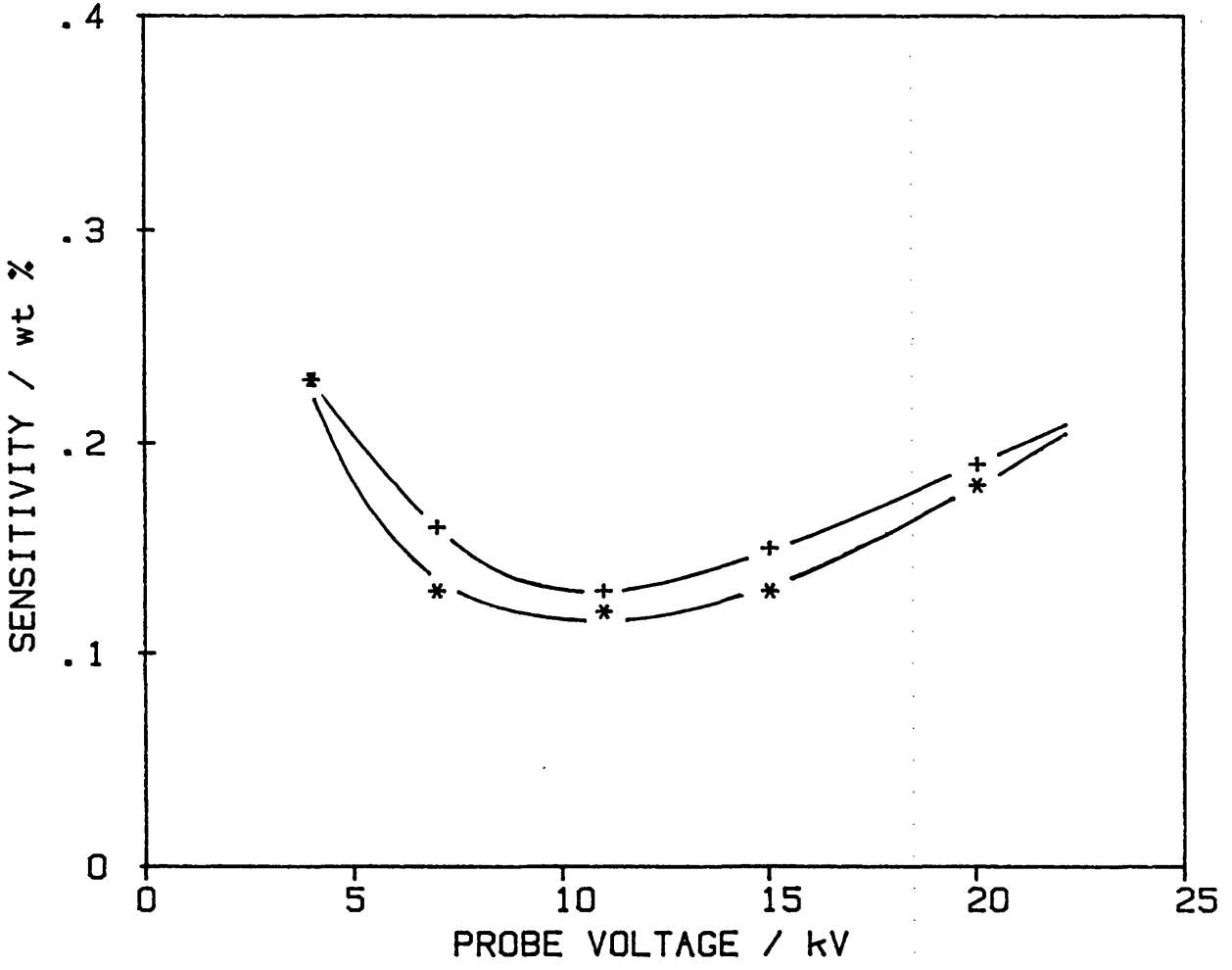

Fig. 8.13 Sensitivity of ED analysis for oxygen, measured using alumina (Al_2O_3) with background removal by ; linear interpolation (+) and calculation using a reference standard. Formvar window.

the voltage initially gives better sensitivity as the x-rays are generated nearer to the specimen surface and soft x-ray count rates are increased. As the voltage is further reduced however the falling value of overvoltage leads to lower count rates, poor statistical accuracy and hence poor sensitivity.

The improvements attainable by reducing the absorption path become more significant the lower the energy of the characteristic x-ray line so the minimum in the curve moves from 11 kV for oxygen, to 7 kV for nitrogen to only 5 kV for carbon. The sensitivities (weight %) at these points are 0.12 for oxygen (in Al_2O_3), 0.5 for nitrogen (in Si_3N_4) and 0.3 for carbon (in SiC). These optimum values will depend upon the system being analysed. For example the sensitivity figure for carbon in Fe_3C tends to be better (about 0.18) than in SiC because, although the background level is higher, absorption of carbon x-rays is lower than in SiC.

It is interesting to note that when analysing for oxygen, the use of a high probe voltage (20 kV) does not worsen the sensitivity to any great extent. In the case of carbon however there is a much greater dependence upon voltage and it would often be desirable to work with probes of less than 10 kV. It appears that 7 or 8 kV would provide near optimum sensitivity for the light elements examined here.

9. CONCLUSIONS

The low energy ED spectrum has been studied in detail to provide a better understanding of the problems relating to quantitative light element analysis. In order to overcome these problems existing processing techniques have been examined and new ones developed to allow measurement of soft x-ray peak intensities. It has also been demonstrated that the new methods provide measurements in good agreement with those obtained by WDS. Unlike previous ED work where inappropriate methods have been employed, the accuracy of this approach has allowed a more realistic assessment of sensitivity for light elements.

A major problem in some types of ED analyser is the limitation in soft x-ray work of the dead time correction. The cause is inherent in the electronics of the system and can only be overcome if the manufacturers adopt a more appropriate correction method. The experiments revealed that errors can be incurred even in conventional analysis with a beryllium window, if significant low energy peaks are present. But when peak intensity ratios are taken, cancellation reduces the errors to less than 10%. However, when a formvar window was used to obtain light element data the errors were much larger and an alternative correction method was required. The approach developed here was based upon the use of a mathematical expression for the recording behaviour of the system and measurement

of the maximum recording rate which could be achieved for the spectrum concerned. This allowed the live time of an analysis to be calculated rapidly from the 'real' time, and also accounted for differences in the system's dead time when processing low energy x-rays.

Close attention was paid to the way in which signals from the x-ray detector are discriminated from those due to random noise. This is particularly important when analysing soft x-rays which produce very small signals close to the noise level. It was shown that two different approaches adopted by manufacturers lead to different representations of the low energy spectrum. It is obviously important that these effects are clearly understood before quantitative measurements are attempted in this low energy region.

To maximise efficiency for soft x-ray analysis the low energy threshold level must be reduced to about 80 eV. But the fact that noise levels are typically over 100 eV in ED systems means that a certain number of noise counts must inevitably appear in the spectrum. The presence of these counts can interfere with the very low energy peaks such as carbon and boron so a method was developed here to allow their removal from any spectrum. A separate noise recording is made, scaled to the appropriate live time and then subtracted from the original spectrum.

The technique for noise removal revealed a previously unidentified artefact in the low energy spectrum and this

was termed the spur. It was characterised by carrying out experiments with differing analysis conditions and its size was found to bear a simple relationship to the total counts in the spectrum. The method adopted for its removal was based on a mathematical expression describing its shape.

Once dead time effects and artefacts had been accounted for, a remaining problem was the x-ray continuum. Several methods used to deal with continuum in conventional ED analysis were examined including mathematical filtering and explicit calculation. The method developed here however, was based on the use of a reference standard; the main advantage being that detector efficiency is incorporated in the spectrum from the standard and need not be explicitly known. The modification of the reference spectrum to predict continuum levels for another spectrum is carried out using corrections for atomic number and absorption effects analogous to those used in ZAF procedures. Here the problem of calculating mass absoption coefficients for x-rays below 1.5 keV was solved by use of a new technique for obtaining polynomial approximations to experimental data.

When used in conjunction with methods for dealing with artefacts, the reference standard approach allowed reliable prediction of background for energies as low as 0.1 keV in ED spectra.

The problem of overlap is well known in EDS but was

expected to be rather worse in the low energy region. Deconvolution techniques were therefore examined and a method developed using least squares fitting of peaks from standards. The determination of errors arising from counting statistics was given special attention and incorporated in the technique. It was then applied to computer generated data to illustrate the minimum errors which could be expected in different overlap situations.

It remained only to demonstrate the accuracy of the new spectrum processing techniques, and this was done in two series of practical analyses, one involving single light element peaks and the other presenting severe overlap problems. Specimen-to-standard ratios were first measured by WDS to obtain accurate values, then the analyses were repeated using EDS. Results showed that when the new processing techniques were applied the ED data agreed well with WDS measurements for light elements. When overlapping L lines from heavy elements were present it was found that their measurement was severly limited by changes in relative intensities within each L series. Nevertheless results for the light element K lines were generally within a few percent of the WD values after deconvolution.

The accuracy of the new method enabled confident assessment of ED sensitivity for light elements. In a further series of experiments the dependence of sensitivity on probe voltage was determined leading to the recommendation of 7 to 8 kV for optimum performance

with light elements. The actual sensitivities were found to be in the region of 0.5 to 0.1% for carbon, nitrogen and oxygen. However, variations are expected in different samples and results will obviously suffer when overlap occurs.

REFERENCES

Aitken, D.W. and Woo, E. (1971). In: Russ, J.C. ed., Energy Dispersion X-ray Analysis; Toronto 1970: X-ray and Electron Probe Analysis, ASTM STP 485, pp. 36-56. Philadelphia: ASTM.

Barbi, N.C. and Lister, D.B. (1981). In: Heinrich, K.F.J., Newbury, D.E., Myklebust, R.L. and Fiori, C.E. eds., Energy Dispersive X-ray Spectrometry, NBS SP 604, pp. 35-44. Washington DC : National Bureau of Standards.

Barbi, N.C., Sandborg, A.O., Russ, J.C. and Soderquist, C.E. (1974). In: Johari, O.M. ed., Scanning Electron Microscopy, 1974, Vol.I, pp. 151-158. Chicago, IL USA : SEM Inc.

Barclay Jones, W. and Carpenter, R.A. (1968). Advances in X-ray Analysis, 11, 214-229.

Bartosek, J., Masek, J., Adams, F. and Hoste, J. (1972). Nucl. Instrum. and Methods, 104, 221.

Beaman, D. R. and Isasi, J.A. (1970). Anal. Chem., 42, 1540-1568.

Beaman, D.R., Isasi, J.A., Birnbaum, H.K. and Lewis, R. (1972). J. Phys. E, 5, 767-776.

Bloomfield, D. J., Love, G. and Scott, V.D. (1981). In: Goringe, M.J., ed. Electron Microscopy and Analysis. Inst. Phys. Conf. Ser. No. 61,pp. 181-182. Inst. of Physics.

Bowman, H.R., Hyde, E.K., Thompson, S.G. and Jared, R.C. (1966). Science, 151, 562-568.

Brouwer, G. and Jansen, J.A. (1973). Anal. Chem., 45, 2239-2247.

Castaing, R. (1951). Thesis University of Paris.

Cochran, W.T., Cooley, J.W., Favin, D.L., Helms, H.D., Kaenel, R.A., Lang, W.W., Maling, G.C., Nelson, D.E., Rader, C.M. and Welch, P.D., (1967). IEEE Trans. Audio and Electroacoustics, AU-15, 45.

Colby, J. W. (1972). In: Shinoda, G., Kohra, K. and Ichinokawa, T. eds., Proc. 6th Int. Conf. X-ray Optics and Microanalysis, Osaka 1971, p. 247. Japan : University of Tokyo Press.

Connelly, A.L. and Black, W.W. (1970). Nucl. Instrum. and Methods, 82, 141-148.

Cosslett, V.E. and Duncumb, P., (1956). Nature, 177, p 1172.

Covell, D.F., Sandomire, M.M. and Eichen, M.S. (1960). Anal. Chem., 32, 1086.

Dolby, R.M. (1959). Proc. Phys. Soc. 73, p81.

Dolby, R.M. (1963). J. Sci. Instrum. 40, p345.

Duncumb, P. and Reed, S.J.B., (1968). In: Heinrich, K.F.J. ed., Quantitative Electron Probe Microanalysis, NBS SP 298, pp.133-154. Washington DC: National Bureau of Standards.

Elad, E. (1971). In: Russ, J.C. ed., Energy Dispersion X-ray Analysis; Toronto 1970 : X-ray and Electron Probe Analysis, ASTM STP 485, pp.57-81. Philadelphia : ASTM.

Fano, U. (1947). Phys. Rev., 72(1), 26-29.

Fiori, C.E., Myklebust, R.L. and Gorlen, K. (1981). In: Heinrich, K.F.J., Newbury, D.E., Myklebust, R.L. and Fiori, C.E. eds., Energy Dispersive X-ray Spectrometry, NBS SP 604, pp.233-272. Washington DC: National Bureau of Standards.

Fiori, C.E., Myklebust, R.L., Heinrich, K.F.J and Yakowitz, H. (1976). Anal. Chem., 48, 172-176.

Fiori, C.E. and Newbury, D.E. (1978). In: Johari, O.M. ed., Scanning Electron Microscopy, 1978, Vol I, pp. 401-422. IL USA:SEM Inc.

Fitzgerald, R. and Gantzel, P. (1971). In: Russ, J.C. ed., Energy Dispersion X-ray Analysis; Toronto 1970: X-ray and Electron Probe Analysis, ASTM STP 485, pp. 3-35. Philadelphia: ASTM.

Fitzgerald R., Keil, K. and Heinrich, K.F.J. (1968). Science, 159, 528-529.

Harms, J. (1967). Nuc. Instrum. and Methods, 53, 192-196.

Heinrich, K.F.J. (1966). In: McKinley, T.D., Heinrich, K.F.J. and Wittry, D.B., eds., The Electron Microprobe, pp. 296-377. New York : John Wiley and Sons Inc.

Henke, B.L. and Ebisu, E.S. (1973). Adv. X-ray Analysis, 17, 150-213.

Holliday, J.E. (1966). In: McKinley, T.D., Heinrich, K.F.J. and Wittry, D.B. eds. The Electron Microprobe, pp.3-22, New York: John Wiley and Sons Inc.

Inouye, T., Harper, T. and Rasmussen, N.C. (1969). Nucl. Instrum. and Methods, 67, 125-132.

Jaklevic, J.M. and Goulding, F. S. (1971). IEEE Trans. Nucl. Sci., NS-18 (1), 187-191.

Johann, H.H. (1931). Zeit. Phys. 69, 185.

Johansson T. (1932). Naturwiss, 20, 758.

Kramers, H.A. (1923). Phil. Mag., 46, 836.

Langheinrich, A.P. and Forster, J.W. (1968). Advances in X-ray Analysis, 11, 275-286.

Love, G. (1975). Thesis, University of Bath.

Love, G., Cox, M.G.C. and Scott, V.D. (1974). J. Phys. D, 7, 2131.

Love, G., Cox, M.G.C. and Scott, V.D. (1978). J. Phys. D, 11, 7-21.

Love, G. and Scott, V.D. (1978). J. Phys. D, 11, 1369-1376.

Love, G. and Scott, V.D. (1981). Scanning, 4, 111-130.

Love, G., Scott, V.D., Dennis, N.M.T. and Laurenson, L. (1981). Scanning, 4, 32-39.

Mariscotti, M.A. (1967). Nucl. Instrum. and Methods, 50, 309.

McCarthy, J.J. and Schamber, F.H. (1981). In: Heinrich, K.F.J., Newbury, D.E., Myklebust, R.L. and Fiori, C.E. eds., Energy Dispersive X-ray Spectrometry,

NBS SP 604, pp. 273-296. Washington DC : National Bureau of Standards.

Moseley, H.G.J. (1913). Phil. Mag., 26, 1024.

Moseley, H.G.J. (1914). Phil. Mag., 27, 703.

Myklebust, R.L., Fiori, C.E. and Heinrich, K.F.J. (1981). In: Heinrich, K.F.J., Newbury, D.E., Myklebust, R.L. and Fiori, C.E. eds., Energy Dispersive X-ray Spectrometry, NBS SP 604, pp.365-380. Washington DC: National Bureau of Standards.

Nash, J.C. (1979). Compact Numerical Methods for Computers : Linear Algebra and Function Minimisation. Bristol:Adam Hilger Ltd.

Pell, E.M. (1960). J. Appl. Phys., 31(2), 291-302.

Philibert, J. (1963). In: Patee, H.H., Cosslett, V.E. and Engstrom, A. eds., X-ray Optics and X-ray Microanalysis, p.379. New York:Academic Press.

Ralston, A. and Rabinowitz, P. (1978). A First Course in Numerical Analysis, 2nd edition. New York: McGraw-Hill Book Company.

Ranzetta, G.V.T. and Scott, V.D. (1964). Brit. J. Appl. Phys. 15, p263.

Rao-Sahib, T.S. and Wittry, D.B. (1974). J. Appl. Phys., 45, 5060-5068.

Reed, S.J.B. (1972a). J. Phys. E, 5, 997-999.

Reed, S.J.B. (1972b). J. Phys. E, 5, 994-996.

Reed, S.J.B. (1975a). Electron Microprobe Analysis, Cambridge: Cambridge University Press.

Reed, S.J.B. (1975b). X-ray Spectrom., 4, 14-17.

Reed, S.J.B. and Ware, N.G. (1972). J. Phys. E, 5, 582-584.

Reed, S.J.B. and Ware, N.G. (1973). X-ray Spectrom., 2(2), 69-74.

Robertson, A., Prestwich, W.V. and Kennett, T.J. (1972). Nucl. Instrum. and Methods, 100, 317-324

Russ, J.C. (1971). In: Russ, J.C. ed., Energy Dispersion X-ray Analysis; Toronto 1970: X-ray and Electron Probe Analysis, ASTM STP, 485 pp. 217-231. Philadelphia:ASTM.

Russ, J.C. (1975). Edax Editor, 5(4), 1.

Russ, J.C. (1977a). X-ray Spectrom., 6(1), 37-55.

Russ, J.C. (1977b). In: Johari, O.M. ed., Scanning Electron Microscopy, 1977, Vol I, p.298. IL USA: SEM Inc.

Russ, J.C. (1978). Edax Editor, 8(2), 20.

Russ, J.C. Baerwaldt, G.C. and McMillan, W.R. (1976). X-ray Spectrom. 5(3), 212-222.

Russ, J.C. and Sandborg, A.O. (1981). In: Heinrich, K.F.J., Newbury, D.E., Myklebust, R.L. and Fiori, C.E. eds., Energy Dispersive X-ray Spectrometry, NBS SP 604, pp.71-95. Washington DC:National Bureau of Standards.

Russ, J.C., Sandborg, A.O., Barnhart, M.W., Soderquist, C.E., Lichtinger, R.W. and Walsh, C.J. (1973). Adv. X-ray Anal., 16, 284.

Ryder, P.L. (1981). In: Heinrich, K.F.J., Newbury, D.E., Myklebust, R.L. and Fiori, C.E. eds., Energy Dispersive X-ray Spectrometry, NBS SP 604, pp.177-192. Washington DC: National Bureau of Standards.

Sandborg, A.O. and Merkle, A.B. (1981). In: Johari, O.M. ed., Scanning Electron Microscopy, 1981, pp. 63-70. Chicago, IL USA:SEM Inc.

Sayce, L.A. and Franks, A. (1964). Proc. Roy. Soc. A282, 353.

Schamber, F.H. (1981). In: Heinrich, K.F.J., Newbury, D.E., Myklebust, R.L. and Fiori, C.E. eds., Energy Dispersive X-ray Spectrometry, NBS SP 604, pp.193-231. Washington DC: National Bureau of Standards.

Scott, V.D. (1974). In: Advances in Analysis of Microstructural Features by Electron-beam Techniques, p.141. London: The Metals Society.

Smith, D.G.W. and Gold, C.M. (1976). Adv. X-ray Analysis, 19, 191-201.

Smith,D.G.W. and Gold, C.M. (1979). In: Newbury, D.E. ed., Microbeam Analysis 1979, p.273. San Francisco: San Francisco Press.

Smith, D.G.W., Gold, C.M. and Tomlinson, D.A. (1975). X-ray Spectrom., 4, 149-156.

Statham, P.J. (1976). X-Ray Spectrom., 5, 154-168.

Statham, P.J. (1977). Anal. Chem., 49(14), 2149-2154.

Statham, P.J. (1978). X-ray Spectrom., 7(3), 132-137.

Statham, P.J. (1981a). In: Heinrich, K.F.J., Newbury, D.E., Myklebust, R.L. and Fiori, C.E. eds., Energy Dispersive X-ray Spectrometry, NBS SP 604, pp.127-139 Washington DC: National Bureau of Standards.

Statham, P.J. (1981b). In: Heinrich, K.F.J., Newbury, D.E., Myklebust, R.L. and Fiori, C.E. eds., Energy Dispersive X-ray Spectrometry, NBS SP 604 pp.141-164. Washington DC: National Bureau of Standards.

Statham, P.J. (1981c). J. Microscopy, 123(1), 1-23.

Statham, P.J. (1983). J. Microsc., 130(2), pp.165-176.

Ware, N.G. and Reed, S.J.B. (1973). J. Phys. E, 6, 286-288.

Westlake, J.R. (1968). A Handbook of Numerical Matrix Inversion and Solutions of Linear Equations. New York: John Wiley and Sons Inc.

Whiddington, R. (1912). Proc. Roy. Soc. A86, p.360.

Williams, C.W. (1968). IEEE Trans. Nucl. Sci. NS 15(1), 297-302.

Williams, D.B. and Goldstein J.I. (1981). In: Heinrich, K.F.J, Newbury, D.E., Myklebust, R.L. and Fiori, C.E., eds., Energy Dispersive X-ray Spectrometry, NBS SP 604, pp.341-349. Washington DC: National Bureau of Standards.

Williams, G. (1971). In: Russ, J.C.ed., Energy Dispersion X-ray Analysis; Toronto 1970: X-ray and Electron Probe Analysis, ASTM STP 485, pp. 125-139. Philadelphia:ASTM.